Mechanistic Investigation of Sulfur Dioxide reduction using second sphere modified porphyrins

Thesis submitted to Jadavpur University

for the Degree of

Doctor of Philosophy (Science)

in

Chemistry

by

Aishik Bhattacharya

School of Chemical Sciences

Indian Association for the Cultivation of Science,

Jadavpur, Kolkata-700032

West Bengal, India

2023

Indian Association for the Cultivation of Science
2A and 2B Raja S. C. Mullick Road, Kolkata, INDIA-700032
Somdatta Ghosh Dey, Ph.D.
Professor, School of Chemical Sciences Phone: +913324734971
(Ext 1376)
Email: icsgd@iacs.res.in

CERTIFICATE FROM THE SUPERVISOR

This is to certify that the thesis entitled **"Mechanistic Investigation of Sulfur Dioxide reduction using second sphere modified porphyrins"** submitted by **Mr. *Aishik Bhattacharya,*** who got his name registered on 05/09/2018 for the award of Ph. D. (Science) degree of Jadavpur University, is absolutely based upon his own work under the supervision of **Professor Somdatta Ghosh Dey** and that neither this thesis nor any part of it has been submitted for either any degree / diploma or any other academic award anywhere before.

Somdatta Ghosh Dey

.....

Signature of the supervisor
date with official seal

Dr. Somdatta Ghosh Dey
Professor
School of Chemical Sciences
Indian Association for the Cultivation of Science
Jadavpur, Kolkata - 700032

DECLARATION

I hereby declare that the research work presented in this thesis entitled **"Mechanistic Investigation of Sulfur Dioxide reduction using second sphere modified porphyrins"** is the result of the studies carried out by me under the supervision of ***Professor Somdatta Ghosh Dey*** at the School of Chemical Sciences, Indian Association for the Cultivation of Science, Kolkata, and the same has not been submitted elsewhere for any other degree or diploma.

Aishik Bhattacharya

Date: 28.09.2023

Aishik Bhattacharya

(227/18/Chem./26)

Dedicated to FAILURE

Acknowledgement

No journey in this world can be an individual endeavour, and especially the journey of PhD. It was, it is and it will always be an endeavour in mutual cooperation. My PhD journey also would have been incomplete without many people and I need to thank them here. First of all, a big gratitude goes to Prof. Somdatta Ghosh Dey, for whom I was here and who was my supervisor, I can't thank you enough Ma'am. Then I must pay my due respects to Prof. Abhishek Dey, on whose ideas I have worked in my entire PhD tenure. If I was a part of anything meaningful, then the credit for all the ideas goes to Prof. Dey, without whom all the beautiful and exciting science I was a part of, would not have happened. Then I must thank all of my lab mates and colleagues, who made life so much easier and fun. Be it my seniors, my batchmates or my juniors. Not all of them are my colleagues, some of them are my brothers and sisters and some of them are my closest friends. You all know who you are. I must then thank the entire IACS fraternity, without whose support this journey would have been even more difficult. All the instrument operators, who meticulously recorded my data, all the canteen staffs, all the admin office staffs, all the security people, all the housekeeping staffs and all the academic and non-academic personnel of IACS, they all work hard so that our life gets a bit easier. The funding agency, UGC without whose timely disbursal of my monthly fellowship and HRA, I would not have been able to complete this PhD. My family, my soon to be family, my friends, I am grateful to all of you and do acknowledge you for your support. And last but not the least, I must thank myself for completing this journey, even when I had a thousand reasons not to. And I sincerely apologize to everyone whom I have hurt intentionally or unintentionally in this brief tenure of PhD. I wish for a world where logic and scientific thinking flourishes hand in hand with empathy, because we have got only one planet where we have signs of life, till now.

Aishik Bhattacharya

PREFACE

The work presented in this thesis entitled "**Mechanistic Investigation of Sulfur Dioxide reduction using second sphere modified porphyrins**" was initiated by the author in September, 2016 in the School of Chemical Sciences, Indian Association for the Cultivation of Science, Kolkata, under the supervision of Prof. Somdatta Ghosh Dey.

Bio-inorganic chemistry is that particular domain of Inorganic Chemistry, which studies the chemical reaction happening in the biological systems from the viewpoint of Inorganic Chemistry. To achieve that goal, it employs the principles of Organic Chemistry, Inorganic Chemistry and Spectroscopy, which falls under the domain of Quantum Chemistry. Bio-inorganic Chemistry covers a wide domain of interest, and one among them being the mechanistic investigations of biological reactions, going on inside biological systems, driven forward by the most efficient catalysts of nature, the enzymes. Human beings lacking the billions of years of time frame to evolve catalysts as efficient as enzymes, prudentially turn towards nature to understand and design biological systems and enzyme catalysts, to drive forward reactions of its own interest. One such reaction of interest being reduction of the pollutant, Sulfur Dioxide (SO_2), which is most efficiently handled by Sulfite Reductase enzymes present in some anaerobic bacteria and Archaea. The mechanism of the SO_2 reduction reaction carried out by the Siroheme based Sulfite reductase enzymes is still unelucidated. This work employs synthetic model complexes, that structurally and functionally mimics the complex active site architecture of the enzyme active sites, to study SO_2 reduction reaction, from a viewpoint of Bio-Inorganic Chemistry, employing principles of Organic, Inorganic Chemistry along with Spectroscopy.

The Chapter 1, which is a General Introduction chapter, introduces the necessity of SO_2 reduction along with the different techniques employed to reduce it. Then it gives a background in the Sulfite Reductase enzymes, describing their active site architecture, the knowledge we have about SO_2 reduction mechanism, till date. This is followed by the necessity of using synthetic model complexes and how they can be employed to study the reaction mechanisms of different biological transformations.

Chapter 2 discusses about the different instrumentation methods and experimental details used to study the reaction mechanisms. It describes in details the instruments which were used, the method of sample preparations has been detailed for a clear understanding of the protocols.

The Chapter 3 investigates the reduction of SO_2 using $Fe^{II}TPP$. It describes the mechanistic investigation where in due course of SO_2 reduction, a novel hexacoordinated MeOH bound

Fe^{III}TPP-SO was generated. The incipient SO was then released from the Fe^{III}TPP, generating Fe^{III}TPP and a very unstable Sulfur Monoxide (SO), which was trapped with the help of a cheltropic adduct formation between 2,3-Dimethylbutadiene and the *in situ* released SO. The trapping of the SO goes on to prove the generation of the MeOH-Fe^{III}TPP-SO intermediate, which has been also identified with the help of other spectroscopic and DFT calculations.

The 4th Chapter is about further investigation of the SO_2 reduction reaction, at lower temperatures. It also introduces another intermediate, that is generated before the generation of the Intermediate described in Chapter 3, the MeOH-Fe^{III}TPP-SO. The new intermediate is a Low Spin, MeOH bound Fe^{III}TPP-SO_2^-, which undergoes protonation and subsequent dehydration to make way for the MeOH-Fe^{III}TPP-SO intermediate. These two novel intermediates have been properly identified and their distinctive Resonance Raman shifts were reported by performing the S^{32}/S^{34} isotope dependant studies. The identification of these intermediates outside protein matrix, for the first time gives new insight into the SO_2 reduction reaction mechanism, performed by Sulfite Redutase enzymes.

The 5th Chapter introduces SO_2 reduction using second sphere modified porphyrins. This has been performed by using Fe^{II}Pydn ligand, which has a pendant Pyridine attached to it and hangs near the distal binding site of Fe^{II}, where SO_2 binds. The signals associated with the MeOH-Fe^{III}-SO_2^- intermediate was also observed with Fe^{III}Pydn porphyrin. A comparative SO_2 reduction rate study was done using Fe^{II}Pydn and Fe^{II}TPP, where it was observed that there is a rate difference on introducing second sphere modification over the Porphyrin. This implies the influence of second sphere interaction, just like in the biological SO_2 reduction performed by the Sulfite Reducatse enzyme.

So, the entire thesis deals in the mechanistic elucidation of SO_2 reduction reaction, using Fe based porphyrins and second sphere modified porphyrins.

Aishik Bhattacharya

Table of Contents

Chapter 1

General Introduction

1.1 Importance of SO_2 reduction:

With industrial revolution, human civilisation has changed enormously. Spinoffs of the revolution are many processes like petroleum refining, fossil fuel burning, metal smelting, to make human life easier. But all these processes give rise to harmful waste products leading to global environmental pollution. A significant pollution among that is air pollution, of which Sulphur and its oxides are a chief air pollutant.[1]

Sulphur ($^{32}S_{16}$) happens to be the 10th most abundant element in the universe and the 8th most abundant element in microbial biomass.[2] Mostly S exists in these 3 states: elemental S (S_8, having formal oxidation state 0), SO_4^{2-} (formal oxidation state +6) and S^{2-} (formal oxidation state -2). Apart from these there are intermediate oxidation states. Among them the +4-oxidation state of S, in which it's found in SO_2 or SO_3^{2-} state is of utmost importance. Since in these states and +6 oxidation states where S is in higher oxidation states and causes environmental damage.

Sulfur Dioxide (SO_2) is an atmospheric pollutant that is emitted from fossil fuel burning and smelters. An estimated >100 Tg of SO_2 is emitted annually; mostly from human activities[3]. This reactive gas-phase air pollutant SO_2 causes respiratory troubles and cardiovascular deaths. By reacting with O_3, OH radicals and H_2O_2, it gets oxidised to H_2SO_4, which is again a cause of acid rains.[4] Apart from direct effects, SO_2 gets oxidized in the atmosphere to sulphates which is the major component of particulate matter (PM 2.5) that is detrimental to human health.[5] SO_2 is added to atmosphere due to both anthropogenic and natural volcanic activities. As a result, it has added to the burden of global warming.[6] A concerted global effort has led to a reduction in SO_2 emission in some countries, but it has been increasing substantially in developing nations that largely relies on coal for power generation.[7] Fixation of SO_2 by reducing it to sulfur or sulfides is an attractive approach to eliminate this pollutant and generate valuable stock chemicals.[8] It's imperative that to reduce the global burden of air pollution, acid rain and global warming, SO_2 has to be removed from the environment. An efficient way of doing this is by reducing SO_2 (where S is in +4 oxidation state) to its lower oxidation states. Due to certain limitations of the industrially widespread methods, it's necessary to look for alternative, more benign methods of SO_2 reduction.

1.2 Metal catalyst based SO_2 reduction:

Limestone-gypsum wet flue gas desulfurization is a widely used technique to remove SO_2 from coal-fired power plant exhaust fumes.[9] Various other methods of SO_2 reduction are used industrially, like SO_2 reduction using H_2/CO at higher temperatures on activated Carbon bed,

or catalytic SO_2 reduction using H_2 over Sn-Zr based catalysts[10]. There are some methods which use Non Thermal Plasma combined with a metallic catalyst to reduce SO_2 into its elemental form[11]. But the problem with all the above methods is either the requirement of high temperature or uber reactive Non-Thermal Plasma, which requires a very controlled atmosphere as its pre-requisite. Due to certain limitations of the industrially widespread methods, it's imperative to look for alternative, more benign methods of SO_2 reduction. V, Nb, Ta oxyfluoride complexes are capable of forming side-on SO complexes when reacted with SO_2.[12] Cobalt based Tetraphenylporphyrin complexes with SO_2 have been known since 1970s[13], while Ru and Fe based porphyrin catalysts are also known to reduce HSO_3^- to H_2S.[14] Reduction of SO_2 by molecular systems are rare, except for some reports on Copper Koneramine complexes[15] and needs to be explored to marshal newer methods for SO_x valorization.

1.3 Biological SO_2 reduction:

The biogeochemical cycle of Sulphur is maintained by bacterial oxidation and bacterial reduction of different analogues of Sulphur (Figure 1). A host of microbial organisms recycle SO_x as a part of the geochemical sulfur cycle and, recently, these organisms have been used to valorize sulfur from an alkaline extract of flue gas which contains SO_2. Here Single Catalytic Desulfurization and Denitrification process is used, where the reactor is prepared with sulfate reducing bacteria, through which if alkaline extract of flue gas is passed, it leads to simultaneous reduction of SO_2 to S^{2-}.[16]

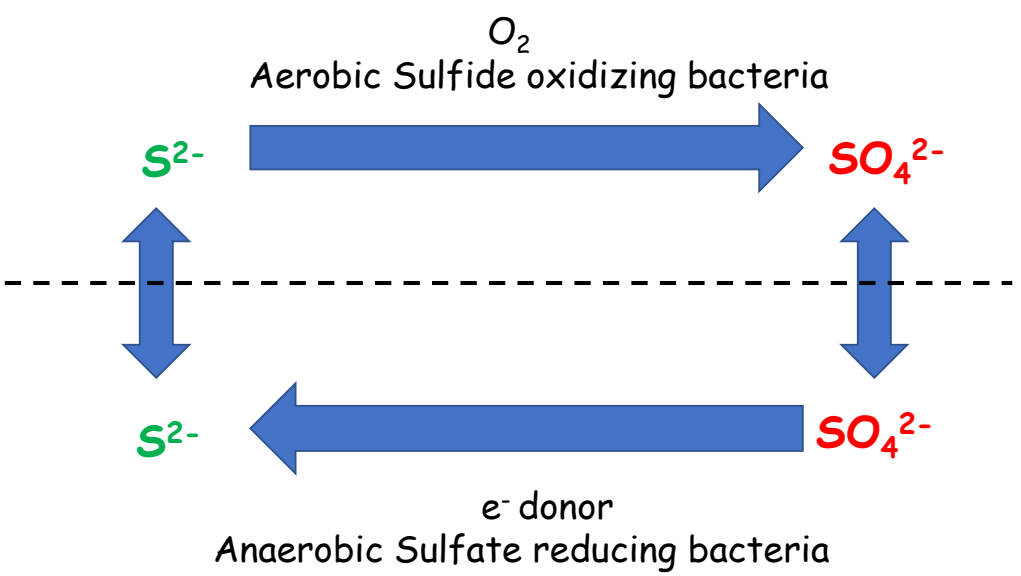

Figure 1. Schematic representation of the cyclic reactions prevailing in a microbial sulfur cycle between sulfate reducing and sulfide oxidizing bacteria.[17]

In nature Sulphur is handled by Sulphate reducing and Sulfide oxidizing bacteria. We are targeting a means of reducing Sulphur, the way nature does, so that we are able to mitigate the harmful effects of oxidised forms of Sulphur as a pollutant. Hence, we would turn our attention on Sulphate reducing bacteria and gain inspiration from them about how they reduce Sulphate into Sulphide. In nature SO_4^{2-} via an enzymatic pathway is converted into SO_3^{2-} (which is chemically similar to SO_2, in both cases S being in +4 oxidation state) and then reduced by Sulphur reducing anaerobes. These bacteria reduce SO_2 or Sulphite via a $6e^-/6H^+$ reduction process to generate S^{2-} (sulphide anion).

1.3.1 Sulfite Reductase:

This $6e^-/6H^+$ reduction rection of Sulphite to Sulphide is facilitated by an enzyme present in these bacteria, known as Sulphite Reductase, which is also found in some archaea, plants and fungi.[18] This enzyme is a member of Oxidoreductase family of enzymes, falling under classification EC 1.8.1.2.[19] There are two different types of Sulfite Reductase enzymes: Assimilatory and Dissimilatory Sulfite Reductases. Assimilatory Sulfite Reductases (ASiR) have been extracted from *Escheria coli* bacteria while the Dissimilatory Sulfite Reductases (DSiR) have been extracted from Sulfate reducing bacteria. The DSiRs can again be classified into two classes: Desulfoviridin, extracted from *Desulfovibrio gigas* and Desulforubridin, extracted from *Desulfovibrio desulfuricans*. The ASiR catalyses Assimilatory Sulfite reduction, a minor pathway facilitating biosynthesis of cysteinyl amino acids, while the DSir catalyses Dissimilatory Sulfite reduction, which is a large-scale process linked to cellular respiration. The Dissimilatory pathway is observed in anaerobes, which evolved this pathway for cellular respiration in early anoxic conditions of earth.[20] The basic difference between Assimilatory and Dissimilatory pathway is the end product; in the former S^{2-} produced from SO_3^{2-} or SO_4^{2-} is assimilated in the cell to generate S containing biomolecules like Cysteine, which is further metabolised into Methionine, Glutathione and many other compounds.[21] While in the dissimilatory pathway, S^{2-} is generated from SO_4^{2-}, which acts as a terminal e^- acceptor. The generated S^{2-} in the dissimilatory pathway is released as Trithionates ($S_3O_3^{2-}$) or Thiosulphate ($S_2O_3^{2-}$).[22] This reduction of SO_3^{2-} (generated from SO_4^{2-} via some other enzymatic pathways) to S^{2-} proceeds via a $6e^-/6H^+$ pathway, the mechanism of which is still not clearly understood.[23] There is another uncommon DSiR, isolated from *Wolinella succinogenes* known as SirA having Octahaem cytochrome c MccA, which is a haem c-copper sulphite reductase, that also catalyses the $6e^-/6H^+$ reduction of SO_2 to S^{2-}.[24]

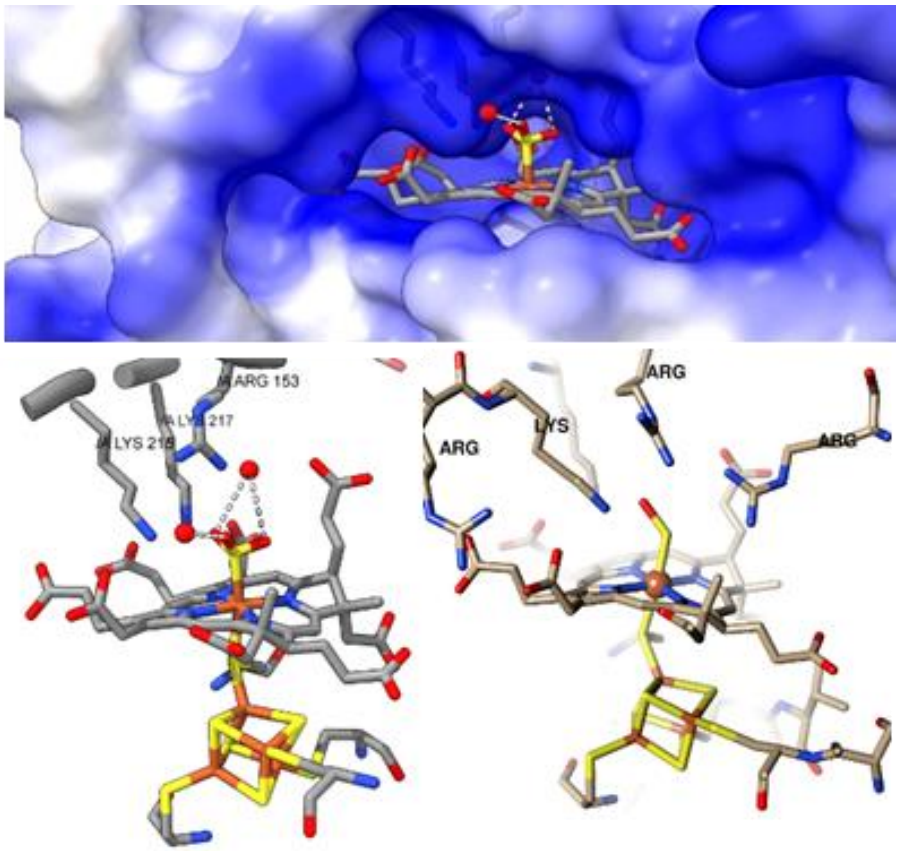

Figure 2. (top) Active site of SiR on the surface of the protein (pdb id: 2GEP [25]) (bottom left) Active site of sulfite reductase bound to SO_3^{2-} and (bottom right) Structure of the partially reduced SO_x species observed crystallographically (pdb id: 7GEP[25]). Color code: Fe → orange, S → yellow, P → light orange, O → red, N → blue and C → grey. The distal pendant residues are labelled

Despite their difference in final products, both the ASiR and DSiR share common structures. Both the ASiR (extracted from *Escheria coli*) and DSiR (extracted from *Desulfovibrio desulfuricans*) contain pentacoordinate high spin siroheme moiety, however there is another type of ASiR (extracted from *Desulfovibrio vulgaris*) that has hexacoordinate low spin siroheme centre.[26] The Siroheme moiety of the heme chromophore belonging to ASiR is iron tetrahydroporphyrin of the isobacteriochlorin family, with octacarboxylic acid substitution around the porphyrin (Figure 3).

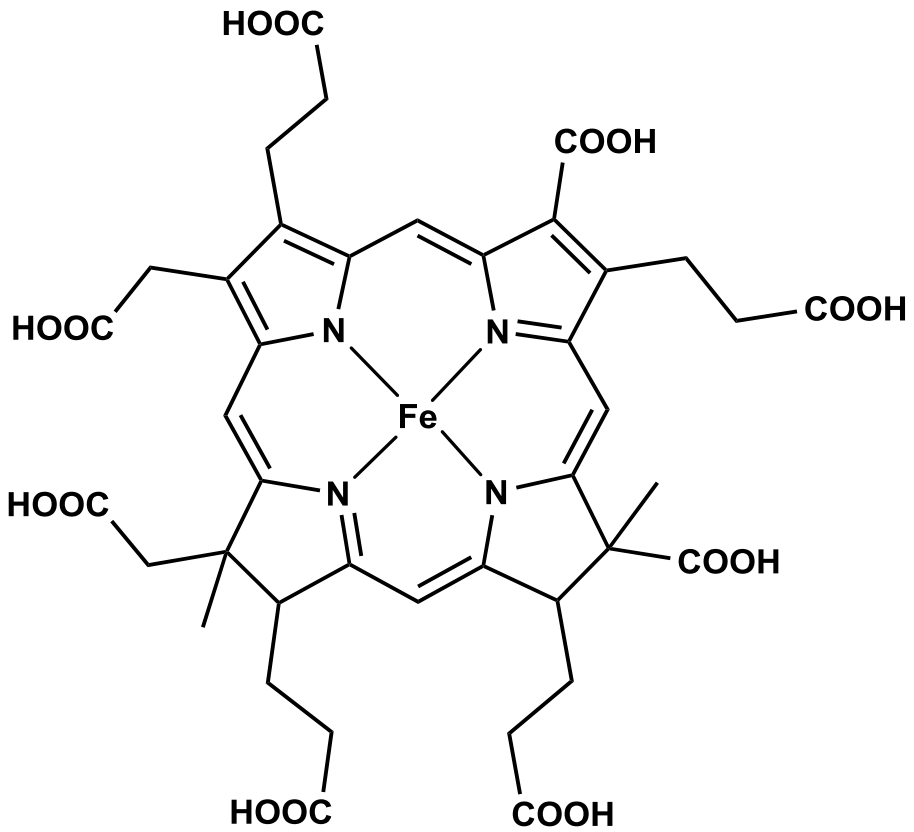

Figure 3. Siroheme moiety of isobacteriochlorin family, present in ASiR and DSiR[27]

There are some differences in the absorption spectra and EPR spectra of the ASiR and DSiR extracted from *E. coli* and *D. desulfuricans* but this difference is due to variation in their local environment, while residing inside their respective proteins.[28] The SiRs feature a siroheme cofactor (Figure 3) in its active site which is a member of the isobacteriochlorin family of heme cofactors.[29] The most extensively studied active site among the different Sulfite Reductaes are ASiR from *E. coli*. The active site of the ASiR extracted from *E. coli* apart from having the siroheme moiety of the isobacteriochlorin family, via its proximal binding site, is covalently bridged to a Cysteine thiolate ligand, which again bridges it to a Fe_4S_4 cluster (Figure 2, bottom).[30] The Fe_4S_4 cluster acts as an e^- pump and transfers e^- via the Cysteine thiolate linkage to the Siroheme moiety, as a result of which the ASiR active site reduces the SO_3^{2-} ion to S^{2-} ions.[31] The Siroheme moiety remains in High Spin S = 5/2 state and the Fe_4S_4 cluster Fe centres are in the +2 diamagnetic oxidation state. The High Spin Fe centre of Siroheme is exchange coupled with the cluster. All the oxidation state and exchange coupling have been evidenced from EPR and Mössbauer spectroscopy on the isolated enzymes.[32] These observations have been further backed up by other spectroscopic evidences in the form of ^{57}Fe ENDOR (electron-nuclear double resonance), rR spectroscopy by Soret band excitation[33] paramagnetic NMR[34] and some crystallographic studies.[35]

The siroheme active site sits on the surface of the protein and in a positively charged cavity containing several lysine and arginine residues (Figure 2, top). These residues stabilize the binding of the substrate and intermediates via H-bonding (Figure 2, bottom left) and provide protons needed for the reduction of SO_3^{2-} to H_2S. The choice of Siroheme as the porphyrin macrocycle is due to its enhanced flexibility because of partial saturation, that results in increased e^- availability, which helps in reduction of SO_3^{2-}.[30] A series of iron-sulfur clusters provide the $6e^-$ needed for this reaction which funnels through the proximal Fe_4S_4 cluster that bridge with the siroheme cofactor (Figure 2).

Now that we have a fair idea about the active site structure of the SiR enzymes, it would be prudent to discuss about the exact mechanism by which the reduction of SO_3^{2-} occurs. The reduction of SO_3^{2-} by the ASiR and DSiR starts with binding of the trigonal bipyramidal SO_3^{2-} anion to the Fe center of the Siroheme moiety via the S atom. The partial saturation and flexibility of the Siroheme macrocycle makes it conducive for e^- donation and binding with the Sulfite anion.[30] Charge flow from Siroheme into the S atom of the Sulfite anion leads to its reduction +4 oxidation state to its lower oxidation states. Most likely, e^- from the Fe atom of Siroheme, flows into the S-O 3d-2p Π^* anti-bonding orbital, weakening the bond. After subsequent reduction of S center from +4 to +2 oxidation state and weakening of S-O bond, the O atoms are protonated by nearby H_2O molecules or by the Arginine or Lysine residue present around the active. Due to protonation of the O atoms, it leads to release of H_2O molecules, where the O atoms come from the Sulfite anions, that lead to generation of Fe bound Sulfoxy intermediates of oxidation state +2.[36] This is followed by subsequent reduction steps, which lead to S^{2-} anion, but the mechanism is not clear. The reduction of SO_2 with the reduced ferrous siroheme active site of SiR has been investigated in detail using a combination of spectroscopic and theoretical techniques.[31, 37-38] The proposed mechanism of action for this overall $6H^+/6e^-$ reduction of sulfite to sulfide by SiR is debatable. Using the X-ray structures of SO_3^{2-} bound active site and structures of other small molecules and anions bound SiR (e.g. NO_2^-, NO, CO, CN^-), involvement of three consecutive $2H^+/2e^-$ reduction steps which are all accompanied by water elimination (Figure 4) was proposed.[24]

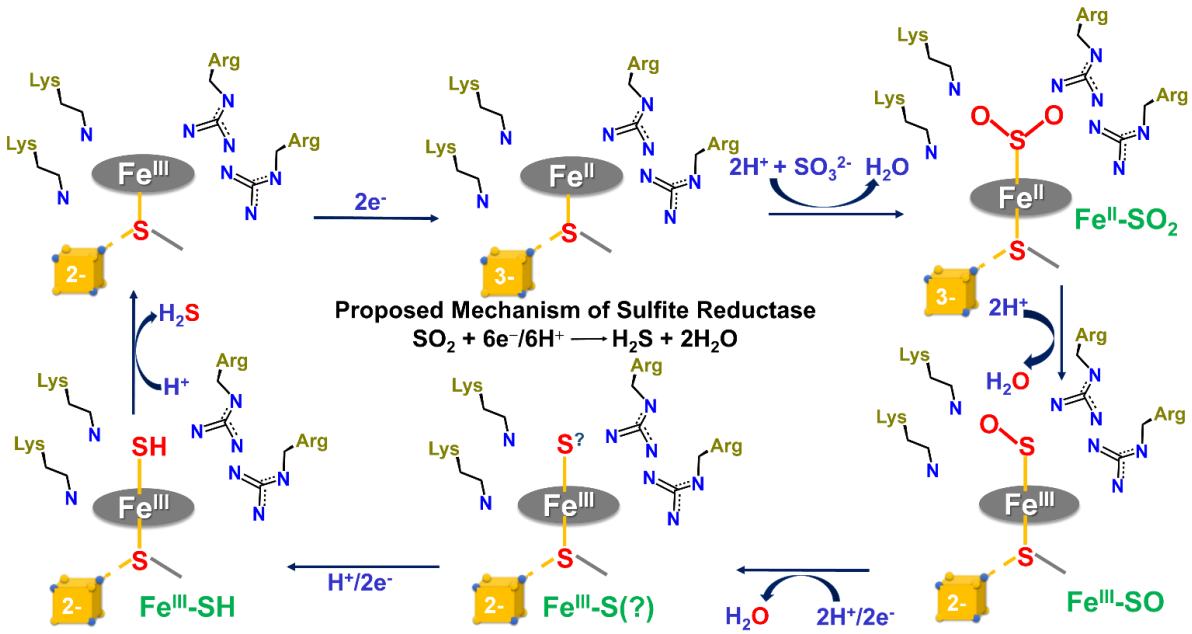

Figure 4. Proposed mechanism of SO_2 reduction by the sulfite reductase. The grey ring represents the heme and the yellow cube represents the Fe_4S_4 cluster – blue and yellow spheres of the yellow cube represent iron and sulfide centers, respectively. The pendant lysine and arginine are indicated. In this proposed mechanism, the reaction proceeds via three $2e^-/2H^+$ steps.

The binding of SO_2 (after water elimination from SO_3^{2-}) to the open co-ordination site of siroheme is followed by its $2e^-$ reductions and water elimination to result in an unusual sulfur monoxide (SO) bound $[Fe^{III}\text{-}SO]^+$ species (Figure 1, bottom right and Figure 2) where the formal oxidation state of the central sulfur is +2 i.e. $2e^-$ reduced relative to +4 in SO_2. Two subsequent $2e^-/2H^+$ reductions and water eliminations yield the final H_2S product of this $6e^-/6H^+$ reduction of SO_2. So, the proposed mechanism is three subsequent $2e^-/2H^+$ reduction of SO_3^{2-} to S^{2-}, accompanied by release of three molecules of H_2O.[25, 39] Alternatively, Stroupe and co-workers used site-directed mutants of the distal Arg and Lys residues to argue for six sequential $1H^+/1e^-$ steps instead. This mechanism is a coupled 'push-pull' mechanism, where the electrons are pushed from the active site Siroheme cofactor and high proton concentrations are donated from distal Arginine and Lysine cages to pull charges from the substrates.[40] Nonetheless, both mechanisms entail the formation of several unusual siroheme bound SO_x species that have not been observed outside the protein matrix in heme systems. Oxidation of the sulfide bound crystals provided crystallographic evidence for the formation of a partially reduced SO_x species. The electron density was fitted to a bent $[Fe^{III}\text{-}SO]^+$ species with a Fe-S distance of 2.2 Å and a S-O distance of 1.6 Å.[25, 30] Unfortunately, the resolution of the structure was not high enough to allow unambiguous determination of the nature of this intermediate in the SO_2 reduction cycle. To have some preliminary idea about electronic

structure of the complex, Enemark Feltham notation comes in handy. Here the total number of Metal d-orbital e^-s and the Π* e^-s of the Ligand, in the Metal(M)-Ligand(L) complex is denoted as $[M\text{-}L]^x$ (where x is the sum of the e^-s. Formally, a $[Fe^{III}\text{-}SO]^+$ species is a $[Fe\text{-}SO]^7$ (5 e^- from Fe^{3+} d-orbitals and 2 e^- from S=O Π* anti-bonding orbitals) species according to Enemark-Feltham notation,[41] which could be similar to the $[FeNO]^7$ intermediate involved in the reduction of NO_2^- in nitrite reductases (NiR). The nature of this $[Fe^{III}\text{-}SO]^+$ species has not yet been understood as it is yet to be actualized in synthetic systems.

1.3.2 Similarities between Nitrite and Sulfite Reductase:

The active sites of SiR are closely related to the active site of NiR which reduce NO_2^- to NH_4^+.[42] The Assimilatory Ferredoxin Nitrite Reductase isolated from Spinach and Chlorella, which catalyzes NO_2^- to NH_4^+, a $6e^-$ reduction reaction also contains a siroheme cofactor in its active site. The spectral properties of both the ASiR and Assimilatory Nitrite Reductases are pretty similar. This assimilatory reduction reaction of NO_2^- to NH_4^+ proceeds via $2e^-$ reduction of NO_2^- initially, followed immediately by direct $6e^-$ reduction to NH_4^+. This entire process is catalyzed by Assimilatory Nitrite Reductase, having a siroheme moiety of isobacteriochlorin class, that is exchange coupled to Fe_4S_4 cluster.[43] It has also been observed that pentahaem Cyctochrome c Nitrite Reeductase (ccNiR), isolated from *Wolinella succinogenes* apart from catalyzing the reduction of NO_2^- to NH_4^+, also catalyzes the reduction of SO_3^{2-} to S^{2-}. Thus ccNiR acts as a common point of intersection between the biogeochemical cycles of Nitrogen and Sulphur.[44] The ASiR isolated from *E. coli* are also capable of catalyzing NO_2^- to NH_4^+ reaction. So, as it is understood that, there are certain SiR which are capable of catalyzing both the SO_3^{2-} to S^{2-} and NO_2^- to NH_4^+ reaction, again there are certain NiR, which are capable of catalyzing both of these reactions. So, the active sites found in the SiR and NiR are often capable of driving forward both these reactions. The Siroheme moiety coupled to Fe_4S_4 cluster is a strong candidate for catalyzing these multi-e^- multi-H^+ reduction reactions to facilitate respiration or biological synthesis of important biomolecules. Since Fe(II) tetraphenylporphyrin ($Fe^{II}TPP$) can reduce NO_2^- just like siroheme based NiR which, in turn, can also reduce sulfite, it is possible that $Fe^{II}TPP$ may reduce SO_2 like the siroheme based SiR.[44]

1.4 Model complex based SO_2 reduction:

Enzymes are biological catalysts designed over billions of years, directed by the driving force of evolution by natural selection. Human life is insignificantly short on the grand time scale of nature. So, we don't have the abundance of time to perfect the human made catalysts by

letting evolution and natural selection choose the most efficient ones. So, the most pragmatic solution at our disposal is to emulate and study the evolutionally designed natural catalysts over billions of years and employ certain aspects of them in designing our own catalysts, to drive forward some reactions which are of interest to us. Another possible alternative for us would be directly employing the enzymes to catalyze those reactions. However, quite a few practical problems arise here while doing so. Some of them are: difficulty in obtaining high molecular mass membrane bound proteins, their tedious isolation and purification processes and finally obtaining them on large industrial scales to catalyze reactions of our choice. These practical problems bar us from directly employing enzymes, the most efficient catalysts at our disposal from solving real world problems. So, we go with the best possible alternative, which is employing synthetic model complexes, which fuses the best of both worlds, gaining mechanistic insights from the enzymes about how to catalyze a process and then rationally designing the catalyst so that it's available on a large scale, so that some real-world problems can be solved. This is called Bio-inspired catalysis.[45] Research on synthetic model porphyrins for decades have led to quite a few advancements in the direction of small molecules activation. The synthetic model complexes of oxy-hemoglobin, structural and functional models of Cytochrome c Oxidase,[46] Horseradish Peroxidase, nitric oxide reductase,[47-48] Nitrite Reductase,[49] etc. have made our understanding about the working mechanisms of those enzymes much clear, as well as gave us new insights about catalyzing small molecules activation using other catalysts.

1.4.1 Using Porphyrin model complex:

Porphyrin is a bulky tetrapyrrolic ligand, where the pyrrole rings are bridged at their α Carbon atoms via methine linkages. The extensive conjugation in the heterocyclic porphyrin ligands impart intense colour to these ligands. Interestingly, the word porphyrin has a Greek origin which roughly translates into purple. This purple colour in porphyrin comes from the n-Π* transition of porphyrin e^- in the visible region.

Deprotonated porphyrin being a dianionic ligand and also having a central hole of proper size is perfectly suited to accommodate a di-cationic metal ion to produce a tetracoordinated structure forming four Nitrogen-Metal bonds. The resulting macrocycle after binding a metal is called metalloporphyrin. When the metalloporphyrin contains Fe metal, it's called heme. Heme metalloporphyrins are perhaps the most widely used natural catalyst present in enzyme active sites, to drive forward a range of biological reactions. The utilization of porphyrin macrocycles as a ligand framework is justifiable because of the following advantages they offer:

1. The porphyrin macrocycles can accommodate a variety of transition metals and can provide the central metal a rigid and stable binding site.
2. The tetracoordinated square planar geometry afforded by the 4 N-M bonds is the most suitable location for substrate binding and activation.
3. The resulting metal complexes are quite robust in a diverse range of media, ranging from organic to aqueous media and from highly basic to acidic environments.
4. The tunability of porphyrin ligands by introduction of several e^- donating or withdrawing functional groups, proximal trans axial ligands, intramolecular proton relay, accessible redox sites, and sterically bulky hydrophilic or hydrophobic groups.

All these features make metalated porphyrins an excellent choice as an active site of different enzymes. Which in turn makes it also a better choice as a functional and structural model complex to study the working mechanisms of different enzymes and also to design efficient bio-inspired catalysts based on them.

1.4.2 Using Fe Tetraphenylporphyrin complex:

The SO_2 or SO_3^{2-} reduction carried out by the enzymes like Sulfite and Nitrite Reductases are performed in the most efficient and benign ways. To achieve the goal of SO_2 reduction in the most efficient way, it's worth emulating the process in which these enzymes perform these multi-e^- multi-H^+ reduction reactions. However, one problem remains is their mechanistic intricacies. All of these processes, performed by these enzymes have been observed in protein matrices and exact step-by-step mechanism of the reduction reactions are also not clear. What we have are piecemeal information from which we try to collate a mechanistic scheme. So, in order to achieve the goal of SO_2 reduction in an efficient way, it's worth studying the mechanism, using which the enzymes like SiR and NiR carry out the reduction reactions. What better way can there be to study reaction mechanism than using synthetic model complexes? This helps us in tuning certain aspects of the reaction and study the mechanism of the reaction, exclusively from a chemical angle. Fe^{II} Tetraphenylporphyrin ($Fe^{II}TPP$) is capable of binding with NO_2^- and reducing it to NO, emulating the activity of Assimilatory Nitrite Reductase, at least partially.[50] Since $Fe^{II}TPP$ can reduce NO_2^- just like siroheme based NiR which, in turn, can also reduce sulfite, it is possible that $Fe^{II}TPP$ may reduce SO_2 like the siroheme based SiR. However, this has been difficult to achieve. While initial vibrational data indicated the formation of SO_2 adduct of $Fe^{II}TPP$ at 20 K,[51] efforts to isolate the adduct or isolate reduced sulfur products failed despite several attempts to do so[52-

[54] and sulfate/sulfite bound Fe(II) porphyrins were isolated instead in non-protic organic solvents. Thus, even though a heme cofactor reduces SO_2 in nature, reduction of SO_2 by iron porphyrins has not been achieved outside of the protein matrix. $Fe^{II}TPP$ having no second sphere modification provides the basic active site to probe the SO_2 reduction reaction, acting as a functional analogue of the heme active site. So, we have used $Fe^{II}TPP$ to study the reaction mechanism of SO_2 reduction, with the hope of emulating the biological reaction, outside a protein matrix. This also helped us in controlling the reaction conditions, allowing us in gaining critical insights about the reaction mechanism. The porphyrin used have been presented below:

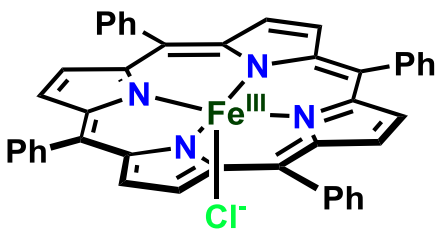

Figure 5. $Fe^{III}TPP$-Cl, the Fe Tetraphenylporphyrin model complex used for SO_2 reduction

1.4.3 Using second sphere modified Fe porphyrin complexes for SO_2 reduction:

A significant number of enzymes in nature are heme containing enzymes, while some other are siroheme containing enzymes. Where iron porphyrin moiety remains in the primary coordination sphere, but the divergence in enzyme functions happen due to their difference in distal environment. Most enzymes differ in the amino acid residues and their orientation, present in their distal environment and that makes a world of difference in their enzymatic activity. Naturally occurring enzymes have evolved to include sophisticated active sites wherein apart from the inner co-ordination spheres of the metals, the non-covalent secondary interactions like hydrophobicity, hydrogen bonding and electrostatics often play a major role in modulating the reactivities of the active sites. These non-covalent interactions are exhibited by the distal amino acid residues in the active site structure of metalloenzyme during small molecule activation that has been well established in literature.[55-56] The distal environment of siroheme containing ASiR and DSiR active site is different in the amino acid residues present around the distal binding site of the siroheme moiety. Due to this difference in distal environment, the products generated from DSiR and ASiR are different. So, it's also prudent to modify the distal environment around porphyrins by using second sphere modified porphyrins and probe the SO_2 reduction reaction using them. Here we have used Fe Pydn porphyrin, which is a second sphere modified porphyrin to perform SO_2 reduction so that we

can understand the role of the distal amino acid residues in tuning SO_2 reduction. The FePydn porphyrin was synthesized by Bhunia et al.[57] The porphyrin used have been presented below

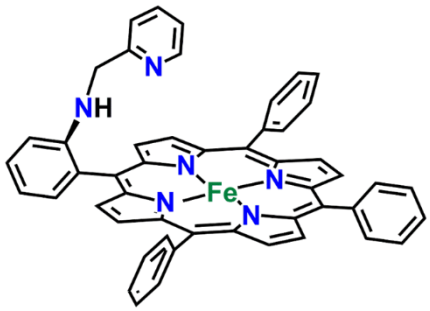

Figure 6. Fe^{II} Pydn, the Fe pyridyl model complex used for SO_2 reduction

1.5 References:

1. Fowler, D.; Brimblecombe, P.; Burrows, J.; Heal, M. R.; Grennfelt, P.; Stevenson, D. S.; Jowett, A.; Nemitz, E.; Coyle, M.; Liu, X.; Chang, Y.; Fuller, G. W.; Sutton, M. A.; Klimont, Z.; Unsworth, M. H.; Vieno, M., A chronology of global air quality. *Philosophical Transactions of the Royal Society A: Mathematical, Physical and Engineering Sciences* **2020,** *378* (2183), 20190314.

2. 15 - Sulfur. In *Chemistry of the Elements (Second Edition)*, Greenwood, N. N.; Earnshaw, A., Eds. Butterworth-Heinemann: Oxford, 1997; pp 645-746.

3. Zhong, Q.; Shen, H.; Yun, X.; Chen, Y.; Ren, Y. a.; Xu, H.; Shen, G.; Du, W.; Meng, J.; Li, W.; Ma, J.; Tao, S., Global Sulfur Dioxide Emissions and the Driving Forces. *Environmental Science & Technology* **2020,** *54* (11), 6508-6517.

4. Qu, Z.; Henze, D. K.; Li, C.; Theys, N.; Wang, Y.; Wang, J.; Wang, W.; Han, J.; Shim, C.; Dickerson, R. R.; Ren, X., SO2 Emission Estimates Using OMI SO2 Retrievals for 2005–2017. *Journal of Geophysical Research: Atmospheres* **2019,** *124* (14), 8336-8359.

5. Huang, Y.; Shen, H.; Chen, H.; Wang, R.; Zhang, Y.; Su, S.; Chen, Y.; Lin, N.; Zhuo, S.; Zhong, Q.; Wang, X.; Liu, J.; Li, B.; Liu, W.; Tao, S., Quantification of Global Primary Emissions of PM2.5, PM10, and TSP from Combustion and Industrial Process Sources. *Environmental Science & Technology* **2014,** *48* (23), 13834-13843.

6. Ward, P. L., Sulfur dioxide initiates global climate change in four ways. *Thin Solid Films* **2009,** *517* (11), 3188-3203.

7. Kato, N.; Akimoto, H., Anthropogenic emissions of SO2 and NOx in Asia: emission inventories. *Atmospheric Environment. Part A. General Topics* **1992,** *26* (16), 2997-3017.

8. McNeill, V. F., Addressing the Global Air Pollution Crisis: Chemistry's Role. *Trends in Chemistry* **2019,** *1* (1), 5-8.

9. Feng, T.; Huo, M.; Zhao, X.; Wang, T.; Xia, X.; Ma, C., Reduction of SO2 to elemental sulfur with H2 and mixed H2/CO gas in an activated carbon bed. *Chemical Engineering Research and Design* **2017,** *121*, 191-199.

10. Han, G. B.; Park, N.-K.; Yoon, S. H.; Lee, T. J.; Han, G. Y., Direct Reduction of Sulfur Dioxide to Elemental Sulfur with Hydrogen over Sn−Zr-Based Catalysts. *Industrial & Engineering Chemistry Research* **2008,** *47* (14), 4658-4664.

11. AlQahtani, M. S.; Knecht, S. D.; Wang, X.; Bilén, S. G.; Song, C., One-Step Low-Temperature Reduction of Sulfur Dioxide to Elemental Sulfur by Plasma-Enhanced Catalysis. *ACS Catalysis* **2020,** *10* (9), 5272-5277.

12. Wei, R.; Chen, X.; Gong, Y., Side-On Sulfur Monoxide Complexes of Tantalum, Niobium, and Vanadium Oxyfluorides. *Inorganic Chemistry* **2019,** *58* (6), 3807-3814.

13. Wayland, B. B.; Mohajer, D., An electron spin resonance study of the interaction of sulphur dioxide with tetraphenylporphyrincobalt(II). *Journal of the Chemical Society, Chemical Communications* **1972,** (13), 776-777.

14. Kline, M. A.; Barley, M. H.; Meyer, T. J., Electrocatalytic reduction of bisulfite to hydrogen sulfide based on a water-soluble iron porphyrin. *Inorganic Chemistry* **1987,** *26* (14), 2196-2197.

15. Chahal, M.; Raje, S.; Kotana, G.; Angamuthu, R., Binding enabled catalytic activation of SO2 by copper koneramine complexes under ambient conditions. *Green Chemistry* **2019,** *21* (23), 6372-6380.

16. Sun, J.; Li, L.; Zhou, G.; Wang, X.; Zhang, L.; Liu, Y.; Yang, J.; Lü, X.; Jiang, F., Biological Sulfur Reduction To Generate H2S As a Reducing Agent To Achieve Simultaneous Catalytic Removal of SO2 and NO and Sulfur Recovery from Flue Gas. *Environmental Science & Technology* **2018,** *52* (8), 4754-4762.

17. Lens, P., Sulfur Cycle. In *Encyclopedia of Microbiology (Third Edition)*, Schaechter, M., Ed. Academic Press: Oxford, 2009; pp 361-369.

18. Brychkova, G.; Yarmolinsky, D.; Ventura, Y.; Sagi, M., A Novel In-Gel Assay and an Improved Kinetic Assay for Determining In Vitro Sulfite Reductase Activity in Plants. *Plant and Cell Physiology* **2012,** *53* (8), 1507-1516.

19. Siegel, L.; Murphy, M.; Kamin, H., Reduced Nicotinamide Adenine Dinucleotide Phosphate-Sulfite Reductase of Enterobacteria. *Journal of Biological Chemistry* **1973,** *248*, 251-264.

20. Grein, F.; Ramos, A. R.; Venceslau, S. S.; Pereira, I. A. C., Unifying concepts in anaerobic respiration: Insights from dissimilatory sulfur metabolism. *Biochimica et Biophysica Acta (BBA) - Bioenergetics* **2013,** *1827* (2), 145-160.

21. Leustek, T.; Martin, M. N.; Bick, J. A.; Davies, J. P., PATHWAYS AND REGULATION OF SULFUR METABOLISM REVEALED THROUGH MOLECULAR AND GENETIC STUDIES. *Annual review of plant physiology and plant molecular biology* **2000,** *51*, 141-165.

22. Kobayashi, K.; Takahashi, E.; Ishimoto, M., Biochemical Studies on Sulfate-reducing Bacteria

XI. Purification and Some Properties of Sulfite Reductase, Desulfoviridin. *The Journal of Biochemistry* **1972,** *72* (4), 879-887.

23. Barton, L. L.; Fauque, G. D., Chapter 2 Biochemistry, Physiology and Biotechnology of Sulfate-Reducing Bacteria. In *Advances in Applied Microbiology*, Academic Press: 2009; Vol. 68, pp 41-98.

24. Hermann, B.; Kern, M.; La Pietra, L.; Simon, J.; Einsle, O., The octahaem MccA is a haem c–copper sulfite reductase. *Nature* **2015,** *520* (7549), 706-709.

25. Crane, B. R.; Siegel, L. M.; Getzoff, E. D., Probing the Catalytic Mechanism of Sulfite Reductase by X-ray Crystallography: Structures of the Escherichia coli Hemoprotein in Complex with Substrates, Inhibitors, Intermediates, and Products. *Biochemistry* **1997,** *36* (40), 12120-12137.

26. Wolfe, B. M.; Lui, S. M.; Cowan, J. A., Desulfoviridin, a multimeric-dissimilatory sulfite reductase from Desulfovibrio vulgaris (Hildenborough) Purification, characterization, kinetics and EPR studies. *European Journal of Biochemistry* **1994,** *223* (1), 79-89.

27. Murphy, M. J.; Siegel, L. M.; Kamin, H.; Rosenthal, D., Reduced Nicotinamide Adenine Dinucleotide Phosphate-Sulfite Reductase of Enterobacteria: II. IDENTIFICATION OF A NEW CLASS OF HEME PROSTHETIC GROUP: AN IRON-TETRAHYDROPORPHYRIN (ISOBACTERIOCHLORIN TYPE) WITH EIGHT CARBOXYLIC ACID GROUPS. *Journal of Biological Chemistry* **1973,** *248* (8), 2801-2814.

28. Murphy, M. J.; Siegel, L. M.; Kamin, H.; DerVartanian, D. V.; Lee, J. P.; LeGall, J.; Peck, H. D., Jr., An iron tetrahydroporphyrin prosthetic group common to both assimilatory and dissimilatory sulfite reductases. *Biochemical and biophysical research communications* **1973,** *54* (1), 82-8.

29. Murphy, M. J.; Siegel, L. M.; Tove, S. R.; Kamin, H., Siroheme: a new prosthetic group participating in six-electron reduction reactions catalyzed by both sulfite and nitrite reductases. *Proc Natl Acad Sci U S A* **1974,** *71* (3), 612-616.

30. Crane, B. R.; Siegel, L. M.; Getzoff, E. D., Sulfite Reductase Structure at 1.6 Å: Evolution and Catalysis for Reduction of Inorganic Anions. *Science* **1995,** *270* (5233), 59-67.

31. Brânzanic, A. M. V.; Ryde, U.; Silaghi-Dumitrescu, R., Why does sulfite reductase employ siroheme? *Chemical Communications* **2019,** *55* (93), 14047-14049.

32. Moura, I.; LeGall, J.; Lino, A. R.; Peck, H. D.; Fauque, G.; Xavier, A. V.; DerVartanian, D. V.; Moura, J. J. G.; Huynh, B. H., Characterization of two dissimilatory sulfite reductases (desulforubidin and desulfoviridin) from the sulfate-reducing bacteria. Moessbauer and EPR studies. *Journal of the American Chemical Society* **1988,** *110* (4), 1075-1082.

33. Han, S. H.; Madden, J. F.; Siegel, L. M.; Spiro, T. G., Resonance Raman studies of Escherichia coli sulfite reductase hemoprotein. 3. Bound ligand vibrational modes. *Biochemistry* **1989,** *28* (13), 5477-85.

34. Kaufman, J.; Spicer, L. D.; Siegel, L. M., Proton NMR of Escherichia coli sulfite reductase: the unligated hemeprotein subunit. *Biochemistry* **1993,** *32* (11), 2853-2867.

35. McRee, D.; Richardson, D.; Richardson, J.; Siegel, L., The heme and Fe4S4 cluster in the crystallographic structure of Escherichia coli sulfite reductase. *Journal of Biological Chemistry* **1986,** *261* (22), 10277-10281.

36. Santos, A. A.; Venceslau, S. S.; Grein, F.; Leavitt, W. D.; Dahl, C.; Johnston, D. T.; Pereira, I. A. C., A protein trisulfide couples dissimilatory sulfate reduction to energy conservation. *Science* **2015,** *350* (6267), 1541-1545.

37. Mirts, E. N.; Petrik, I. D.; Hosseinzadeh, P.; Nilges, M. J.; Lu, Y., A designed heme-[4Fe-4S] metalloenzyme catalyzes sulfite reduction like the native enzyme. *Science* **2018,** *361* (6407), 1098-1101.

38. Silaghi-Dumitrescu, R.; Makarov, S. V., Siroheme-containing sulfite reductase: A density functional investigation of the mechanism. *International Journal of Quantum Chemistry* **2012,** *112* (3), 900-908.

39. Parey, K.; Warkentin, E.; Kroneck, P. M. H.; Ermler, U., Reaction Cycle of the Dissimilatory Sulfite Reductase from Archaeoglobus fulgidus. *Biochemistry* **2010,** *49* (41), 8912-8921.

40. Smith, K. W.; Stroupe, M. E., Mutational Analysis of Sulfite Reductase Hemoprotein Reveals the Mechanism for Coordinated Electron and Proton Transfer. *Biochemistry* **2012,** *51* (49), 9857-9868.

41. Enemark, J. H.; Feltham, R. D., Principles of structure, bonding, and reactivity for metal nitrosyl complexes. *Coordination Chemistry Reviews* **1974,** *13* (4), 339-406.

42. Maia, L. B.; Moura, J. J. G., How Biology Handles Nitrite. *Chemical Reviews* **2014,** *114* (10), 5273-5357.

43. Daniel-Vedele, F.; Dorbe, M.-F.; Godon, C.; Truong, H.-N.; Caboche, M. In *Molecular Genetics of Nitrate Assimilation in Solanaceous Species*, Plant Molecular Biology, Berlin, Heidelberg, 1994//; Coruzzi, G.; Puigdomènech, P., Eds. Springer Berlin Heidelberg: Berlin, Heidelberg, 1994; pp 129-139.

44. Lukat, P.; Rudolf, M.; Stach, P.; Messerschmidt, A.; Kroneck, P. M. H.; Simon, J.; Einsle, O., Binding and Reduction of Sulfite by Cytochrome c Nitrite Reductase. *Biochemistry* **2008,** *47* (7), 2080-2086.

45. Fontecave, M.; Artero, V., Bioinspired catalysis at the crossroads between biology and chemistry: A remarkable example of an electrocatalytic material mimicking hydrogenases. *Comptes Rendus Chimie* **2011,** *14* (4), 362-371.

46. Collman, J. P.; Boulatov, R.; Sunderland, C. J.; Fu, L., Functional Analogues of Cytochrome c Oxidase, Myoglobin, and Hemoglobin. *Chemical Reviews* **2004,** *104* (2), 561-588.

47. Collman, J. P.; Yang, Y.; Dey, A.; Decréau, R. A.; Ghosh, S.; Ohta, T.; Solomon, E. I., A functional nitric oxide reductase model. *Proceedings of the National Academy of Sciences* **2008,** *105* (41), 15660-15665.

48. Collman, J. P.; Dey, A.; Yang, Y.; Ghosh, S.; Decréau, R. A., O2 reduction by a functional heme/nonheme bis-iron NOR model complex. *Proceedings of the National Academy of Sciences* **2009,** *106* (26), 10528-10533.

49. Campbell, W. H., NITRATE REDUCTASE STRUCTURE, FUNCTION AND REGULATION: Bridging the Gap between Biochemistry and Physiology. *Annual review of plant physiology and plant molecular biology* **1999,** *50* (1), 277-303.

50. Finnegan, M. G.; Lappin, A.; Scheidt, W. R., Instability of the nitrite/iron (III) porphyrinate system. *Inorganic Chemistry* **1990,** *29* (2), 181-185.

51. Kuroi, T.; Nakamoto, K., Matrix-isolation infrared spectra of oxy(tetraphenylporphyrinato)iron(II) containing CS2 and SO2 as axial ligands. *Journal of Molecular Structure* **1986,** *146*, 111-121.

52. Reynolds, M. S.; Holm, R. H., Binding of oxysulfur anions to macrocyclic iron(II,III): [(Fe(TPP))2SO4] and Fe(Me6[14]-4,11-dieneN4)(S2O5)]. *Inorganica Chimica Acta* **1989,** *155* (1), 113-123.

53. Cocolios, P.; Lagrange, G.; Guilard, R.; Oumous, H.; Lecomte, C., Alkane (or arene)-sulphinato and -sulphonato-iron(III) porphyrins: synthesis and physicochemical properties; crystal structure of benzenesulphinato(5,10,15,20-tetraphenylporphyrinato)iron(III). *Journal of the Chemical Society, Dalton Transactions* **1984,** (4), 567-574.

54. Scheidt, W. R.; Lee, Y. J.; Finnegan, M. G., Reactions of sulfur dioxide with iron porphyrinates and the crystal structure of (hydrogen sulfato)(tetraphenylporphinato)iron(III) hemibenzene solvate. *Inorganic Chemistry* **1988,** *27* (26), 4725-4730.

55. Simon, J.; Kroneck, P. M. H., Chapter Two - Microbial Sulfite Respiration. In *Advances in Microbial Physiology*, Poole, R. K., Ed. Academic Press: 2013; Vol. 62, pp 45-117.

56. Poulos, T. L., Heme Enzyme Structure and Function. *Chemical Reviews* **2014,** *114* (7), 3919-3962.

57. Bhunia, S.; Rana, A.; Roy, P.; Martin, D. J.; Pegis, M. L.; Roy, B.; Dey, A., Rational Design of Mononuclear Iron Porphyrins for Facile and Selective 4e–/4H+ O2 Reduction: Activation of O–O Bond by 2nd Sphere Hydrogen Bonding. *Journal of the American Chemical Society* **2018,** *140* (30), 9444-9457.

Chapter 2

Experimental details: Instrumentation and Methods

2.1. Instrumental details:

Absorption spectra were obtained by a UV-Vis diode array spectrophotometer (Agilent 8453). EPR experiments were performed at 77 K in a liquid nitrogen finger Dewar. EPR spectra were obtained by a JEOL FA200 spectrophotometer with the following parameters- modulation width: 10 Gauss; amplitude: 20; time constant: 300 ms; power: 2 mW; frequency: 9.25 GHz. The EPR data was simulated using JEOL Anisotropic Simulation software. For GC-MS an Agilent 7890B GC system with a 5977A MS detector was used. Mössbauer spectra were recorded using an alternating constant WissEl Mössbauer spectrometer, consisting of an MR 360 drive unit, an MVT 1000 velocity transducer, and an LND45431 proportional counter mounted on an MB-600 Mössbauer bench with cryostat stand. The system was operated in a horizontal transmission geometry with source (^{57}Co in Rh-matrix), absorber and detector in a linear arrangement. The temperature was controlled and maintained using MBBC-N20106 Mössbauer cryostat for liquid nitrogen connected with Lake Shore-325 temperature controller unit. Measurements were performed at 95K. Data acquisition was performed using a 512-channel analyzer. Isomer shifts were referenced versus α-iron metal foil at the same temperature. The simulation of experimental data was performed using the Normos-A Mössbauer Fit programmes Site and Dist. Resonance Raman (rR) data were collected using 413.1 nm excitation from a Kr^+ ion source (Sabre Coherent Inc.) and a Trivista 555 triple spectrophotometer (gratings used in the three stages were 900, 900, and 2400 grooves/mm) fit with an electronically cooled Pixis CCD camera (Princeton Instruments). The irradiation power kept at the sample is 8-10 mW, so that photodegradation does not take place. All the data were collected at 77 K in a liquid N_2 cooled finger Dewar after preparing the reaction mixtures at their respective reaction temperature and freezing them after a stipulated time. The FT-IR data were measured on a Perkin Elmer spectrophotometer (Frontier) instrument. The CaF_2 windows for FTIR spectroscopy were purchased from Sigma-Aldrich. Data were collected by dropcasting the sample over CaF_2 window and taking dry hexane/air background in $LiTaO_3$ mode at room temperature.

2.2. Materials:

All the reagents used were of the best commercially available quality. H_2SO_4 (98%, Merck), Na_2SO_3 (anhydrous, Merck), Silica (Merck), Na_2SO4 (Merck), all were bought from respective vendors and used without further purification. Benzaldehyde (Spectrochem), Pyrrole (Spectrochem), Glacial Acetic acid (Spectrochem), Na_2S (Spectrochem) were bought from respective vendors. 2,4,6-Trimethylpyridine (Sigma-Aldrich), Ferrous Bromide (anhydrous, Sigma-Aldrich), HCl (37%, Merck), were used for Fe^{III}TPP synthesis. $^{57}FeCl_2$ was provided by

Prof. Nicolai Lehnart's group (University of Michigan). Tetrahydrofuran, Methanol, Hexane were sourced from Finar Chemicals and used only after subjecting them to adequate drying and distilling procedures. Dry and pure SO_2 gas was passed through a solution of conc. H_2SO_4 to remove any moisture and tested using GC-MS prior to use (Figure S1). The solubility of SO_2 in THF (after 20 mins purging) is assumed to be 0.3-0.5 M as is the case for commercial sources of the same (https://www.sigmaaldrich.com/catalog/product/aldrich/901592). All solvents used were dried and degassed before use.

2.3. Methods:

All the methods of synthesis, sample preparations have been mentioned at the beginning of each chapter, in the Experimental section.

Chapter 3

Reduction of Sulfur Dioxide to Sulfur Monoxide by Ferrous Porphyrin

3.1 Introduction

SO_2 is a harmful gas-phase air pollutant and exposure to which beyond a permissible limit can have detrimental effect on respiratory and cardiovascular health.[1] The problem of SO_2 pollution is further compounded by its atmospheric oxidation to Sulfphates leading to acid rain and particulate matter ($PM_{2.5}$) generation, leading to 4.2 million premature death.[2] Due to anthropogenic activities, around > 100 Tg y^{-1} of SO_2 is emitted globally.[3] The baton of SO_2 emission has gradually passed on from developed countries to developing countries, due to their growing economic activities. In this case India is leading the charge owing to its growing electricity demands and lack of emission controls.[4] Fixation of SO_2 by reducing it to sulfur or sulfides is an attractive approach to eliminate this pollutant and generate valuable stock chemicals. SO_2 fixation by its reduction to its lower valent forms like Sulfur or Sulfides might be an attractive approach to fight the pollution and generate valuable stock chemicals, but most of these approaches require H_2/CO, high temperature and supported metal oxide heterogeneous catalysts.[5-7] To achieve the goal of SO_2 reduction, many potential candidates for its reduction were synthesized. There is precedence of transition metal complexes bound to SO_2/SO indicative of the reactivity of the transition metals with SO_2 and SO.[8-12]But examples of SO_2 reduction are few and far between and they need to be explored to find newer methods of SO_2 mitigation.[13]Sulfur is naturally handled in an entirely different way, where a plethora of microbial organisms recruit enzymes to interconvert Sulfur to its different oxidation states, maintaining the biogeochemical cycle of Sulfur. The enzyme responsible for Sulfur metabolism is Sulfite Reductase (SiR), which catalyzes the $6e^-/6H^+$ reduction of SO_3^{2-} to S^{2-}.[14]

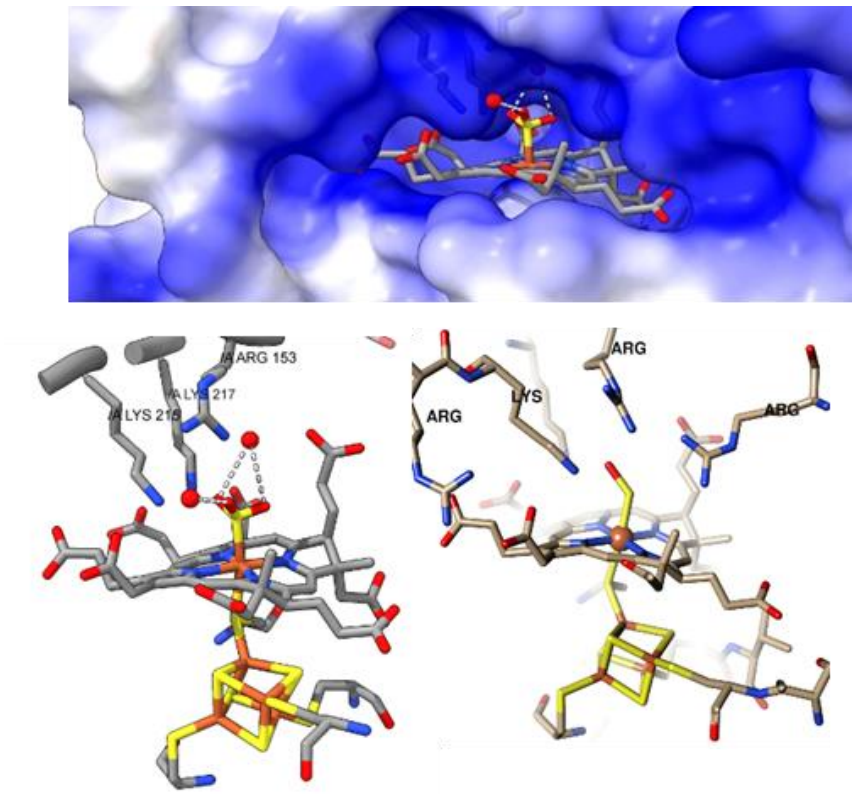

Figure 3.1 (top) Active site of SiR on the surface of the protein (pdb id: 2GEP[15]); (bottom left) active site of sulfite reductase bound to SO_3^{2-}; and (bottom right) structure of the partially reduced SO_x species observed crystallographically (pdb id: 7GEP[15]). Color code: Fe → orange, S → yellow, P → light orange, O → red, N → blue and C → grey. The distal pendant residues are labelled

The active site of SiR enzyme contains a siroheme-Fe/S center (Figure 1) composed of a reduced porphyrin ring of isobacteriochlorin class bridged to a [4Fe-4S] cubane cluster via a Cysteine thiolate linkage.[16] The siroheme active site sits on the surface of the protein and in a positively charged cavity containing several lysine and arginine residues (Figure 1, top). The siroheme active site resides on the protein surface, inside a positively charged cavity surrounded by lysine and arginine catalytic residues (Figure 1, top). These catalytic residues help to stabilize substrate binding to the metal centre and the intermediates generated in due course of the reduction reaction via H-bonding and also by providing the protons required for the reduction of SO_3^{2-} to S^{2-} (Figure 1, bottom left). A series of iron-sulfur clusters provide the $6e^-$ needed for this reaction which funnels through the proximal Fe_4S_4 cluster that bridge with the siroheme cofactor (Figure 1). The $6e^-$ required for the reduction reaction is supplied by a series of iron-sulfur clusters, which direct them through the proximal Fe_4S_4 cluster that is covalently linked with the siroheme cofactor (Figure 1). The reduction of SO_3^{2-} by the reduced siroheme active site of SiR has been studied extensively employing spectroscopic and theoretical techniques, helping in unearthing a lot of information about the reaction

mechanism.[17-21] The proposed mechanism of action for this overall $6H^+/6e^-$ reduction of sulfite to sulfide by SiR is debatable. Using the X-ray structures of SO_3^{2-} bound active site and structures of other small molecules and anions bound SiR (e.g. NO_2^-, NO, CO, CN^-), involvement of three consecutive $2H^+/2e^-$ reduction steps which are all accompanied by water elimination (Figure 2) was proposed.[15, 22, 23]

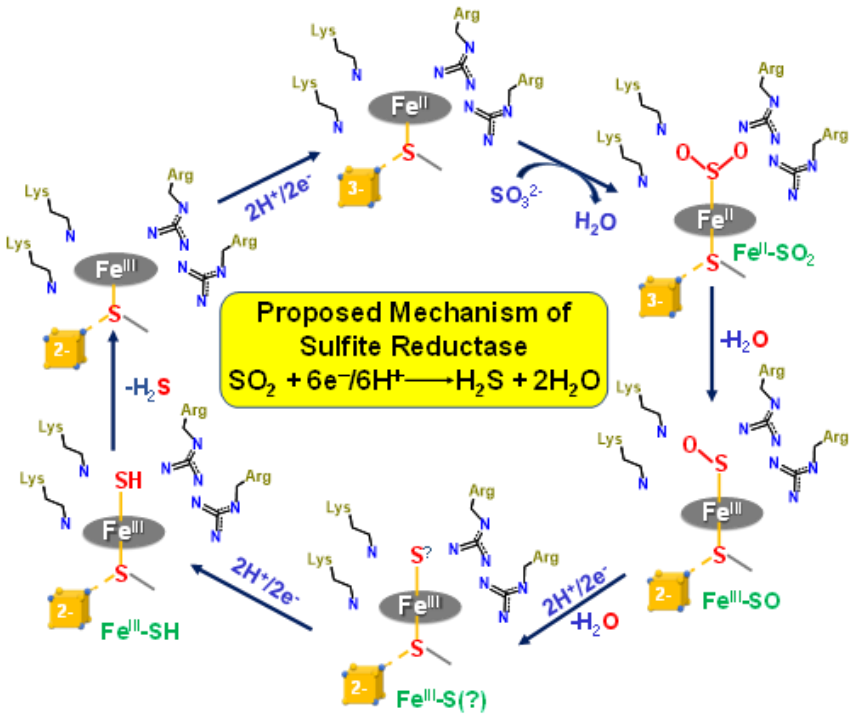

Figure 3.2 Proposed mechanism of SO_2 reduction by the sulfite reductase. The grey ring represents the heme and the yellow cube represents the Fe_4S_4 cluster – blue and yellow spheres represent iron and sulfide centers, respectively. The pendant lysine and arginine are indicated. In this proposedmechanism, the reaction proceeds via three $2e^-/2H^+$ steps.

The binding of SO_2 to the open coordination site (post water elimination from SO_3^{2-}) of siroheme is followed by its $2e^-$ reductions and water elimination, which leads to generation of an unusual sulfur monoxide (SO) bound $[Fe^{III}\text{-}SO]^+$ species (Figure 1, bottom right and Figure 2) where Sulfur has a formal oxidation state of +2 after $2e^-$ reduction from SO_2. Two subsequent $2e^-/2H^+$ reductions and water eliminations yield the final H_2S product of this $6e^-/6H^+$ reduction of SO_2. Alternatively, Stroupe and co-workers used site-directed mutants of the distal Arg and Lys residues to argue for six sequential $1H^+/1e^-$ steps instead.[24] Nonetheless, both mechanisms entail the formation of several unusual siroheme bound SO_x species that have not been observed outside the protein matrix in heme systems. The electron density was fitted to a bent $[Fe^{III}\text{-}SO]^+$ species with a Fe-S distance of 2.2 Å and a S-O distance of 1.6 Å.[15] The nature of this $[Fe^{III}\text{-}SO]^+$ species has not yet been understood as it is yet to be actualized

in synthetic systems. The active site of Nitrite Reductase also contains a Siroheme moiety covalently linked to Fe_4S_4 cluster via a cysteine thiolate linkage. The active site of Nitrite Reductase is responsible for another $6e^-/6H^+$ reduction reaction, the reduction of NO_3^- to NH_4^+.[16, 25]There are precedence of NO_2^- reduction by Fe^{II} tetraphenylporphyrin ($Fe^{II}TPP$), which function as model complexes of siroheme based Nitrite reductase, which in turn can also reduce SO_3^{2-}.[26] Hence it might be possible for $Fe^{II}TPP$ to reduce SO_2 just like siroheme based NiR.[27]But there was a lot of difficulty in achieving this goal. Vibrational data of matrix cocondensation reaction products of $Fe^{II}TPP$ with SO_2 gave indication of formation of SO_2 adducts of $Fe^{II}TPP$ at 20K[28], but their isolation despite several attempts, were an exercise in futility.[29, 30]Heme cofactors naturally reduce SO_2 but its reduction outside the protein matrix has not been achieved yet, in synthetic model complexes.

In this work we have investigated the reaction of SO_2 with $Fe^{II}TPP$ in organic solvent.The reaction indicates that SO_2 is reduced by $Fe^{II}TPP$ by a $2e^-$ reduction reaction into Sulfur Monoxide (SO) via a $[Fe^{III}\text{-}SO]^+$ intermediate.This mimics the first step in the catalytic cycle of SiR.

3.2 Experimental Section:

3.2.1 Materials:

All the reagents used were of the best commercially available quality. H_2SO_4 (98%, Merck), Na_2SO_3 (anhydrous, Merck), Silica (Merck), Na_2SO4 (Merck), all were bought from respective vendors and used without further purification. Benzaldehyde (Spectrochem), Pyrrole (Spectrochem), Glacial Acetic acid (Spectrochem), Na_2S (Spectrochem) were bought from respective vendors. 2,4,6-Trimethylpyridine (Sigma-Aldrich), Ferrous Bromide (anhydrous, Sigma-Aldrich), HCl (37%, Merck), were used for $Fe^{III}TPP$ synthesis. $^{57}FeCl_2$ was provided by Prof. Nicolai Lehnart's group (University of Michigan). Tetrahydrofuran, Methanol, Hexane were sourced from Finar Chemicals and used only after subjecting them to adequate drying and distilling procedures. Dry and pure SO_2 gas was passed through a solution of conc. H_2SO_4 to remove any moisture and tested using GC-MS prior to use (Figure S1). The solubility of SO_2 in THF (after 20 mins purging) is assumed to be 0.3-0.5 M as is the case for commercial sources of the same (https://www.sigmaaldrich.com/catalog/product/aldrich/901592). All solvents used were dried and degassed before use. Absorption spectra were obtained by a UV-Vis diode array spectrophotometer (Agilent 8453). EPR experiments were performed at 77 K in a liquid nitrogen finger Dewar. EPR spectra were obtained by a JEOL FA200 spectrophotometer with the following parameters- modulation width: 10 gauss; amplitude: 20; time constant: 300 ms; power: 2 mW; frequency: 9.25 GHz. The EPR data was simulated

using JEOL Anisotropic Simulation software. For GC-MS an Agilent 7890B GC system with a 5977A MS detector was used. Mössbauer spectra were recorded using an alternating constant WissEl Mössbauer spectrometer, consisting of an MR 360 drive unit, an MVT 1000 velocity transducer, and an LND45431 proportional counter mounted on an MB-600 Mössbauer bench with cryostat stand. The system was operated in a horizontal transmission geometry with source (^{57}Co in Rh-matrix), absorber and detector in a linear arrangement. The temperature was controlled and maintained using MBBC-N20106 Mössbauer cryostat for liquid nitrogen connected with Lake Shore-325 temperature controller unit. Measurements were performed at 95K. Data acquisition was performed using a 512-channel analyzer. Isomer shifts were referenced versus α-iron metal foil at the same temperature. The simulation of experimental data was performed using the Normos-A Mössbauer Fit programmes Site and Dist. Resonance Raman (rR) data were collected using 413.1 nm excitation from a Kr^+ ion source (Sabre Coherent Inc.) and a Trivista 555 triple spectrophotometer (gratings used in the three stages were 900, 900, and 2400 grooves/mm) fit with an electronically cooled Pixis CCD camera (Princeton Instruments). The irradiation power kept at the sample is 8-10 mW, so that photodegradation does not take place. All the data were collected at 77 K in a liquid N_2 cooled finger Dewar after preparing the reaction mixtures at their respective reaction temperature and freezing them after a stipulated time. The FT-IR data were measured on a Perkin Elmer spectrophotometer (Frontier) instrument. The CaF_2 windows for FTIR spectroscopy were purchased from Sigma-Aldrich. Data were collected by dropcasting the sample over CaF_2 window and taking dry hexane/air background in $LiTaO_3$ mode at room temperature.

3.2.2 Methods:

3.2.2 a) Synthesis:

Synthesis of Tetraphenylporphyrin (TPP):

Freshly distilled pyrrole (56 ml, 0.8 mol) and 80 ml (0.8 mol) of reagent grade benzaldehyde are added to 3 lit. of refluxing reagent grade propionic acid. (Note: crystalline material is not direct,ly obtained if acetic acid is used.) After refluxing for 30 min, the solution is cooled to room temperature and filtered, and the filter cake is washed thoroughly with methanol. After a hot water wash, the resulting purple crystals are air dried, and finally dried in vacuo to remove adsorbed acid to yield 25 g (20%, yield) of TPP. Spectrophotometric analysis shows that only 1% of the TPP yield remains in the filtrate and also that the filtered material is about 3% tetraphenylchlorin (TPC) by weight. This method was developed by Adler *et al.*[31]

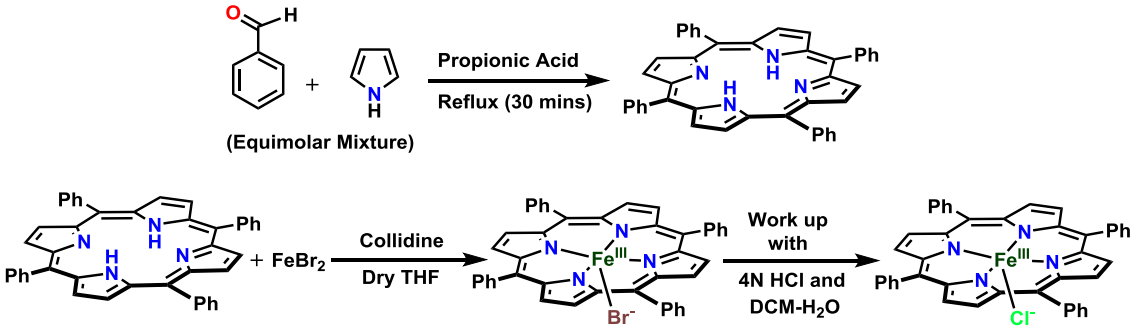

Scheme 3.1 Synthesis of TPP and Fe^{III}TPP by the reported procedure of Adler *et al*[31]

Synthesis of Fe^{III}TPP:

The synthesized 100mg, 0.162 mmol TPP was dissolved in dry degassed THF solvent inside a glove box and then stirred with 98.6 mg, 0.810 mmol 2,4,6-trimethyl pyridine (Collidine) for 30 minutes for the purpose of deprotonation of the pyrrolic protons. Then 350 mg, 1.62 mmol $FeBr_2$ metallic salt was added into the solution and left under stirring condition and the reaction was followed by TLC until disappearance of the TPP spot and appearance of a new spot. The reaction mixture was taken out of the glove box, the THF was removed from the reaction mixture *in vacuo* and the reaction was worked up with DCM and water after treating with 4N HCl to remove excess $FeBr_2$.The organic layer was dried with Na_2SO_4 and evaporated through a rotary evaporator. The solid compund was purified by column chromatography using 5:95 MeOH-DCM solution to afford the Fe^{III}TPP-Cl (HCl being the source of Cl^- in the resulting compound) (Scheme 1).

3.2.2 b) Sample preparation for UV-Vis Spectroscopy:

Synthesized Fe^{III}TPP was dissolved in THF to prepare 1 mM solution. It was subjected to reduction using a 0.5 eq. (20 mM stock solution) of Na_2S dissolved in dry degassed methanol.[32] The reduction was monitored using UV-Vis spectroscopy. Pure and dry SO_2 gas was bubbled in dry degassed THF to prepare a saturated solution of SO_2 in THF. 10-80 µL of SO_2 saturated THF (0.3-0.5 M) was added to the ferrous porphyrin and the absorption was recorded. For the kinetic runs, data at 0.5 s intervals were recorded.

3.2.2 c) Sulfur Monoxide Transfer:

A solution of Fe^{II}TPP (712 mg, 1011 mmol) prepared in THF, was bubbled with dry and pure SO_2 gas for a minute at 193K. The reaction mixture was then transferred to a reaction vessel containing degassed 2,3-Dimethyl-1,3-butadiene (~2 ml, 10110 mmol, 10-fold excess), the addition was done at 273K and the reaction was allowed to continue for 72 hours under

nitrogen atmosphere. Aliquot from reaction mixture was taken out and they were drop cast on CaF_2 window and their IR was recorded to identify the products. For the purpose of GC-MS, solvent was removed from reaction mixture by rotary evaporator and DMB-SO & DMB-SO_2 adducts were separated out from reaction mixtures by column chromatography, using Hexane as eluent. The eluted adducts were subjected to GC-MS for product identification. A control reaction was also set up in absence of $Fe^{II}TPP$ and the procedures were followed to record GC-MS and IR spectroscopy for product identification.

3.2.2 d) Sample preparation for Mössbauer spectroscopy:

Sample preparation for Mössbauer spectroscopy: ^{57}Fe enriched $Fe^{III}TPP$ was synthesized using the same protocol as described in SI (Scheme S1 & Synthesis of $Fe^{III}TPP$-Cl) using $^{57}FeCl_2$. A 300 µL, 10mM solution of $Fe^{III}TPP$-Cl was prepared in dry degassed THF inside the glovebox, which was then reduced to $Fe^{II}TPP$ using 0.5eq Na_2S dissolved in dry degassed MeOH. The $Fe^{II}TPP$ produced was separated into two 150 µL solutions in two different sealed anaerobic vials and they were injected with 150 µL saturated solution of dry and pure SO_2 gas in THF at 233K and at RT respectively to afford 300 µL solutions of 5 mM concentration reaction mixture each. Maintaining the reactions at their respective temperatures, they were allowed to proceed for 10 minutes and then, 150 µL of the reaction mixtures were separately transferred to custom-made Nylon capsules and frozen with liquid N_2, and attached to the sample holder (immersed into liquid N_2) using a screw joint, and inserted into the cryostat (maintained at 95 K for data collection). To record Mössbauer data of $Fe^{II}TPP$+$Fe^{III}TPP$-Cl samples, 5mM, 200 µL solution of ^{57}Fe rich $Fe^{III}TPP$-Cl was prepared in dry degassed THF inside the glovebox. It was half-reduced using 0.25 eq Na_2S dissolved in dry degassed MeOH, so that the sample consists of equal amount of $Fe^{II}TPP$ and $Fe^{III}TPP$-Cl. Then 150 µL of the sample was taken in custom-made Nylon capsule and frozen in liquid N_2 inside the glovebox. The remaining procedures were same for data collection.

3.2.2 e) Sample Preparation for EPR and Raman Spectroscopy:

$Fe^{III}TPP$ was reduced to $Fe^{II}TPP$ inside the glovebox using 0.5eq. Na_2S dissolved in dry degassed MeOH. In EPR Tubes, 20 µL, 5 mM solution of $Fe^{II}TPP$ were taken and maintained at different temperatures like 233K, RT. Then they were injected with an 80 µL saturated solution of dry and pure SO_2 gas in THF to afford a 100 µL solution of 1 mM concentration reaction mixture. The reaction mixtures were allowed to progress for required time before freezing them in liq. N_2 for EPR analysis and resonance Raman analysis.

3.2.2 f) DFT Calculations:

The density functional calculations are performed using Gaussian 03 software package. Geometry optimisation was done with the B3lyp functional with an unrestricted formalism. For MeOH bound SO complex a mixed basis set with 6-311g* on Fe and 6-31g* on C, H, N, S, O have been used for optimization and frequency calculations.[33] Tight SCF convergence and the 6-311+g* basis set has been used on all the atoms for a single point energy calculation using the PCM model and convergence criterion of 10^{-10} Hartree.[34] Mulliken orbital populations are calculated using QMForge, and molecular orbital contours are generated using Gaussview software. The ground state wave function of Fe^{III}-LS-SO complexes have been calculated using the contribution of Fe and S, O in the unoccupied molecular orbitals. Mössbauer parameter ΔEq is calculated using PROP=EFG keyword in the optimised geometry of Fe^{III}-LS-SO with 6-311+g* all basis set. Isomer shift values are calculated using the software developed by Emile Bominaar.

3.3 Results and Discussion:

3.3.1 UV-Visible studies:

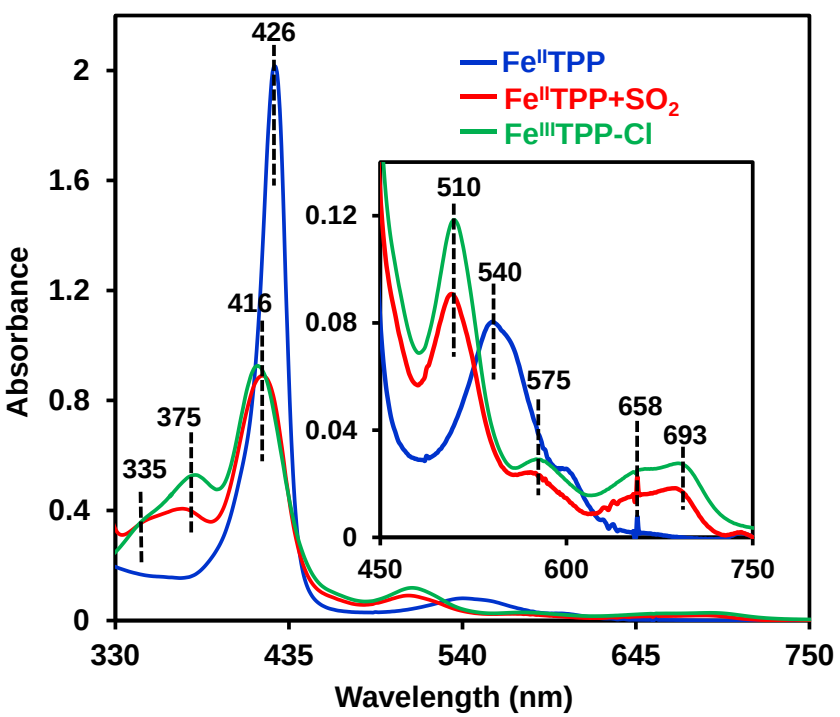

Figure 3.3 Absorption data of the Fe^{II}TPP (blue), the resulting species of the RT reaction Fe^{II}TPP+SO_2 (red) and Fe^{III}TPP-Cl (green), showing the Soret bands. Inset: Q-band region of the given spectra

Upon injecting $Fe^{II}TPP$ (10 μM solution) with saturated solution of SO_2 in THF solvent (800 mM) at room temperature (RT), there occurs a distinct change in UV features. The characteristic Soret and Q-band of $Fe^{II}TPP$ at 426 nm and 540 nm respectively (Figure 3, blue) shifts to 416 nm and 510 nm (Figure 3, red), which are characteristic of $Fe^{III}TPP$. Upon comparing the $Fe^{II}TPP+SO_2$ (Figure 3, red) spectra with reference $Fe^{III}TPP$-Cl spectra (Figure 3, green), we find that their characteristic match. This means, upon SO_2 injection there has been an oxidation of the $Fe^{II}TPP$ to $Fe^{III}TPP$-Cl.

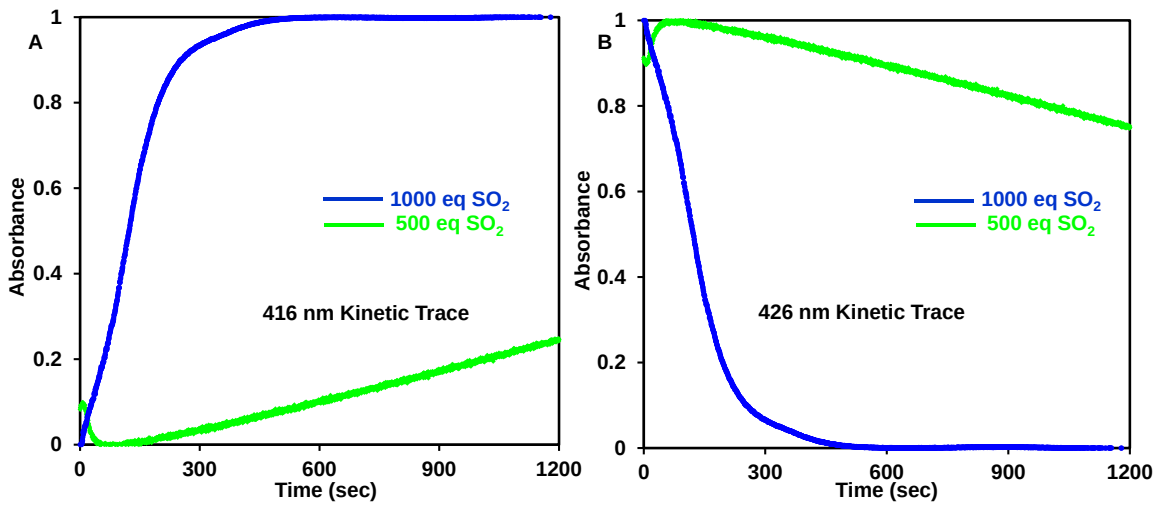

Figure 3.4 Overlay of kinetics data of 417 nm and 426 nm trace after addition of 500 eq (A) and 1000 eq (B) SO_2-THF in $Fe^{II}TPP$

The kinetics of the above reaction was followed by taking time traces of 416 nm and 426 nm bands at two different SO_2 concentrations, keeping the concentration of the $Fe^{II}TPP$ constant (Figure 4 A&B). This indicates that there is an SO_2 concentration dependance in the above reaction.

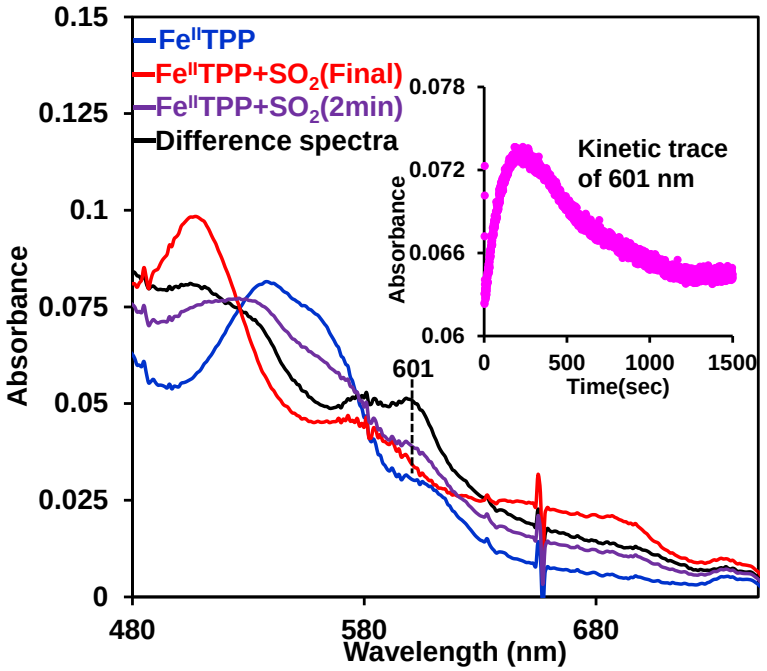

Figure 3.5 UV absorption spectrum of reactant Fe^{II}TPP (blue), the final spectrum of the RT reaction Fe^{II}TPP+SO$_2$ (red) and spectrum recorded for the RT reaction Fe^{II}TPP+SO$_2$ at 2min (violet) where the new absorption feature at 601 nm corresponding to the intermediate is observed. The spectrum of the intermediate (black) can be obtained by subtracting the red spectrum and blue spectrum from the violet spectrum. Inset: kinetic trace of 601 nm after addition of 1000 eq SO$_2$-THF (pink).

To probe for the involvement of any intermediate associated in the reaction of Fe^{II}TPP with SO$_2$, we studied the reaction at lower concentrations of SO$_2$. The reaction of Fe^{II}TPP with SO$_2$ at RT was studied employing UV-Vis spectroscopy keeping the SO$_2$ concentrations relatively lower. The UV-Kinetics revealed generation of a new peak at 601 nm (Figure 5, violet) which was absent in both starting spectra of Fe^{II}TPP (Figure 5, blue) and final spectra of Fe^{II}TPP+SO$_2$ (Figure 5, red). Subtracting the components of starting Fe^{II}TPP and final spectra of Fe^{II}TPP+SO$_2$ spectra from the spectra of Fe^{II}TPP+SO$_2$ at 2 min, revealed the peak at 601 nm prominently. The time trace of the 601 nm peak (Figure 5, inset, pink) informed that the species corresponding to the 601 nm peak maximizes at 200 sec and decays thereafter. This indicated that there might be an involvement of an intermediate in the reaction of Fe^{II}TPP+SO$_2$. The isolation of intermediate under these conditions is inherently difficult and that encouraged us to probe the reaction utilizing other spectroscopic techniques and different temperature conditions.

3.3.2 EPR Spectroscopic studies:

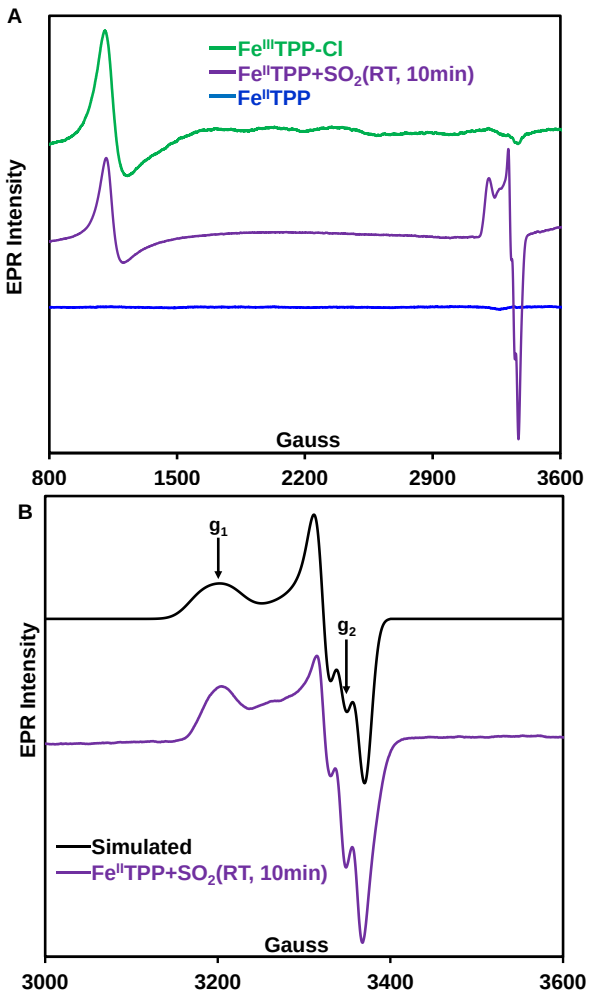

Figure 3.6 (A) EPR spectra of frozen samples of Fe^{III}TPP-Cl (green), Fe^{II}TPP (blue) and the Room Temperature reaction mixture of $Fe^{II}TPP+SO_2$ frozen after 10 minutes (violet). X-band EPR data were recorded at 77K. (B) Comparison of experimental data of the Room Temperature reaction mixture $Fe^{II}TPP+SO_2$ (violet) and simulated data (black).

The $Fe^{II}TPP+SO_2$ reaction was probed using EPR spectroscopy. Allowing the said reaction to proceed for 10 minutes at RT and then freezing it in liq. N_2, its X-band EPR was recorded at 77K. The EPR spectra of the reaction mixture showed two new species when SO_2 was added to the EPR silent Fe^{II}TPP (Figure 6A, blue) reactant. First, a signal at g=5.96 which is characteristic of a high spin Fe^{III} species is observed (Figure 6A, green). Additionally, another signal having g_1 and g_2 values of 2.06 and 1.98 are observed which indicate the formation of a low-spin S=1/2 Fe^{III} species (Figure 6A, violet) as well. The EPR data was simulated as an S=1/2 system and it was observed that the theoretical and experimental spectra match (Figure 6B), confirming that the species obtained is an S=1/2 species. The S=1/2 EPR species has a nature much different than other low spin ferric species, which usually have very narrow g-

values. The S=1/2 species obtained here is very similar to EPR signals of exchange coupled S=1/2 ferrous nitrosyl adducts of heme and non-heme $[FeNO]^7$ species.[35-38] Analogously, this signal can originate from a $[Fe^{III}\text{-}SO]^+$ or a $[FeSO]^7$ species produced from a $2e^-$ reduction of SO_2 akin to the first reduction step in SiR (Figure 1&2). Although there are no precedence for EPR of metal bound SO complexes, SO has a triplet ground state like O_2[39] and an anti-ferromagnetic coupling of a S=1/2 Fe^{III} with an S=1 SO is expected to result in a S=1/2 ground state with an EPR signal like those reported for $[FeNO]^7$ species, which are described as S=1/2 Fe^{III} center anti-ferromagnetically coupled to an S=1 NO.[37, 40, 41] Note that, these signals are very different from a free SO_2^- radical, which has a typical sharp signal with g values ranging between 2.008-2.005.[42, 43]

3.3.3 Mössbauer Spectroscopic studies:

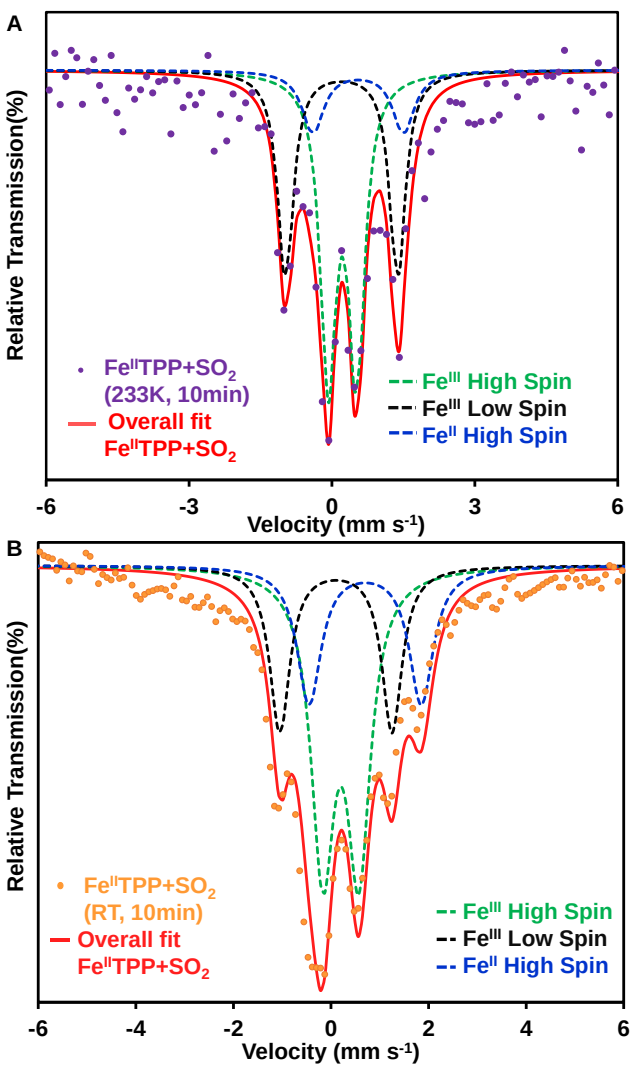

Figure 3.7 (A) Mössbauer spectra of reaction mixture frozen after 10 minutes for the reaction $^{57}Fe^{II}TPP+SO_2$, done at 233K (violet points) along with the data fits (red). (B) Mössbauer spectra of

reaction mixture frozen after 10 minutes for the same reaction done at room temperature (orange points) along with their data fits (red). The relative population of high spin Fe^{III} (green), low spin Fe^{III} (black) and high spin Fe^{II} (blue) species for the reaction done at 233K are 52%, 46% and 2%, respectively. Mössbauer data was recorded at 95K, zero field.

In order to gain more insights about the incipient intermediate in the reaction, the reaction was probed at lower temperatures using Mössbauer spectroscopy so that we could gain insight about its oxidation state and spin state. The $Fe^{II}TPP+SO_2$ reaction was allowed to proceed for 10 minutes under two different temperatures, 233K and RT. The reason for probing the reaction at lower temperature was to slow down the reaction so that the intermediate could be observed properly. After 10 minutes, the reaction mixtures were frozen and their Mössbauer spectra were recorded at 95K, under zero field. The RT and 233K reaction mixtures, both show 3 different components varying in their relative populations. The 233K reaction mixture (Figure 6A, violet) show species having δ_{iso} = 0.22 mm/s and ΔE_q = 0.60 mm/s with 52% population (Figure 6A, green), another species having δ_{iso} = 0.20 mm/s and ΔE_q = 2.35 mm/s with 46% population (Figure 6A, black) and a minor species having δ_{iso} = 0.55 mm/s and ΔE_q = 1.90 mm/s with ~2% population (Figure 6A, blue). From the observed δ_{iso} and ΔE_q values it can be said that the reaction mixture contains three different species. A high spin $Fe^{III}TPP$ species, which was previously confirmed by the g=5.96 signal in EPR, a low spin $Fe^{III}TPP$ species, the existence of which was reinforced by g values of 2.06 and 1.98 from EPR and another unreacted $Fe^{II}TPP$ species which was EPR silent. [44-47]The difference between the reaction mixture obtained at 233K and RT is in between the relative population of the species. The population of low spin $Fe^{III}TPP$ decreases as we move from 233K to RT, while the population of high spin $Fe^{III}TPP$ increases as we move from 233K to RT. This implies that the low spin $Fe^{III}TPP$ was an intermediate which had higher population at lower temperature than at RT. So, the low spin iron center of the intermediate species is $[Fe^{III}\text{-}SO]^+$, and it is best described as an S=1/2 Fe^{III} center anti-ferromagnetically coupled to an S=1 SO, resulting in an overall S=1/2 ground state. It has to be also kept in mind that the Mössbauer data obtained from 233K and RT reaction mixture is different from the spectra obtained from frozen sample of $Fe^{II}TPP+Fe^{III}TPP\text{-}Cl$ (Figure 7). This goes on to prove that the low spin Fe^{III} species obtained is indeed an intermediate and not a spectra of $Fe^{III}TPP\text{-}Cl$.

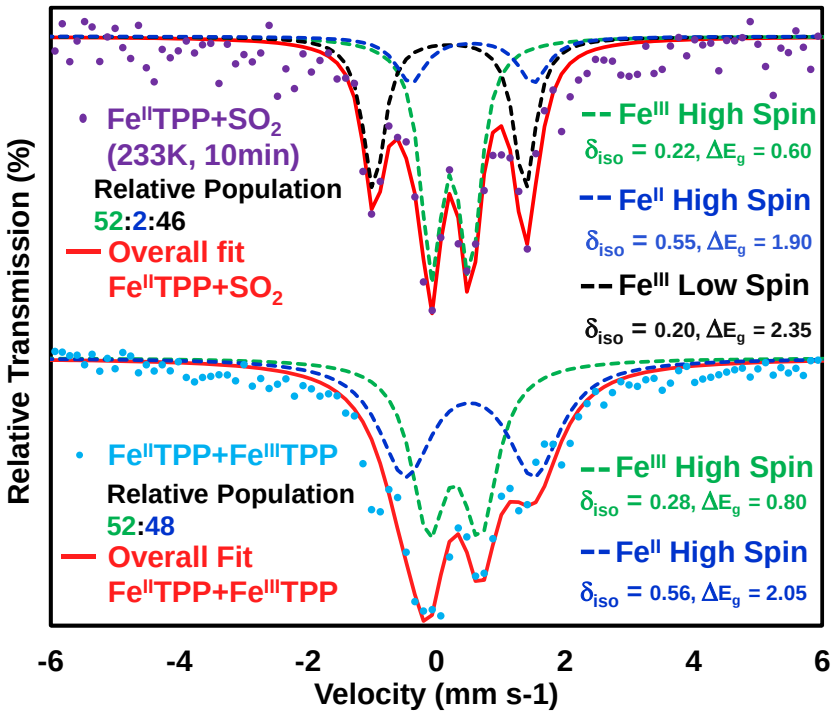

Figure 3.8 (Top) Mössbauer spectra of reaction mixture frozen after 10 minutes for the reaction $^{57}Fe^{II}TPP+SO_2$, done at 233K (violet points) along with the data fits (red); (bottom) Mossbauer data of frozen sample of $Fe^{II}TPP+Fe^{III}TPP$ (blue points) along with its data fit (red). The components are Fe^{III} High Spin (green), Fe^{II} High Spin (blue) and Fe^{III} Low Spin (black) given along with their isomeric shift, quadruple splitting value and relative populations (mentioned in respective spectra colour) are given. The Mossbauer data was redorded at 95K, zero field.

The UV-Vis data of the $Fe^{II}TPP+SO_2$ reaction at RT shows only a high spin ferric porphyrin species as the final product (Figure 3), which is consistent with the observed decay of the S=1/2 $[Fe^{III}\text{-}SO]^+$ intermediate species trapped at 233K and eventual conversion to the high spin ferric porphyrin product at higher temperatures. Below a table listing the Mössbauer parameters are provided.

Components	d_{iso} (mm s^{-1})	ΔE_q (mm s^{-1})	% population
Fe^{III}-HS	0.22	0.60	52
Fe^{III}-LS	0.20	2.35	46
Fe^{II}-HS	0.55	1.90	2

Table 3.1 Mössbauer parameters obtained from the reaction done at 233K

3.3.4 Resonance Raman Spectroscopic studies:

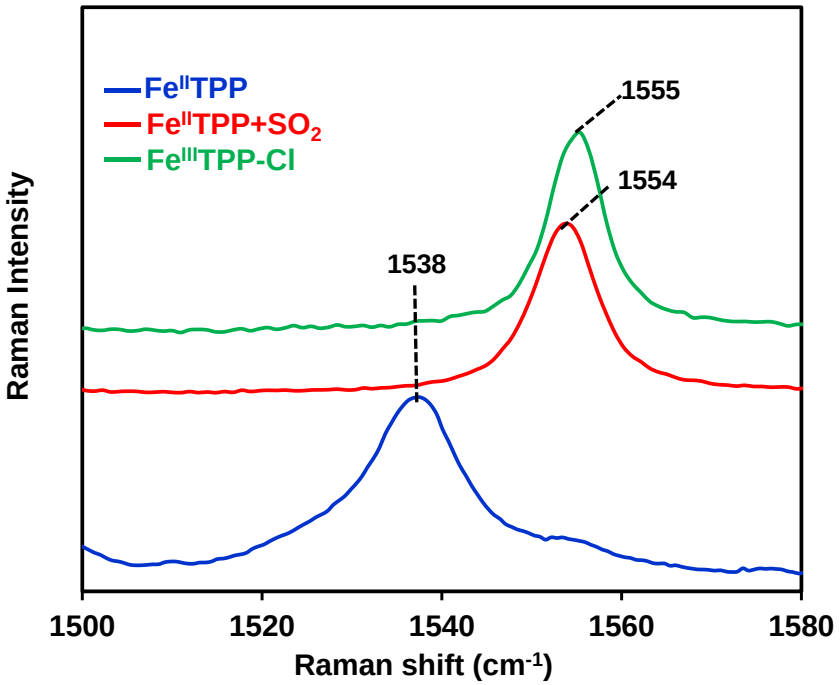

Figure 3.9 The resonance Raman data of Fe^{II}TPP (blue), the resulting species of the RT reaction Fe^{II}TPP+SO_2 (red) and Fe^{III}TPP-Cl (green).

The Fe^{II}TPP+SO_2 reaction was studied with the help of resonance Raman spectroscopy to investigate the nature of the intermediate and gain further insights about the type of bonding present in the reaction. The resonance Raman data of the starting Fe^{II}TPP exhibits a ν_2 vibration at 1538 cm^{-1} (Figure 3B, blue) characteristic of high spin ferrous porphyrin.[48] Upon addition of SO_2, the ν_2 shifts to 1554 cm^{-1} (Figure 3B, red) which is characteristic of high spin Fe^{III} porphyrin (Figure 3B, green) suggesting that the SO_2 oxidizes the ferrous porphyrin to its ferric state, consistent with the UV-Vis data. The resonance Raman data corroborates the findings from the other spectroscopic investigations like UV-Vis, EPR and Mössbauer of the Fe^{II}TPP+SO_2 reaction at RT.

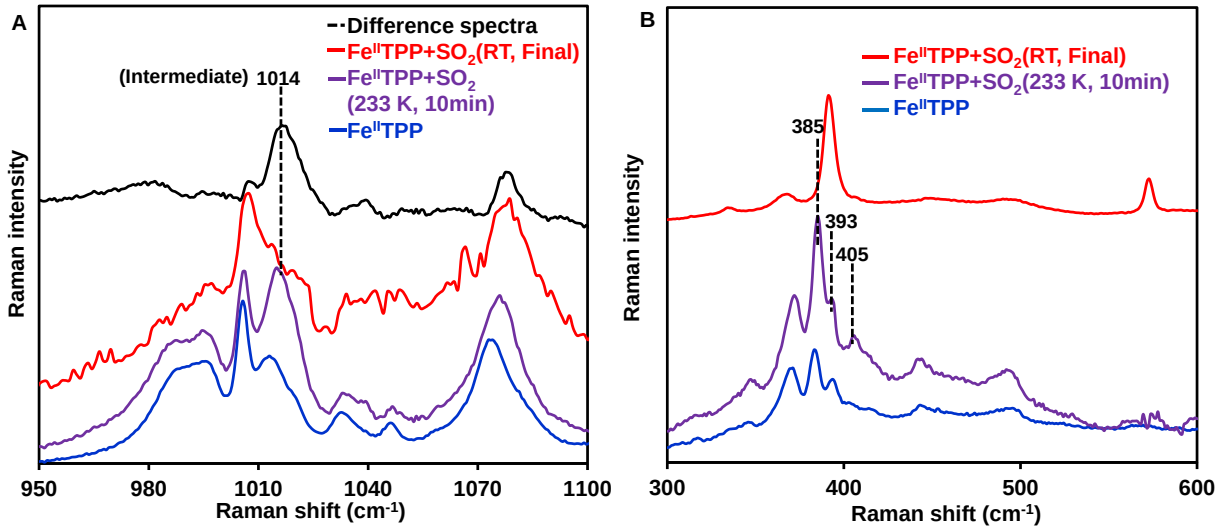

Figure 3.10 (A) resonance Raman spectra of frozen sample of $Fe^{II}TPP$ (blue), reaction mixture of $Fe^{II}TPP + SO_2$ done at 233 K which was frozen after 10 minutes (violet), the frozen sample of the final product of the RT reaction mixture of $Fe^{II}TPP+SO_2$ after letting the reaction mixture stand for a day (red). The Difference spectra (black) obtained by subtracting the blue spectra from violet spectra showing an intermediate feature at 1014 cm^{-1}; (B) Resonance Raman spectra of $Fe^{II}TPP$ (blue line), reaction mixture of $Fe^{II}TPP + SO_2$ at 233K containing intermediate $[Fe^{III}\text{-}SO]^+$ (violet line) and final product of the RT reaction $Fe^{II}TPP + SO_2$ after letting the reaction mixture stand for a day (red line).

To search for intermediate we had to investigate the reaction at lower temperature. So, we studied the reaction at 233K and at RT. The $Fe^{II}TPP+SO_2$ reaction was allowed to proceed for 10 minutes under two different temperatures, 233K and RT. The 233K reaction mixture was frozen after 10 minutes while the RT reaction mixture was frozen after allowing it to stand for a day and then their resonance Raman spectra were recorded. The resonance Raman spectra of the 233K $Fe^{II}TPP+SO_2$ reaction mixture frozen after 10 minutes exhibit υ_8 marker band (Fe-$N_{pyrrole}$ symmetric stretching) at 385 cm^{-1} with a shoulder at 393 cm^{-1} as may be expected due to the presence of both high spin $[Fe^{III}TPP]^+$ species and low spin $[Fe^{III}\text{-}SO]^+$ species in the solution (Figure 9B, violet).[49, 50] New vibrations are observed at 1014 cm^{-1} and at 405 cm^{-1} (Figure 9A&B, violet) which are absent in the reactant $Fe^{II}TPP$ species (Figure 9A&B, blue) as well as in the final product of the RT $Fe^{II}TPP+SO_2$ reaction, obtained after letting the reaction mixture stand for a day (Figure 9A&B, red), respectively. This transient vibration at 1014 cm^{-1} is indicative of the intermediate involved in the reaction. Difference spectra between the intermediate (Figure 9A, violet) and the starting $Fe^{II}TPP$ (Figure 9A, blue) species (after scaling with a solvent peak) clearly indicates the presence of 1014 cm^{-1} band (Figure 9A, black). The 1014 cm^{-1} peak is consistent with the 'S=O' stretch of the $[Fe^{III}\text{-}SO]^+$ intermediate species. (Note that these assignments need isotopically labelled SO_2 to be

confirmed which is expensive and beyond the scope of this investigation.) The results obtained from resonance Raman spectroscopy confirms that an intermediate is indeed obtained in the reaction and it is $[Fe^{III}\text{-}SO]^{+}$ with characteristic 'S=O' stretch at 1014 cm^{-1} and the final product of the reaction being high spin $Fe^{III}TPP$.

3.3.5 X-ray crystallographic studies:

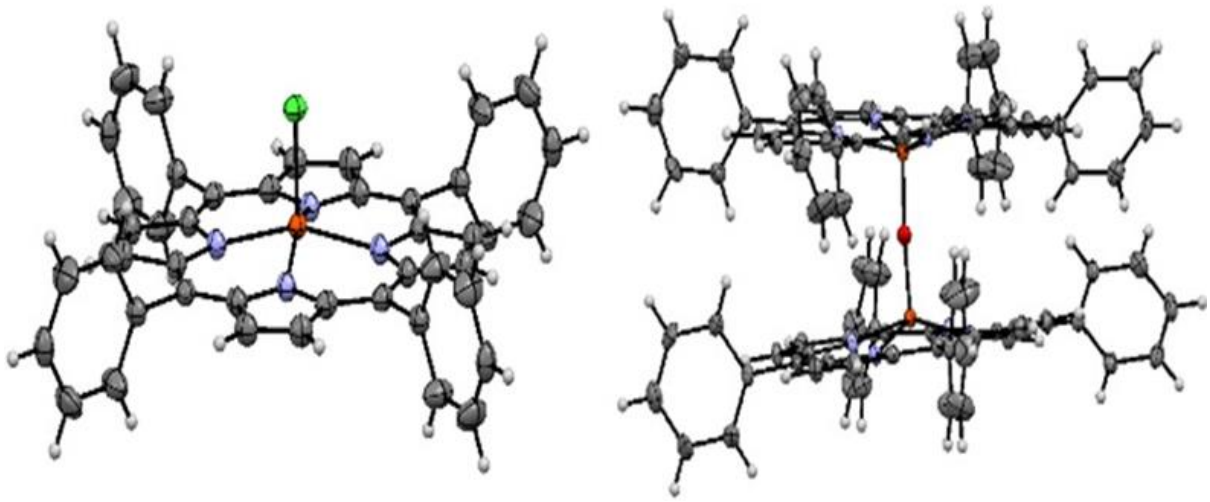

Figure 3.11 (left) Structure of $Fe^{III}TPP\text{-}Cl$ crystallized from the reaction mixture and (right)[51] structure of the μ-oxo dimer formed when the reduced FeTPP is exposed to O_2.[52] Color code: Orange → Fe, green → Cl, red → O, blue →N, grey → C and white → H

In order to ascertain the final product of the $Fe^{II}TPP+SO_2$ reaction at RT, it was allowed to proceed. On letting the reaction mixture to stand at RT for 7 days results in crystallization, affording purple-coloured crystals of ferric tetraphenylporphyrin chloride ($Fe^{III}TPP\text{-}Cl$) species (Figure 10, left). This confirms the obtaining of $Fe^{III}TPP$ species from UV-Vis and rR spectra (Figure 5 & 8, red spectra) of the said reaction at RT. Erstwhile efforts of investigating the reaction of SO_2 with $Fe^{II}TPP$ by Holm and Scheidt resulted in the oxidation of both $Fe^{II}TPP$ and SO_2 to sulphate bridged $Fe^{III}TPP$, likely due to adventitious O_2. In a control experiment, where the $Fe^{II}TPP$ is intentionally exposed to O_2, a μ-oxo dimer species is formed (Figure 10, right) instead of $Fe^{III}TPP\text{-}Cl$. Thus, any possible interference from accidental O_2 leak in the reaction; as well as interference from the reductant used, can be eliminated. This goes on to prove without ambiguity that the eventual product of the reaction of $Fe^{II}TPP+SO_2$ is $Fe^{III}TPP\text{-}Cl$, which is generated only when SO_2 reacts with Ferrous porphyrin. In absence of SO_2 a m-oxo dimer of $Fe^{III}TPP$ is obtained.

3.3.6 DFT studies:

The experimental results were further correlated with the Density functional theory (DFT) calculations. DFT calculations (B3LYP/6-311g*) on a hypothetical model of a solvent (MeOH) bound $[Fe^{III}\text{-}SO]^{+}$ intermediate species indicate a S=1/2 ground state which is 3.8 Kcal/mol and 36.0 Kcal/mol lower in energy than the S=3/2 and S=5/2 states, respectively. The optimized geometry of the $[Fe^{III}\text{-}SO]^{+}$ intermediate species have Fe-S and S-O bond distances of 2.24 Å and 1.54 Å, respectively. These values are reasonably close to the crystallographically observed Fe-S and S-O distances of 2.3 Å and 1.6 Å, respectively.[15] Note that the resolution of the X-tal structure of this species is only 2.5 Å. The SO is bound in a bent end-on fashion with a Fe-S-O angle of 111^{0}. The calculated δ_{iso} and ΔE_q are 0.24 mm/s and 2.25 mm/s, respectively, which agree well with the experimental values of δ_{iso} = 0.20 mm/s and ΔE_q = 2.35 mm/s. The calculated S-O vibration is at 1000 cm^{-1} which is reasonably close to the experimentally observed S-O vibration at 1014 cm^{-1}.

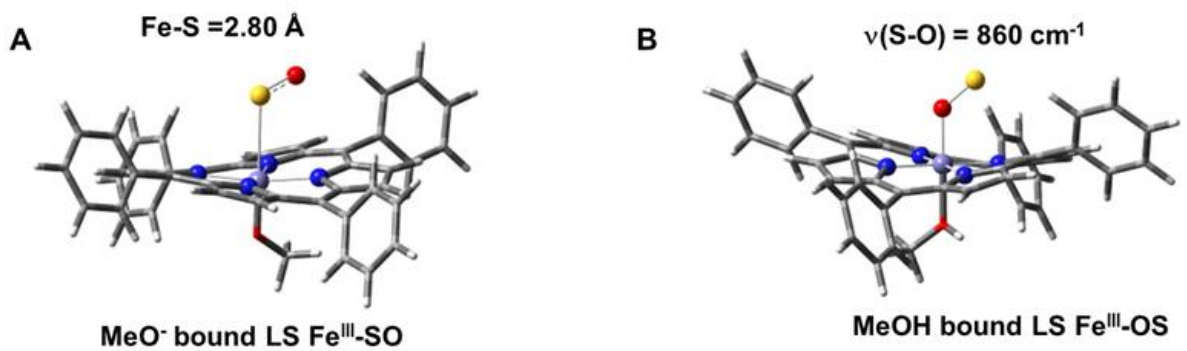

Figure 3.12 DFT optimized structure of the proposed (A) MeO^{-}-$[Fe^{III}\text{-}SO]^{+}$ (B) MeOH-$[Fe^{III}\text{-}OS]^{+}$ species (Fe light blue, N blue, S yellow, O red, C gray and H white)

Neither hypothetical models of the deprotonated MeO- (Figure 11A) bound nor the O-bound isomer of the $[Fe^{III}\text{-}SO]^{+}$ species (Figure 11B) were consistent with the data obtained.

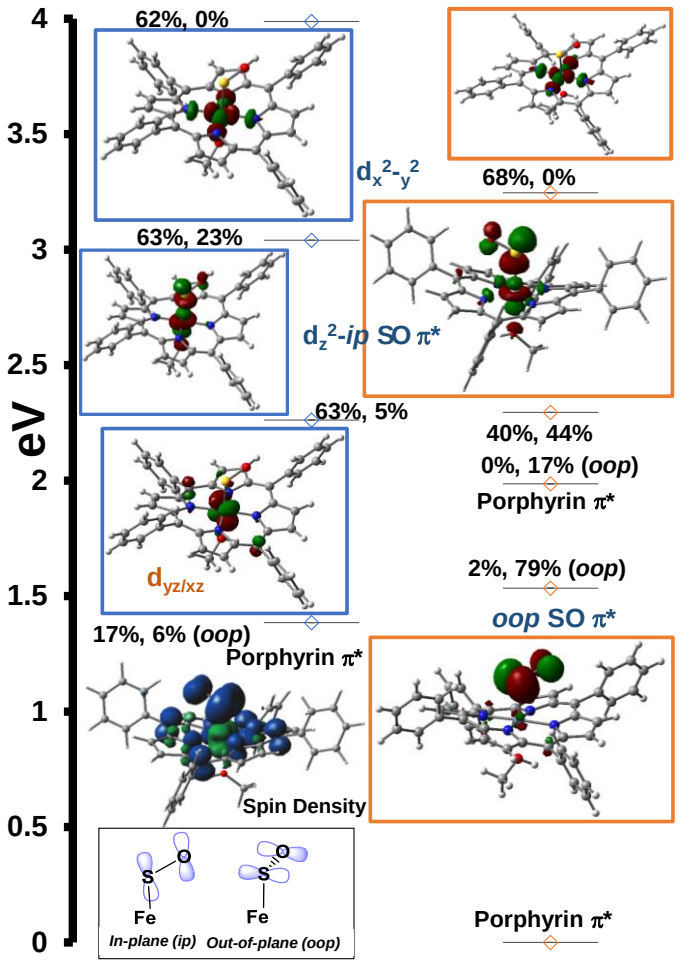

Figure 3.13 (top) DFT optimized structure of the proposed $[Fe^{III}\text{-}SO]^+$ species (Fe light blue, N blue, O red, C gray and H white); (bottom) Molecular orbital diagram of $[Fe^{III}SO]^+$ species. The unoccupied α (orange) and β (blue) orbitals are depicted and their energies are normalized with respect to β LUMO. The coefficients of Fe and SO are indicated.

The MO diagram of the $[Fe^{III}\text{-}SO]^+$ species shows a t_2^5 low-spin Fe^{III} center where the unpaired electron resides in a $d_{xz/yz}$ orbital. The $d_{x^2-y^2}$ orbital is involved in σ bonding with the pyrrolic nitrogen. The triplet SO has singly occupied *in-plane* and *out-of-plane* π* orbitals (inset in Figure 12). The d_{z^2} orbital is involved in forming a σ bond with the *in-plane* SO π* and there is no π bonding between the $d_{xz/yz}$ and the *out-of-plane* SO π* orbital. The S=1/2 Fe^{III} center is anti-ferromagnetically coupled to a triplet S=1 SO (Figure 12, inset) resulting in an overall S=1/2 ground state of the $[FeSO]^7$ entity which is very similar to the ground state of S=1/2 $[FeNO]^7$ species.[53]

The EPR, Mössbauer and resonance Raman data indicate that a mixture of high spin $[Fe^{III}TPP]^+$ and low spin $[Fe^{III}\text{-}SO]^+$ intermediate species are initially produced when SO_2 reacts with $Fe^{II}TPP$. Furthermore, the Mössbauer data indicate that the population of the high spin

[Fe^{III}TPP]$^+$ and low spin [Fe^{III}-SO]$^+$ species is in the ratio of ~0.9:1 suggesting that these two ferric species are produced simultaneously as suggested by the EPR data obtained under the same conditions. These experimental data are suggestive of a 2e$^-$ reduction of SO_2 where one electron is derived from a free Fe^{II}TPP in solution and the other is obtained from the ferrous porphyrin that binds the SO_2 and results in the low-spin [Fe^{III}-SO]$^+$ intermediate (Scheme 1). The protons required for the water elimination can be obtained from MeOH used in the reaction mixture (for dissolving Na_2S reductant) or any residual water in the solvent used. Note that EPR, Mössbauer as well as resonance Raman data indicate that this S=1/2 [Fe^{III}-SO]$^+$ species is an intermediate of the reaction and its solvolysis results in the formation of high spin ferric porphyrin which automatically entails the release of SO.

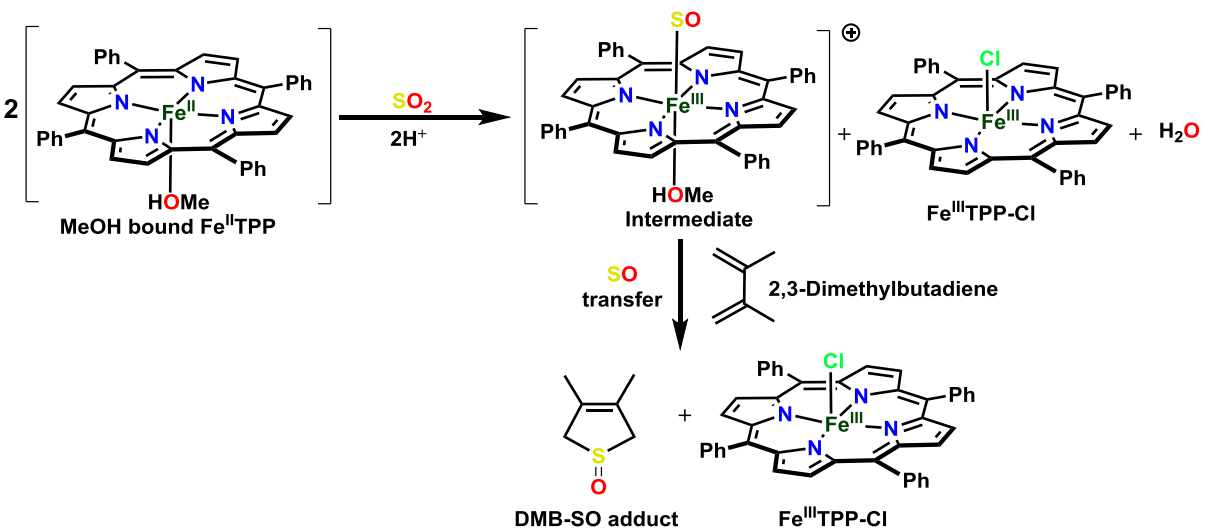

Scheme 3.2 Possible products resulting from 2e$^-$ SO_2 reduction.

3.3.7 SO Trapping:

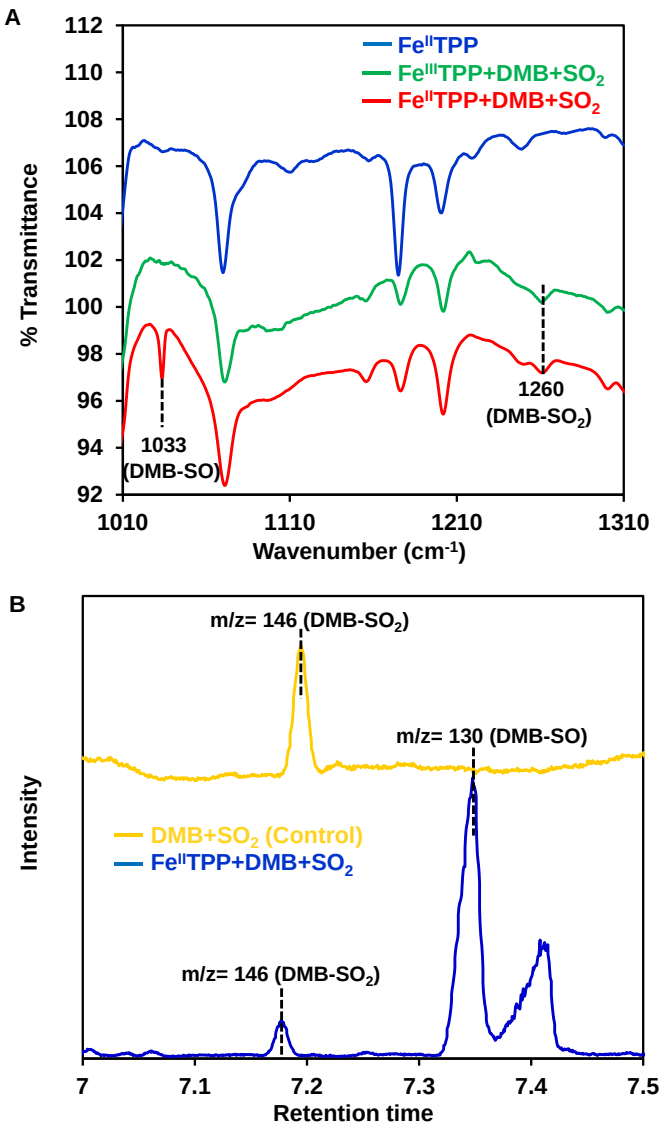

Figure 3.14 (A) FT-IR spectra of reactant $Fe^{II}TPP$ (blue), reaction mixture containing $Fe^{III}TPP+DMB+SO_2$ (green) and the reaction mixture containing $Fe^{II}TPP+DMB+SO_2$ (red). IR samples were drop cast and data recorded in Transmittance mode. (B) GC-MS chromatogram of $Fe^{II}TPP+DMB+SO_2$ reaction mixture (blue) and control reaction mixture of $DMB+SO_2$ (yellow).

SO is an unstable molecule and has a lifetime of < 1s at RT and chemically trapping it is a formidable challenge.[54] In rare cases its formation may be evidenced using an addition reaction with dienes at high temperatures, albeit a very low yielding reaction.[55] The reaction of $Fe^{II}TPP$ with SO_2 when incubated with 2,3-dimethylbutadiene (DMB) exhibits a new vibration in the FTIR spectra at 1033 cm^{-1} (Figure 9A, red) which is absent in the control samples of $Fe^{II}TPP$ (Figure 9A, blue) and $Fe^{III}TPP+DMB+SO_2$ mixture (Figure 9A, green). This 1033 cm^{-1} peak is characteristic of the stretching vibration of the sulfoxide group of the S=O

bound DMB, which can only be generated and trapped in situ when $Fe^{II}TPP$ reacts with SO_2. Whereas, another vibration at 1260 cm^{-1} which is present in both $Fe^{II}TPP+DMB+SO_2$ and in $Fe^{III}TPP+DMB+SO_2$ (Figure 9A, red and green), is characteristic of SO_2 vibration and is present due to the cheletropic reaction of unreacted or excess SO_2 with DMB, irrespective of presence or absence of SO. Note that, a table showing a list of the band frequencies in IR data of the region shown in Figure 9A is also demonstrated as Table 2 below.

IR peaks (cm^{-1})	Mode	Description
1070	C-O	Stretching of cyclic ether of THF
1156	C-C-H, C-C-N	Stretching vibration of porphyrin
1176	C-H	Bending vibration
1202	C-H	Bending vibration
1248	C-N	
1300	N-C-C, C-N-C	Pyrrole half ring modes

Table 3.2 List of the band frequencies and their assignment in the IR data shown in Figure 13 (A)

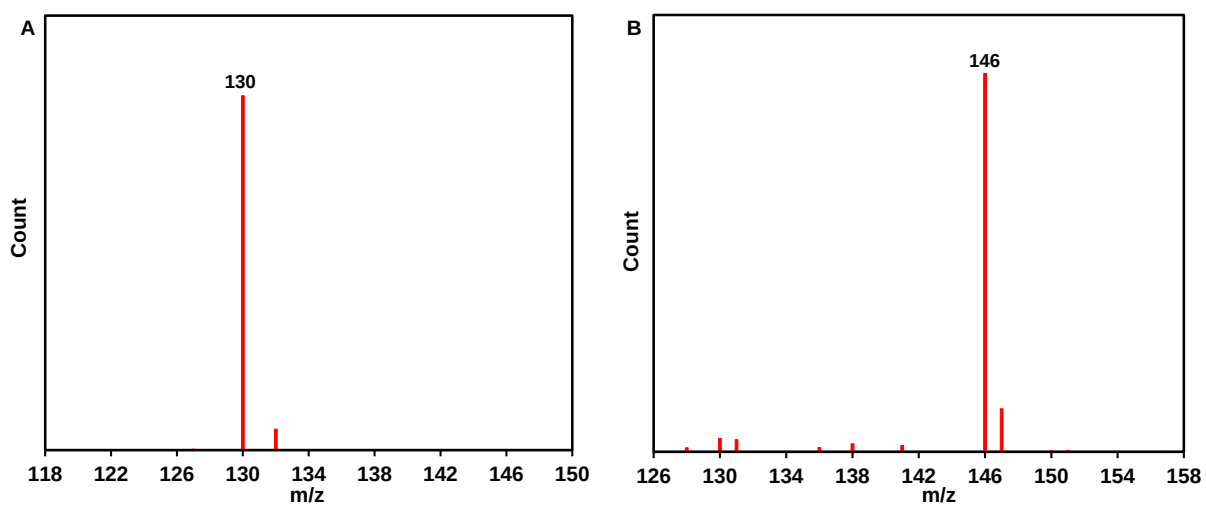

Figure 3.15 The Mass spectra of the corresponding GC-MS chromatograms obtained from the reaction mixture of $Fe^{II}TPP+DMB+SO_2$ and $DMB+SO_2$ control (Fig 13 B). (A) The mass spectra corresponding to the peak obtained at retention time 7.35 min (Fig 13 B, blue) indicating the DMB-SO adduct. (B) The mass spectra corresponding to the peak obtained at retention time 7.19 min (Fig 13 B, yellow) and 7.17 min (Fig 13 B, blue) indicating the DMB-SO_2 adduct.

The transfer of SO to DMB is further confirmed by GCMS data of the reaction mixture $Fe^{II}TPP+DMB+SO_2$ (Figure 9B, blue), having GC-MS peak at retention time 7.35 min with

corresponding mass 130 (Figure 14, A) which is absent in the control of DMB+SO_2 (Figure 9B, yellow) signifying trapping of DMB-SO in the reaction mixture. The reaction mixture also contains a GC-MS peak at the retention time 7.17 min (Figure 13 B, blue), which is also present in the control sample of DMB+SO_2 at retention time 7.19 min (Figure 13 B, yellow), and both having the corresponding mass of 146 (Figure 14, B), confirming generation of cheletropic adduct of DMB-SO_2. Thus in due course of the reaction Fe^{II}TPP+SO_2 incubated with DMB, Sulfoxide is generated in situ and it gets trapped by cheletropic reaction, which is confirmed by IR vibrations at 1033 cm^{-1} and mass peak of 130, and in absence of Fe^{II}TPP, SO_2 itself generates the expected cheletropic reaction adduct in the control samples, confirmed by IR vibrations at 1260 cm^{-1} and mass peaks at 146.[30, 56] A catalytic turnover of 85% ±0.3% is observed for the cheletropic reaction adduct of DMB + SO in presence of Fe^{II}TPP catalyst (calculated from GCMS area).

3.4 Conclusion:

In summary, the data show that ferrous porphyrin can reduce SO_2 similar to the known reactivity of sirohemebased sulfite reductase. The reaction follows a $2e^-/2H^+$ pathway to generate an S=1/2 $[Fe^{III}\text{-}SO]^+$ species which releases SO. Unlike in SiR where the electron is donated by the proximal Fe_4S_4 cluster, here a free Fe^{II} TPP surrogate as the electron donor. The resultant SO species was evidenced by trapping its cheletropic reaction adduct with DMB. This is the first report of chemical reduction of SO_2 by synthetic ferrous porphyrins mimicking the reaction of sulfite reductase outside the protein matrix. The observation of a $[Fe^{III}\text{-}SO]^+$ species outside the protein matrix heralds the possibility of accessing several other unusual intermediates proposed to be involved in the $6e^-/6H^+$ process in this enzyme. These results will enable a deeper understanding of the mechanism of SiR's and aid in mimicking its function in artificial systems.

3.5 References:

(1) Qu, Z.; Henze, D. K.; Li, C.; Theys, N.; Wang, Y.; Wang, J.; Wang, W.; Han, J.; Shim, C.; Dickerson, R. R.; et al. SO2 Emission Estimates Using OMI SO2 Retrievals for 2005–2017. *Journal of Geophysical Research: Atmospheres* **2019**, *124* (14), 8336-8359, https://doi.org/10.1029/2019JD030243. DOI: https://doi.org/10.1029/2019JD030243 (acccessed 2022/08/01).

(2) Seinfeld, J. H.; Pandis, S. N. *Atmospheric Chemistry and Physics: From Air Pollution to Climate Change*; Wiley, 2012.

(3) Zhong, Q.; Shen, H.; Yun, X.; Chen, Y.; Ren, Y. a.; Xu, H.; Shen, G.; Du, W.; Meng, J.; Li, W.; et al. Global Sulfur Dioxide Emissions and the Driving Forces. *Environmental Science & Technology* **2020**, *54* (11), 6508-6517. DOI: 10.1021/acs.est.9b07696.

(4) Lu, Z.; Streets, D. G.; de Foy, B.; Krotkov, N. A. Ozone Monitoring Instrument Observations of Interannual Increases in SO2 Emissions from Indian Coal-Fired Power Plants during 2005–2012. *Environmental Science & Technology* **2013**, *47* (24), 13993-14000. DOI: 10.1021/es4039648.

(5) Feng, T.; Huo, M.; Zhao, X.; Wang, T.; Xia, X.; Ma, C. Reduction of SO2 to elemental sulfur with H2 and mixed H2/CO gas in an activated carbon bed. *Chemical Engineering Research and Design* **2017**, *121*, 191-199. DOI: https://doi.org/10.1016/j.cherd.2017.03.014.

(6) AlQahtani, M. S.; Knecht, S. D.; Wang, X.; Bilén, S. G.; Song, C. One-Step Low-Temperature Reduction of Sulfur Dioxide to Elemental Sulfur by Plasma-Enhanced Catalysis. *ACS Catalysis* **2020**, *10* (9), 5272-5277. DOI: 10.1021/acscatal.0c00299.

(7) Han, G. B.; Park, N.-K.; Yoon, S. H.; Lee, T. J.; Han, G. Y. Direct Reduction of Sulfur Dioxide to Elemental Sulfur with Hydrogen over Sn−Zr-Based Catalysts. *Industrial & Engineering Chemistry Research* **2008**, *47* (14), 4658-4664. DOI: 10.1021/ie800058v.

(8) Wei, R.; Chen, X.; Gong, Y. Side-On Sulfur Monoxide Complexes of Tantalum, Niobium, and Vanadium Oxyfluorides. *Inorganic Chemistry* **2019**, *58* (6), 3807-3814. DOI: 10.1021/acs.inorgchem.8b03411.

(9) Kline, M. A.; Barley, M. H.; Meyer, T. J. Electrocatalytic reduction of bisulfite to hydrogen sulfide based on a water-soluble iron porphyrin. *Inorganic Chemistry* **1987**, *26* (14), 2196-2197. DOI: 10.1021/ic00261a005.

(10) Wayland, B. B.; Mohajer, D. An electron spin resonance study of the interaction of sulphur dioxide with tetraphenylporphyrincobalt(II). *Journal of the Chemical Society, Chemical Communications* **1972**, (13), 776-777, 10.1039/C39720000776. DOI: 10.1039/C39720000776.

(11) Schenk, W. A. Sulfur Oxides as Ligands in Coordination Compounds. *Angewandte Chemie International Edition in English* **1987**, *26* (2), 98-109, https://doi.org/10.1002/anie.198700981. DOI: https://doi.org/10.1002/anie.198700981 (acccessed 2022/08/01).

(12) Gong, J. K.; Fanwick, P. E.; Kubiak, C. P. A sulphur monoxide-bridged dinickel a-frame complex: [Ni2(μ-SO)(PPh2CH2PPh2)2Cl2]. *Journal of the Chemical Society, Chemical*

Communications **1990**, (17), 1190-1191, 10.1039/C39900001190. DOI: 10.1039/C39900001190.

(13) Chahal, M.; Raje, S.; Kotana, G.; Angamuthu, R. Binding enabled catalytic activation of SO2 by copper koneramine complexes under ambient conditions. *Green Chemistry* **2019**, *21* (23), 6372-6380, 10.1039/C9GC02647A. DOI: 10.1039/C9GC02647A.

(14) Crane, B. R.; Getzoff, E. D. The relationship between structure and function for the sulfite reductases. *Current Opinion in Structural Biology* **1996**, *6* (6), 744-756. DOI: https://doi.org/10.1016/S0959-440X(96)80003-0.

(15) Crane, B. R.; Siegel, L. M.; Getzoff, E. D. Probing the Catalytic Mechanism of Sulfite Reductase by X-ray Crystallography: Structures of the Escherichia coli Hemoprotein in Complex with Substrates, Inhibitors, Intermediates, and Products. *Biochemistry* **1997**, *36* (40), 12120-12137. DOI: 10.1021/bi971066i.

(16) Murphy, M. J.; Siegel, L. M.; Tove, S. R.; Kamin, H. Siroheme: A New Prosthetic Group Participating in Six-Electron Reduction Reactions Catalyzed by Both Sulfite and Nitrite Reductases. *Proceedings of the National Academy of Sciences* **1974**, *71* (3), 612-616. DOI: 10.1073/pnas.71.3.612 (acccessed 2022/08/02).

(17) Crane, B. R.; Siegel, L. M.; Getzoff, E. D. Sulfite Reductase Structure at 1.6 Å: Evolution and Catalysis for Reduction of Inorganic Anions. *Science* **1995**, *270* (5233), 59-67. DOI: 10.1126/science.270.5233.59 (acccessed 2022/08/02).

(18) Brânzanic, A. M. V.; Ryde, U.; Silaghi-Dumitrescu, R. Why does sulfite reductase employ siroheme? *Chemical Communications* **2019**, *55* (93), 14047-14049, 10.1039/C9CC05271B. DOI: 10.1039/C9CC05271B.

(19) Lui, S. M.; Cowan, J. A. Direct Reversible Protein Electrochemistry at a Pyrolytic Graphite Electrode. Characterization of the Redox Thermodynamics of the Fe4S4-Siroheme Prosthetic Center in the Hexameric Dissimilatory Sulfite Reductase and the Monomeric Assimilatory Sulfite Reductase from Desulfovibrio vulgaris (Hildenborough). Systematic pH Titration Experiments and Implications for Active Site Chemistry. *Journal of the American Chemical Society* **1994**, *116* (25), 11538-11549. DOI: 10.1021/ja00104a038.

(20) Mirts, E. N.; Petrik, I. D.; Hosseinzadeh, P.; Nilges, M. J.; Lu, Y. A designed heme-[4Fe-4S] metalloenzyme catalyzes sulfite reduction like the native enzyme. *Science* **2018**, *361* (6407), 1098-1101. DOI: 10.1126/science.aat8474 (acccessed 2022/08/02).

(21) Santos, A. A.; Venceslau, S. S.; Grein, F.; Leavitt, W. D.; Dahl, C.; Johnston, D. T.; Pereira, I. A. C. A protein trisulfide couples dissimilatory sulfate reduction to energy

conservation. *Science* **2015**, *350* (6267), 1541-1545. DOI: 10.1126/science.aad3558 (acccessed 2022/08/02).

(22) Hermann, B.; Kern, M.; La Pietra, L.; Simon, J.; Einsle, O. The octahaem MccA is a haem c–copper sulfite reductase. *Nature* **2015**, *520* (7549), 706-709. DOI: 10.1038/nature14109.

(23) Parey, K.; Warkentin, E.; Kroneck, P. M. H.; Ermler, U. Reaction Cycle of the Dissimilatory Sulfite Reductase from Archaeoglobus fulgidus. *Biochemistry* **2010**, *49* (41), 8912-8921. DOI: 10.1021/bi100781f.

(24) Smith, K. W.; Stroupe, M. E. Mutational Analysis of Sulfite Reductase Hemoprotein Reveals the Mechanism for Coordinated Electron and Proton Transfer. *Biochemistry* **2012**, *51* (49), 9857-9868. DOI: 10.1021/bi300947a.

(25) Maia, L. B.; Moura, J. J. G. How Biology Handles Nitrite. *Chemical Reviews* **2014**, *114* (10), 5273-5357. DOI: 10.1021/cr400518y.

(26) Nasri, H.; Wang, Y.; Huynh Boi, H.; Scheidt, W. R. Nitrite-bound five-coordinate low-spin iron(II) model complex for the prosthetic group of nitrite reductase with an unusually large quadrupole splitting. Synthesis, Moessbauer properties, and molecular structure of the complex (nitro)(.alpha.,.alpha.,.alpha.,.alpha.-tetrakis(o-pivalamidophenyl)porphinato)iron(II). *Journal of the American Chemical Society* **1991**, *113* (2), 717-719. DOI: 10.1021/ja00002a075.

(27) Lukat, P.; Rudolf, M.; Stach, P.; Messerschmidt, A.; Kroneck, P. M. H.; Simon, J.; Einsle, O. Binding and Reduction of Sulfite by Cytochrome c Nitrite Reductase. *Biochemistry* **2008**, *47* (7), 2080-2086. DOI: 10.1021/bi7021415.

(28) Kuroi, T.; Nakamoto, K. Matrix-isolation infrared spectra of oxy(tetraphenylporphyrinato)iron(II) containing CS2 and SO2 as axial ligands. *Journal of Molecular Structure* **1986**, *146*, 111-121. DOI: https://doi.org/10.1016/0022-2860(86)80287-3.

(29) Reynolds, M. S.; Holm, R. H. Binding of oxysulfur anions to macrocyclic iron(II,III): [(Fe(TPP))2SO4] and Fe(Me6[14]-4,11-dieneN4)(S2O5)]. *Inorganica Chimica Acta* **1989**, *155* (1), 113-123. DOI: https://doi.org/10.1016/S0020-1693(00)89291-9.

(30) Scheidt, W. R.; Lee, Y. J.; Finnegan, M. G. Reactions of sulfur dioxide with iron porphyrinates and the crystal structure of (hydrogen sulfato)(tetraphenylporphinato)iron(III) hemibenzene solvate. *Inorganic Chemistry* **1988**, *27* (26), 4725-4730. DOI: 10.1021/ic00299a010.

(31) Adler, A. D.; Longo, F. R.; Finarelli, J. D.; Goldmacher, J.; Assour, J.; Korsakoff, L. A simplified synthesis for meso-tetraphenylporphine. *The Journal of Organic Chemistry* **1967**, *32* (2), 476-476. DOI: 10.1021/jo01288a053.

(32) Mittra, K.; Singha, A.; Dey, A. Mechanism of Reduction of Ferric Porphyrins by Sulfide: Identification of a Low Spin FeIII–SH Intermediate. *Inorganic Chemistry* **2017**, *56* (7), 3916-3925. DOI: 10.1021/acs.inorgchem.6b02878.

(33) Perdew, J. P. Density-functional approximation for the correlation energy of the inhomogeneous electron gas. *Physical Review B* **1986**, *33* (12), 8822-8824. DOI: 10.1103/PhysRevB.33.8822.

(34) Pecul, M.; Marchesan, D.; Ruud, K.; Coriani, S. Polarizable continuum model study of solvent effects on electronic circular dichroism parameters. *The Journal of Chemical Physics* **2004**, *122* (2), 024106. DOI: 10.1063/1.1829046 (acccessed 2022/03/28).

(35) Praneeth, V. K. K.; Näther, C.; Peters, G.; Lehnert, N. Spectroscopic Properties and Electronic Structure of Five- and Six-Coordinate Iron(II) Porphyrin NO Complexes: Effect of the Axial N-Donor Ligand. *Inorganic Chemistry* **2006**, *45* (7), 2795-2811. DOI: 10.1021/ic050865j.

(36) Walker, F. A. Models of the Bis-Histidine-Ligated Electron-Transferring Cytochromes. Comparative Geometric and Electronic Structure of Low-Spin Ferro- and Ferrihemes. *Chemical Reviews* **2004**, *104* (2), 589-616. DOI: 10.1021/cr020634j.

(37) Tangen, E.; Conradie, J.; Ghosh, A. The Challenge of Being Straight: Explaining the Linearity of a Low-Spin {FeNO}7 Unit in a Tropocoronand Complex. *Inorganic Chemistry* **2005**, *44* (24), 8699-8706. DOI: 10.1021/ic050781a.

(38) Raynor, J. B. Electron Spin Resonance Spectrum of the Pentacyanonitrosylferrate (I) Anion. *Nature* **1964**, *201* (4925), 1216-1217. DOI: 10.1038/2011216a0.

(39) Ishikawa, Y.; Gong, Y.; Weiner, B. R. Gaussian-2 theoretical and direct ab initio molecular dynamics study of the reaction of O(3P) with thiirane, O(3P) + C2H4S(1A1)→SO(3Σ−) + C2H4(1Ag). *Physical Chemistry Chemical Physics* **2000**, *2* (4), 869-876, 10.1039/A907976I. DOI: 10.1039/A907976I.

(40) Goussias, C.; Deligiannakis, Y.; Sanakis, Y.; Ioannidis, N.; Petrouleas, V. Probing Subtle Coordination Changes in the Iron−Quinone Complex of Photosystem II during Charge Separation, by the Use of NO. *Biochemistry* **2002**, *41* (51), 15212-15223. DOI: 10.1021/bi026223e.

(41) Franz, K. J.; Lippard, S. J. NO Disproportionation Reactivity of Fe Tropocoronand Complexes. *Journal of the American Chemical Society* **1999**, *121* (45), 10504-10512. DOI: 10.1021/ja991664f.

(42) Rinker, R. G.; Gordon, T. P.; Mason, D. M.; Corcoran, W. H. The Presence of the SO2 Radical Ion in Aqueous Solutions of Sodium Dithionite. *The Journal of Physical Chemistry* **1959**, *63* (2), 302-302. DOI: 10.1021/j150572a042.

(43) Livraghi, S.; Paganini, M. C.; Giamello, E. SO2 reactivity on the MgO and CaO surfaces: A CW-EPR study of oxo-sulphur radical anions. *Journal of Molecular Catalysis A: Chemical* **2010**, *322* (1), 39-44. DOI: https://doi.org/10.1016/j.molcata.2010.02.012.

(44) Ellison, M. K.; Schulz, C. E.; Scheidt, W. R. Structural and Electronic Characterization of Nitrosyl(Octaethylporphinato)iron(III) Perchlorate Derivatives. *Inorganic Chemistry* **2000**, *39* (22), 5102-5110. DOI: 10.1021/ic000789e.

(45) Marchant, L.; Sharrock, M.; Hoffman, B. M.; Münck, E. Study of an oxygenated heme complex in frozen solution by Mössbauer emission spectroscopy. *Proc Natl Acad Sci U S A* **1972**, *69* (9), 2396-2399. DOI: 10.1073/pnas.69.9.2396 PubMed.

(46) Iijima, S.; Mizutani, F.; Niwa, O.; Matsumoto, N.; Sunatsuki, Y.; Kojima, M. Mössbauer studies of mixed-valence spin-crossover iron complexes with a hexadentate tripod ligand. *Hyperfine Interactions* **2005**, *166* (1), 397-402. DOI: 10.1007/s10751-006-9299-0.

(47) Wyllie, G. R. A.; Schulz, C. E.; Scheidt, W. R. Five- to Six-Coordination in (Nitrosyl)iron(II) Porphyrinates: Effects of Binding the Sixth Ligand. *Inorganic Chemistry* **2003**, *42* (18), 5722-5734. DOI: 10.1021/ic034473t.

(48) Burke, J. M.; Kincaid, J. R.; Peters, S.; Gagne, R. R.; Collman, J. P.; Spiro, T. G. Structure-sensitive resonance Raman bands of tetraphenyl and "picket fence" porphyrin-iron complexes, including an oxyhemoglobin analog. *Journal of the American Chemical Society* **1978**, *100* (19), 6083-6088. DOI: 10.1021/ja00487a018.

(49) Cheam, T. C.; Krimm, S. Vibrational analysis of crystalline diketopiperazine—I. Raman and i.r. spectra. *Spectrochimica Acta Part A: Molecular Spectroscopy* **1984**, *40* (6), 481-501. DOI: https://doi.org/10.1016/0584-8539(84)80081-1.

(50) Burke, J. M.; Kincaid, J. R.; Spiro, T. G. Resonance Raman spectra and vibrational modes of iron(III) tetraphenylporphine .mu.-oxo dimer. Evidence for phenyl interaction and lack of dimer splitting. *Journal of the American Chemical Society* **1978**, *100* (19), 6077-6083. DOI: 10.1021/ja00487a017.

(51) Silver, J.; Marsh, P. J.; Symons, M. C. R.; Svistunenko, D. A.; Frampton, C. S.; Fern, G. R. Crystal Structure of Bis(4-methylimidazole)tetraphenylporphyrinatoiron(III) Chloride and Related Compounds. Correlation of Ground State with Fe−N Bond Lengths. *Inorganic Chemistry* **2000**, *39* (13), 2874-2881. DOI: 10.1021/ic990848s.

(52) Hoffman, A. B.; Collins, D. M.; Day, V. W.; Fleischer, E. B.; Srivastava, T. S.; Hoard, J. L. Crystal structure and moleculsr stereochemistry of .mu.-oxo-bis[.alpha.,.beta.,.gamma.,.delta.-tetraphenylporphinatoiron(III)]. *Journal of the American Chemical Society* **1972**, *94* (10), 3620-3626. DOI: 10.1021/ja00765a060.

(53) Goodrich, L. E.; Paulat, F.; Praneeth, V. K. K.; Lehnert, N. Electronic Structure of Heme-Nitrosyls and Its Significance for Nitric Oxide Reactivity, Sensing, Transport, and Toxicity in Biological Systems. *Inorganic Chemistry* **2010**, *49* (14), 6293-6316. DOI: 10.1021/ic902304a.

(54) Schenk, P. W.; Steudel, R. New Finding in the Chemistry of the Lower Oxides of Sulfur. *Angewandte Chemie International Edition in English* **1965**, *4* (5), 402-409, https://doi.org/10.1002/anie.196504021. DOI: https://doi.org/10.1002/anie.196504021 (acccessed 2020/12/13).

(55) Dodson, R. M.; Sauers, R. F. Sulphur monoxide: reaction with dienes. *Chemical Communications (London)* **1967**, (22), 1189-1190, 10.1039/C19670001189. DOI: 10.1039/C19670001189.

(56) Cocolios, P.; Lagrange, G.; Guilard, R.; Oumous, H.; Lecomte, C. Alkane (or arene)-sulphinato and -sulphonato-iron(III) porphyrins: synthesis and physicochemical properties; crystal structure of benzenesulphinato(5,10,15,20-tetraphenylporphyrinato)iron(III). *Journal of the Chemical Society, Dalton Transactions* **1984**, (4), 567-574, 10.1039/DT9840000567. DOI: 10.1039/DT9840000567.

Chapter 4

A complete mechanistic study of SO_2 reduction using Ferrous Porphyrin

4.1 Introduction:

The biogeochemical cycle of Sulphur has global importance, both in terms of biological and chemical perspectives. One of its key metabolic pathways happens to be SO_4^{2-} to SO_3^{2-} to S^{2-}.[1] This requires the action of ASiR and DSiR enzymes, which has been isolated from some anaerobic and aerobic bacteria apart from certain prokaryotes.[2] The unravelling of the $6e^-/6H^+$ mechanism has not been done outside protein matrix and there are certain controversies regarding the mechanism. Some propose that it is a series of successive $2e^-/2H^+$ reduction reactions, while some propose it to be a series of six $1e^-/1H^+$ reactions. Nonetheless the first step involves the binding of the S atom, either in the form of SO_3^{2-} or in the form of SO_2. Here the S atom directly binds to the Fe centre of the siroheme moiety followed by e^- transfer from the Fe_4S_4 cluster. The binding of SO_2 (after water elimination from SO_3^{2-}) to the open co-ordination site of siroheme is followed by its $2e^-$ reductions and water elimination to result in an unusual sulfur monoxide (SO) bound $[Fe^{III}\text{-}SO]^+$ species where the formal oxidation state of the central sulfur is +2 i.e. $2e^-$ reduced relative to +4 in SO_2. Two subsequent $2e^-/2H^+$ reductions and water eliminations yield the final H_2S product of this $6e^-/6H^+$ reduction of SO_2. So, the proposed mechanism is three subsequent $2e^-/2H^+$ reduction of SO_3^{2-} to S^{2-}, accompanied by release of three molecules of H_2O.[3-4] Alternatively, Stroupe and co-workers used site-directed mutants of the distal Arg and Lys residues to argue for six sequential $1H^+/1e^-$ steps instead. This mechanism is a coupled 'push-pull' mechanism, where the electrons are pushed from the active site Siroheme cofactor and high proton concentrations are donated from distal Arginine and Lysine cages to pull charges from the substrates.[5] In order to properly elucidate the reaction mechanism of SO_2 reduction, it is required to perform the reaction using a functional and structural model of the heme active site. So, we chose Fe^{II}TPP, which itself is capable of of binding with NO_2^- and reducing it to NO, emulating the activity of Assimilatory Nitrite Reductase, at least partially.[6] Since Fe^{II}TPP can reduce NO_2^- just like siroheme based NiR which, in turn, can also reduce sulfite, it is possible that Fe^{II}TPP may reduce SO_2 like the siroheme based SiR. However, this has been difficult to achieve. While initial vibrational data indicated the formation of SO_2 adduct of Fe^{II}TPP at 20 K,[7] efforts to isolate the adduct or isolate reduced sulfur products failed despite several attempts to do so[8-10] and sulfate/sulfite bound Fe(II) porphyrins were isolated instead in non-protic organic solvents. In our previous work we have already studied the reduction reaction using Fe^{II}TPP. The reaction was probed at RT and at 233K by employing different spectroscopic, synthetic and theoretical calculations. We have stumbled upon a 6C Low Spin MeOH-Fe^{III}TPP-SO intermediate, which is the first instance of isolation of such a novel intermediate. Till date the proposed mechanisms of biological SO_2 reduction entail the formation of several unusual siroheme bound SO_x species that have not been observed outside the protein matrix in heme systems. Several enzyme

crystals were grown in presence of the reactants and intermediate chemical species like SO_3^{2-}, S^{2-} etc. proposed in the SO_2 reduction cycle. Oxidation of the sulfide bound crystals provided crystallographic evidence for the formation of a partially reduced SO_x species. The electron density was fitted to a bent $[Fe^{III}\text{-}SO]^+$ species with a Fe-S distance of 2.2 Å and a S-O distance of 1.6 Å.[3, 11] Unfortunately, the resolution of the structure was not high enough to allow unambiguous determination of the nature of this intermediate in the SO_2 reduction cycle. Formally, a $[Fe^{III}\text{-}SO]^+$ species is a $[Fe\text{-}SO]^7$ (5 e^- from Fe^{3+} d-orbitals and 2 e^- from S=O Π* anti-bonding orbitals) species according to Enemark-Feltham notation,[12] which could be similar to the $[FeNO]^7$ intermediate involved in the reduction of NO_2^- in nitrite reductases (NiR). The nature of this $[Fe^{III}\text{-}SO]^+$ species has not yet been understood as it is yet to be actualized in synthetic systems. Our data shows data show that ferrous porphyrin can reduce SO_2 similar to the known reactivity of siroheme based sulfite reductase. The reaction follows a $2e^-/2H^+$ pathway to generate an S=1/2 $[Fe^{III}\text{-}SO]^+$ species which releases SO. Unlike in SiR where the electron is donated by the proximal Fe_4S_4 cluster, here a free Fe^{II}TPP surrogates as the electron donor. The resultant SO species was evidenced by trapping its cheletropic reaction adduct with DMB. This is the first report of chemical reduction of SO_2 by synthetic ferrous porphyrins mimicking the reaction of sulfite reductase outside the protein matrix. The observation of a $[Fe^{III}\text{-}SO]^+$ species outside the protein matrix heralds the possibility of accessing several other unusual intermediates proposed to be involved in the $6e^-/6H^+$ process in this enzyme. These results will enable a deeper understanding of the mechanism of SiR's and aid in mimicking its function in artificial systems.[13] In this work we have extended our previous work and studied the SO_2 reduction using Fe^{II}TPP in greater detail by tweaking some of the reaction conditions. We went down to lower temperature to discover newer intermediates, we probed the proton dependence of the reaction and we also did some isotope dependant studies using $^{34}SO_2$, which allowed us to report and confirm novel Fe-S bound intermediates. This helped us in proposing a detailed mechanistic scheme of the $2e^-/2H^+$ reduction of SO_2 by Fe^{II}TPP.

4.2 Experimental Section:

4.2.1 Materials:

All the reagents used were of the best commercially available quality. H_2SO_4 (98%, Merck), Na_2SO_3 (anhydrous, Merck), Silica (Merck), Na_2SO4 (Merck), all were bought from respective vendors and used without further purification. Benzaldehyde (Spectrochem), Pyrrole (Spectrochem), Glacial Acetic acid (Spectrochem), Na_2S (Spectrochem) were bought from respective vendors. 2,4,6-Trimethylpyridine (Sigma-Aldrich), Ferrous Bromide (anhydrous,

Sigma-Aldrich), HCl (37%, Merck), were used for $Fe^{III}TPP$ synthesis. $Na_2{}^{34}SO_3$ isotope was bought from Icon Isotopes and used for $^{34}SO_2$ generation. Tetrahydrofuran, Methanol, Hexane were sourced from Finar Chemicals and used only after subjecting them to adequate drying and distilling procedures. Dry and pure SO_2 gas was passed through a solution of conc. H_2SO_4 to remove any moisture and tested using GC-MS prior to use (Figure S1). The solubility of SO_2 in THF (after 20 mins purging) is assumed to be 0.3-0.5 M as is the case for commercial sources of the same (https://www.sigmaaldrich.com/catalog/product/aldrich/901592). All solvents used were dried and degassed before use. Absorption spectra were obtained by a UV-Vis diode array spectrophotometer (Agilent 8453). EPR experiments were performed at 77 K in a liquid nitrogen finger Dewar. EPR spectra were obtained by a JEOL FA200 spectrophotometer with the following parameters- modulation width: 10 gauss; amplitude: 20; time constant: 300 ms; power: 2 mW; frequency: 9.25 GHz. The EPR data was simulated using JEOL Anisotropic Simulation software. Resonance Raman (rR) data were collected using 413.1 nm excitation from a Kr^+ ion source (Sabre Coherent Inc.) and a Trivista 555 triple spectrophotometer (gratings used in the three stages were 900, 900, and 2400 grooves/mm) fit with an electronically cooled Pixis CCD camera (Princeton Instruments). The irradiation power kept at the sample is 8-10 mW, so that photodegradation does not take place. All the data were collected at 77 K in a liquid N_2 cooled finger Dewar after preparing the reaction mixtures at their respective reaction temperature and freezing them after a stipulated time.

4.2.2 Methods:

4.2.2 a) Synthesis:

Synthesis of Tetraphenylporphyrin (TPP):

Freshly distilled pyrrole (56 ml, 0.8 mol) and 80 ml (0.8 mol) of reagent grade benzaldehyde are added to 3 lit. of refluxing reagent grade propionic acid. (Note: crystalline material is not direct,ly obtained if acetic acid is used.) After refluxing for 30 min, the solution is cooled to room temperature and filtered, and the filter cake is washed thoroughly with methanol. After a hot water wash, the resulting purple crystals are air dried, and finally dried in vacuo to remove adsorbed acid to yield 25 g (20%, yield) of TPP. Spectrophotometric analysis shows that only 1% of the TPP yield remains in the filtrate and also that the filtered material is about 3% tetraphenylchlorin (TPC) by weight. This method was developed by Adler *et al.*[14]

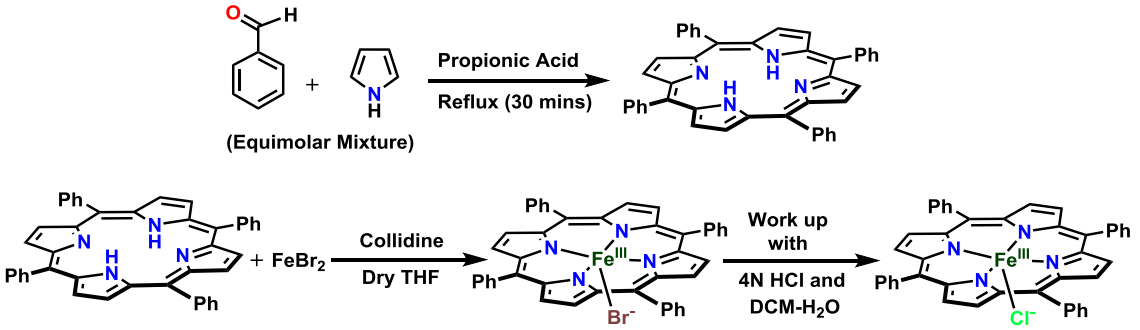

Scheme 1. Synthesis of TPP and Fe^{III}TPP by the reported procedure of Adler *et al*[14]

Synthesis of Fe^{III}TPP:

The synthesized 100mg, 0.162 mmol TPP was dissolved in dry degassed THF solvent inside a glove box and then stirred with 98.6 mg, 0.810 mmol 2,4,6-trimethyl pyridine (Collidine) for 30 minutes for the purpose of deprotonation of the pyrrolic protons. Then 350 mg, 1.62 mmol $FeBr_2$ metallic salt was added into the solution and left under stirring condition and the reaction was followed by TLC until disappearance of the TPP spot and appearance of a new spot. The reaction mixture was taken out of the glove box, the THF was removed from the reaction mixture *in vacuo* and the reaction was worked up with DCM and water after treating with 4N HCl to remove excess $FeBr_2$.The organic layer was dried with Na_2SO_4 and evaporated through a rotary evaporator. The solid compund was purified by column chromatography using 5:95 MeOH-DCM solution to afford the Fe^{III}TPP-Cl (HCl being the source of Cl^- in the resulting compound) (Scheme 1).

4.2.2 b) Sample preparation for UV-Vis Spectroscopy:

Synthesized Fe^{III}TPP was dissolved in THF to prepare 1 mM solution. It was subjected to reduction using a 0.5 eq. (20 mM stock solution) of Na_2S dissolved in dry degassed methanol or dry degassed CD_3OD.[15] The reduction was monitored using UV-Vis spectroscopy. Pure and dry SO_2 gas was bubbled in dry degassed THF to prepare a saturated solution of SO_2 in THF. 10-80 µL of SO_2 saturated THF (0.3-0.5 M) was added to the ferrous porphyrin and the absorption was recorded. For the kinetic runs, data at 0.5 s intervals were recorded.

4.2.2 c) Generation of $^{34}SO_2$ for isotopic shift studies:

80 mg of $Na_2{}^{34}SO_3$ (Icon Isotopes) was taken in an anaerobic vial and sparged with N_2 to remove traces of Oxygen. In another anaerobic vial H_3PO_4 was taken and purged with N_2 to ensure removal of traces of Oxygen. In the vial containing $Na_2{}^{34}SO_3$, the H_3PO_4 was added to generate $^{34}SO_2$ and it was bubbled into another vial containing dry degassed THF, to generate

$^{34}SO_2$ bubbled THF solution. That solution was injected into $Fe^{II}TPP$ solution and subjected to different spectroscopic techniques like resonance Raman and EPR.

4.2.2 d) Sample Preparation for EPR and Raman Spectroscopy:

$Fe^{III}TPP$ was reduced to $Fe^{II}TPP$ inside the glovebox using 0.5eq. Na_2S dissolved in dry degassed MeOH and/or CD_3OD. In EPR Tubes, 20 µL, 5 mM solution of $Fe^{II}TPP$ were taken and maintained at different temperatures like 193K, RT. Then they were injected with an 80 µL saturated solution of dry and pure SO_2 gas in THF (or $^{34}SO_2$ bubbled THF) to afford a 100 µL solution of 1 mM concentration reaction mixture. The reaction mixtures were allowed to progress for required time before freezing them in liq. N_2 for EPR analysis and resonance Raman analysis.

4.2.2 e) DFT Calculations:

The density functional calculations are performed using Gaussian 03 software package. Geometry optimisation was done with the B3lyp functional with an unrestricted formalism. For MeOH bound SO complex a mixed basis set with 6-311g* on Fe and 6-31g* on C, H, N, S, O have been used for optimization and frequency calculations.[16] Tight SCF convergence and the 6-311+g* basis set has been used on all the atoms for a single point energy calculation using the PCM model and convergence criterion of 10^{-10} Hartree.[17] Mulliken orbital populations are calculated using QMForge, and molecular orbital contours are generated using Gaussview software. The ground state wave function of Fe^{III}-LS-SO_2H complexes have been calculated using the contribution of Fe and S, O in the unoccupied molecular orbitals.

4.3 Results and Discussion:

4.3.1 UV-Visible studies:

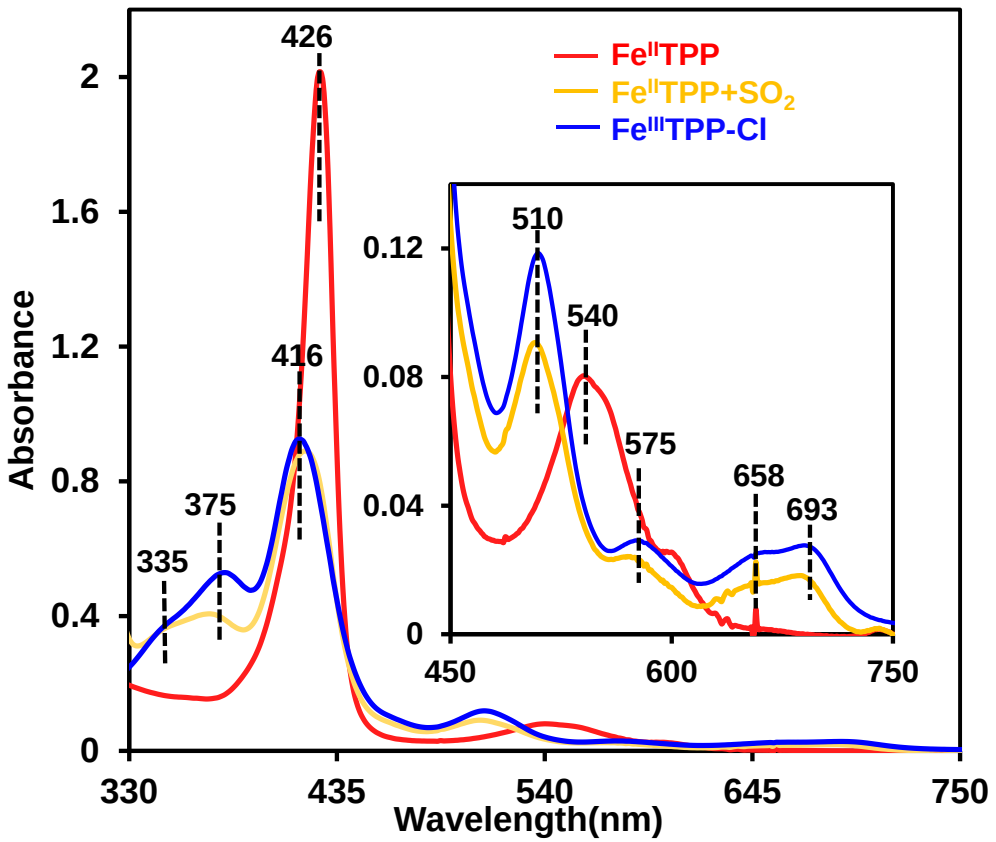

Figure 4.1. Absorption data of the Fe^{II}TPP (red), the resulting species of the RT reaction Fe^{II}TPP+SO_2 (yellow) and Fe^{III}TPP-Cl (blue), showing the Soret bands. Inset: Q-band region of the given spectra

On impregnating a solution of Fe^{II}TPP having characteristic Soret and Q-bands at 426 and 540 nm (Figure 4.1, Red) with a 60 mL solution of saturated SO_2-THF, the Soret and Q-bands shift to 416 and 510 nm along with a Charge Transfer band at 658 and 693 nm (Figure 4.1, Yellow). This new spectrum is similar to Fe^{III}TPP-Cl (Figure 4.1, blue) and this observation shows that Fe^{II}TPP reacting with SO_2 generates Fe^{III}TPP-Cl as its end product.[13]

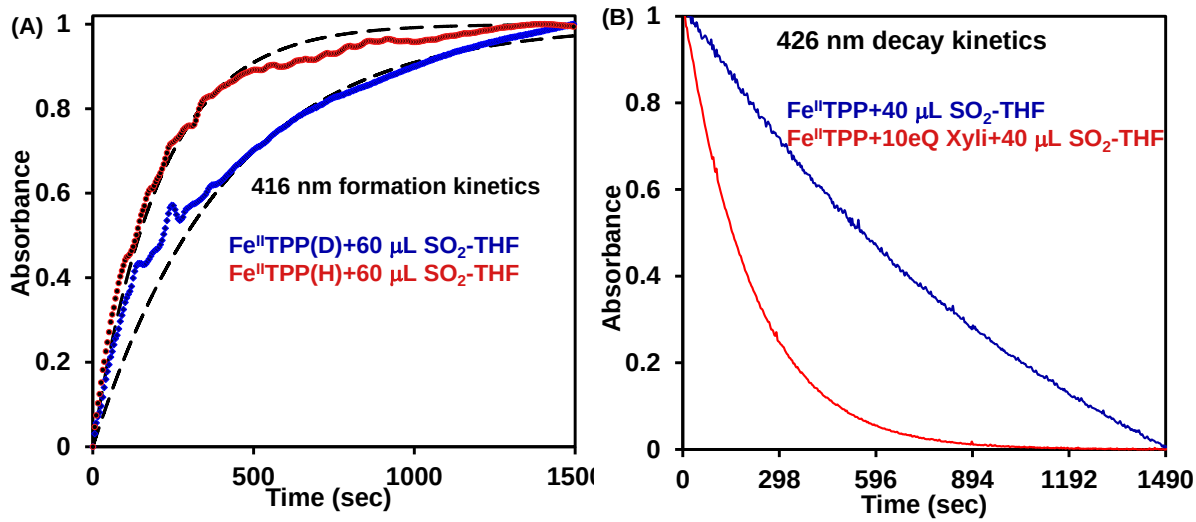

Figure 4.2. (A) Absorbance vs Time Kinetic trace of 416 nm band of $Fe^{II}TPP$ (reduced using CD_3OD, blue and reduced with CH_3OH, red) with 60 mL SO_2-THF, (B) Absorbance vs Time Kinetic trace of 426 nm band of $Fe^{II}TPP$ reaction with 40mL SO_2-THF (blue spectra) and $Fe^{II}TPP$+10eQ Xylidinium Hydrochloride reaction with 40mL SO_2-THF (red spectra). All the experiments have been performed at RT.

On following the time dependent evolution of the 416 nm band in the reaction between $Fe^{II}TPP$ with SO_2 it was observed that the Ferrous Porphyrin prepared using CD_3OD shows a slower reaction than the one prepared using CH_3OH. Here CD_3OD and CH_3OH are purposefully used to understand the proton dependance of the reaction. The first order rate constant using CH_3OH is 0.0048 s^{-1} (Table 1) while the first order rate constant using CD_3OD is 0.0023 s^{-1}, giving a k_H/k_D value of around 2. Hence the reaction twice as slow in presence of CD_3OD proving a strong proton dependance in the rate determining state of the reaction.

UV Kinetics			
Wavelength (nm)	**Rate in MeOH**	**Rate in CD_3OD**	**Kinetic Isotope Effect**
416	**k_H = 0.0048 s^{-1}**	**k_D = 0.0023 s^{-1}**	**k_H/k_D = 2.08**

Table 4.1 The k_H and k_D values reported for the $Fe^{II}TPP+SO_2$ reduction reaction in presence of MeOH and CD_3OD

The time dependent decay kinetics of the 426 nm band in the reaction between $Fe^{II}TPP$ with SO_2 both in presence of an external proton source like Xylidinium Hydrochloride and in its

absence (Figure 4.2, B) was followed. It was observed that the reaction is faster in presence of an external proton source like Xylidinium than in its absence. This goes on to prove that there is involvement of proton in the rate determining step of this reaction. So, our UV experiments give telltale evidences of a proton dependance in the SO_2 reduction using $Fe^{II}TPP$. This calls for further probing of the reaction employing other spectroscopic techniques.

4.3.2 EPR spectroscopic studies:

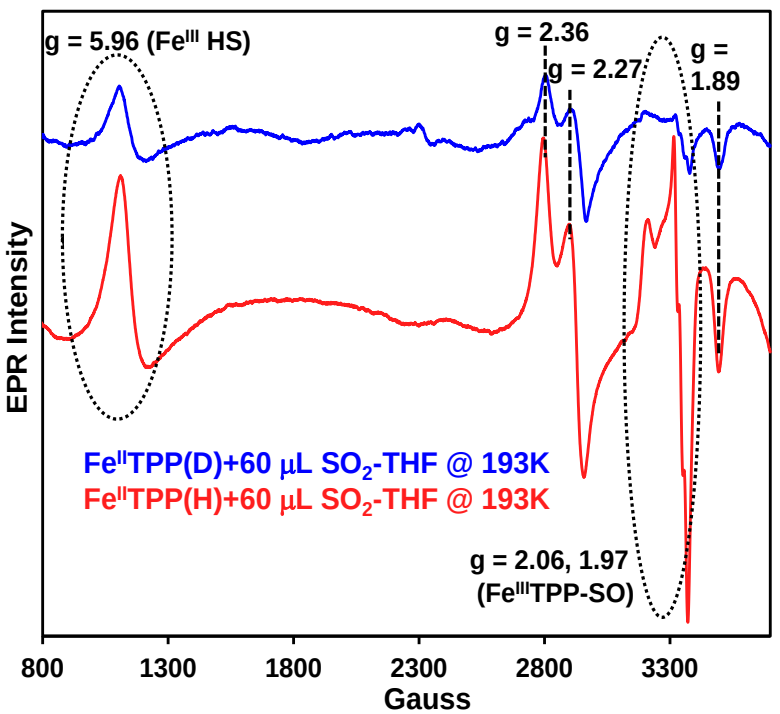

Figure 4.3. EPR spectra of reaction between $Fe^{II}TPP$ (reduced using CD_3OD, blue and reduced using MeOH, red) and saturated SO_2-THF solution, where reaction was allowed to proceed at 193K for 10 minutes and then frozen. X-band EPR data were recorded on the frozen samples at 77K

$Fe^{II}TPP$ on reacting with a saturated solution of SO_2-THF generates $Fe^{III}TPP$ via a Low spin hexa-coordinated MeOH bound $Fe^{III}TPP$-SO intermediate. On probing the reaction mixture by freezing it after allowing the reaction to proceed for 10 minutes at Room Temperature (RT), it is observed that two distinct EPR signals are obtained. An axial signal having g value 5.96, characteristic of High Spin Fe^{III}, which corresponds to the $Fe^{III}TPP$ end product of the reaction and another novel axial signal, having g values of 2.06 and 1.97. This signal is characteristic of the Low Spin MeOH bound $Fe^{III}TPP$-SO intermediate.[13] From the isotope dependent UV kinetics studies, we have observed an k_H/k_D = 2.08, which indicates a proton dependence in this reaction.

So, we studied the reaction using EPR spectroscopy at 193K instead of RT, to find involvement of other proton dependent intermediates. Just like in the UV-Vis experiments, $Fe^{II}TPP$ was prepared from $Fe^{III}TPP$, using Na_2S dissolved in both CD_3OD and MeOH to internally vary the proton source. Then the thus prepared $Fe^{II}TPP$ samples were subjected to SO_2 and the reactions were allowed to proceed at 193K for 10 minutes and they were frozen and had their EPR recorded. It was observed that at 193K when $Fe^{II}TPP$ was injected with SO_2, it generated a rhombic signal having g values at 2.36, 2.27 and 1.89, characteristic of Fe^{III} Low spin signal.[18] Apart from the rhombic signals, the two previously observed EPR signals corresponding to High Spin Fe^{III} and 6C MeOH bound $Fe^{III}TPP$-SO intermediate signals were also observed (Figure 4.3). It was also observed that in the $Fe^{II}TPP$ prepared using CD_3OD, the intensity of all the three EPR signals were lower than the $Fe^{II}TPP$ prepared in MeOH, indicating overall slower reaction kinetics in CD_3OD than MeOH, which corroborates with the k_H/k_D=2.08 observed in UV-Vis kinetics study. Another interesting observation is, the intensity of the axial $Fe^{III}TPP$-SO signal is greater than the rhombic Fe^{III} Low Spin signal in $Fe^{II}TPP$ prepared in MeOH (Figure 4.3, red spectra), while the intensity of the rhombic Fe^{III} Low Spin signal is greater than the axial $Fe^{III}TPP$-SO signal in the $Fe^{II}TPP$ prepared in CD_3OD (Figure 4.3, blue spectra). This shows that there is a proton dependence in the step where the Fe^{III} Low Spin rhombic species gets converted into $Fe^{III}TPP$-SO intermediate species.

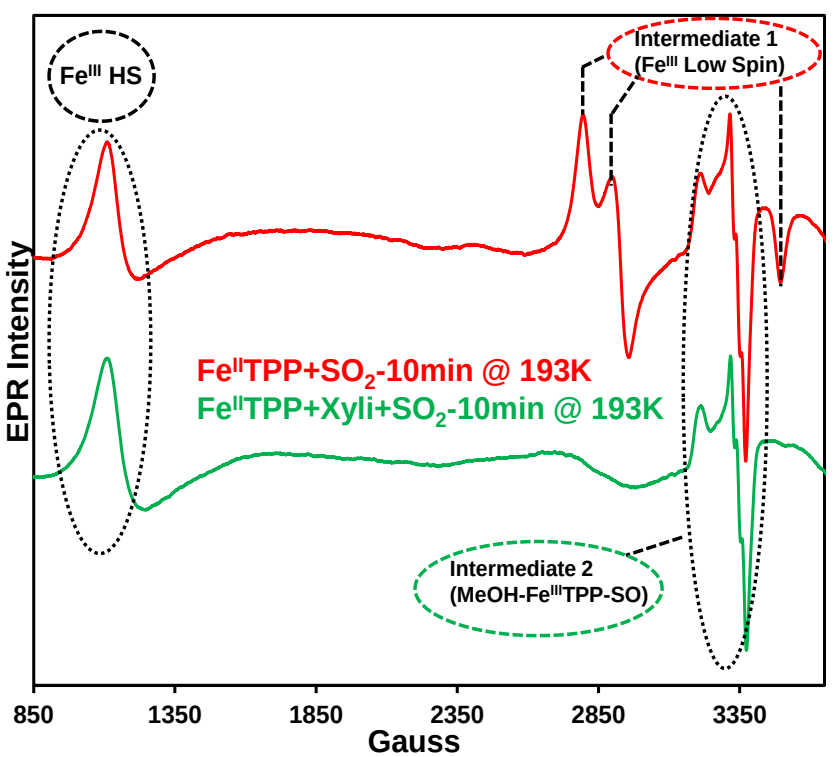

Figure 4.4. EPR spectra of $Fe^{II}TPP+SO_2$ reaction (red), and $Fe^{II}TPP$ (with Xylidinium proton source) $+SO_2$ reaction (green). Both the reactions were performed at 193K and frozen after allowing the reaction to proceed for 10 minutes. X-band EPR data were recorded on the frozen samples at 77K

Having got an indication of proton dependance in the reaction of $Fe^{II}TPP$ with SO_2, it was necessary to confirm that. So, another experiment was devised where the reaction of $Fe^{II}TPP$ with SO_2 was studied in presence and absence of an external proton source, Xylidinium hydrochloride. It was observed that at 193K when $Fe^{II}TPP$ was injected with SO_2, it generated the rhombic signal having g values at 2.36, 2.27 and 1.89 along with the previously observed EPR signals corresponding to High Spin Fe^{III} and 6C MeOH bound $Fe^{III}TPP$-SO intermediate signals (Figure 4.4, red spectra). But the most interesting observation is that, in the $Fe^{II}TPP$ having previously added Xylidinium proton source, on addition of SO_2, the rhombic signal, characteristic of the Fe^{III} Low Spin species, disappears and only the axial signal corresponding to the MeOH bound $Fe^{III}TPP$-SO axial signal remains along with $Fe^{III}TPP$ High Spin signal (Figure 4.4, green spectra). This indicates that the rhombic signal arises due to a Low Spin Fe^{III} intermediate, which in presence of external proton source, makes way for the already identified $Fe^{III}TPP$-SO intermediate. Hence, the EPR data indicates the presence of two different intermediates in the reaction, one being a Low Spin Fe^{III} intermediate (g values of 2.36, 2.27, 1.89), here onwards will be referred to as Intermediate 1. That Intermediate 1, in a proton dependent step, makes way for the already reported 6C Low Spin MeOH bound $Fe^{III}TPP$-SO intermediate, here onwards will be referred to as Intermediate 2. And along with the two intermediates, High Spin Fe^{III} is also generated parallel to them.

In the reaction of $Fe^{II}TPP$ with SO_2, Intermediate 2 has been well characterized but the Fe^{III} Low Spin Intermediate 1 has not yet been characterized. In order to properly characterize the Intermediate 1, it was necessary to generate the said intermediate in exclusion of Intermediate 2. Hence, we designed an experiment which allowed us isolate the Intermediate 1 *in situ*. We performed the reaction using very low concentrations of SO_2. The low concentration was ensured by using 80mg of Na_2SO_3, which after acid addition generated SO_2 gas, which was bubbled into a solution of THF. Using that SO_2 bubbled THF solution, the Intermediate 1 trapping experiments were performed and subjected to EPR and resonance Raman spectroscopy.

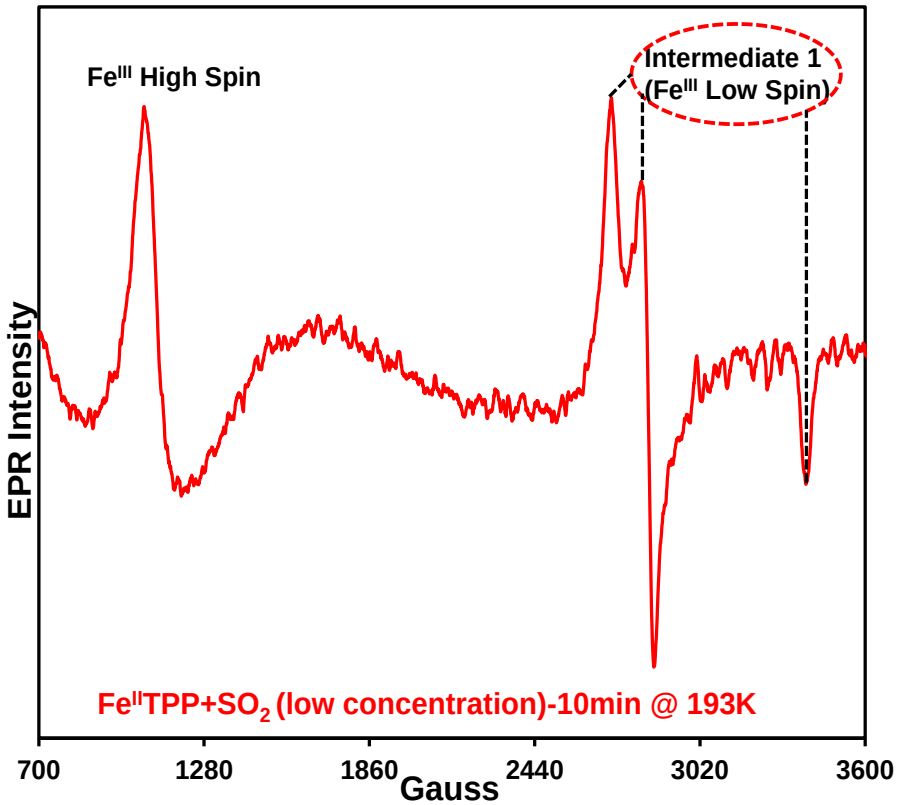

Figure 4.5. EPR spectra of the reaction Fe^{II}TPP with SO_2-THF at very low concentration. The reaction was performed at 193K and frozen after allowing the reaction to proceed for 10 minutes. X-band EPR data were recorded on the frozen samples at 77K

On injecting SO_2-THF solution of very low concentration into the Fe^{II}TPP solution at 193K and allowing the reaction to proceed for 10 minutes, it was observed that the rhombic signal corresponding to Intermediate 1 along with High Spin Fe^{III} was generating. This was an exclusive isolation of Intermediate 1 along with High Spin Fe^{III}, which is always generated for the 2e$^-$ reduction of SO_2 using Fe^{II}TPP.

4.3.3 resonance Raman studies:

The reaction of Fe^{II}TPP with SO_2 generates Fe^{III}TPP as final product and also reduces SO_2 to SO, via a Low Spin MeOH-Fe^{III}-SO intermediate (Intermediate 2) observed at 233K and at RT. The intermediate generates characteristic resonance Raman feature at 1014 cm^{-1}, which corresponds to 'S=O' stretch of the Intermediate 2. But this 'S=O' stretch hasn't been spectroscopically validated using isotopically labelled SO_2, but has been chemically trapped from the system as the Intermediate 2 releases SO to generate High Spin Fe^{III}TPP.[13] For that purpose cheletropic reaction of a diene with the SO was utilized.[19] On performing the reaction at lower temperature of 193K, we stumbled upon another proton dependent Low Spin

intermediate, Intermediate 1. To unearth its properties and to corroborate our experimental findings from UV-Vis and EPR spectroscopic studies, we did record resonance Raman spectroscopic experiments on our reaction mixture.

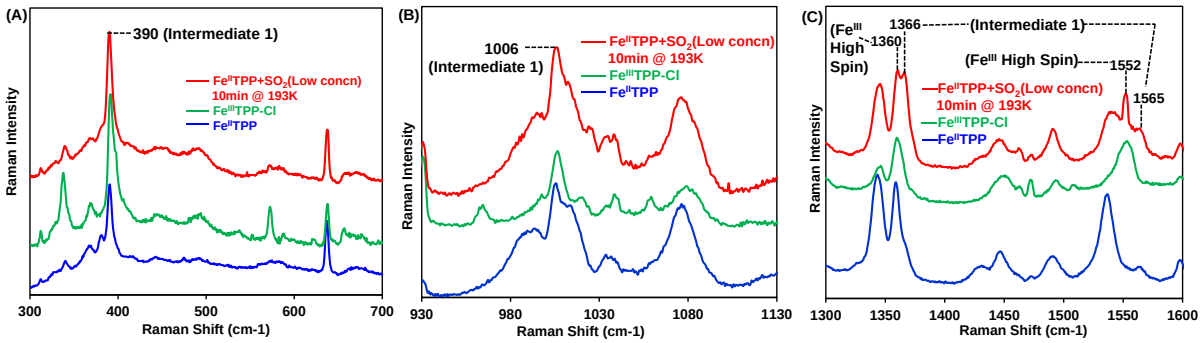

Figure 4.6 resonance Raman data of the reaction Fe^{II}TPP with SO_2-THF at very low concentration (red spectra). The reaction was performed at 193K and frozen after allowing to proceed for 10 minutes. Resonance Raman data of Fe^{III}TPP-Cl (green spectra) and Fe^{II}TPP (blue spectra) of similar concentrations have also been overlayed. (A) shows the lower energy region, (B) shows the moderate energy region and (C) shows the higher energy region. All the spectra were recorded at 77K

The samples prepared for EPR spectroscopy were also subjected to resonance Raman spectroscopy. The reaction mixture at 193K where Fe^{II}TPP was injected with SO_2-THF of very low concentration, which showed rhombic Fe^{III} Low Spin signals corresponding to Intermediate 1 in EPR, yielded some characteristic features in resonance Raman. The band at 390 cm^{-1} (Figure 4.5, A, red spectra), the band at 1006 cm^{-1} (Figure 4.5, B, red spectra) and 1366 cm^{-1} & 1565 cm^{-1} (Figure 4.5, C, red spectra), all are characteristic resonance Raman features of Intermediate 1, also identified from EPR spectroscopy. The 1366 cm^{-1} and 1565 cm^{-1} bands observed for Intermediate 1 are typical of 6 Coordinated Fe^{III} Low Spin n_4 and n_2 oxidation and spin state marker bands respectively.[20] Generation of Intermediate 1 necessitates the simultaneous generation of a High Spin Fe^{III} signal. In the resonance Raman spectra of the higher energy region along with the Low Spin Fe^{III} species, n_4 and n_2 marker bands at 1360 and 1552 cm^{-1}, characteristic of Fe^{III} High Spin species (Figure 4.5, C, red spectra), were also obtained.[20] The observation of Fe^{III} Low Spin species along with Fe^{III} High Spin species in resonance Raman spectra, proves the observation from EPR spectroscopy that Intermediate 1 is generated vis-à-vis Fe^{III} High Spin species.

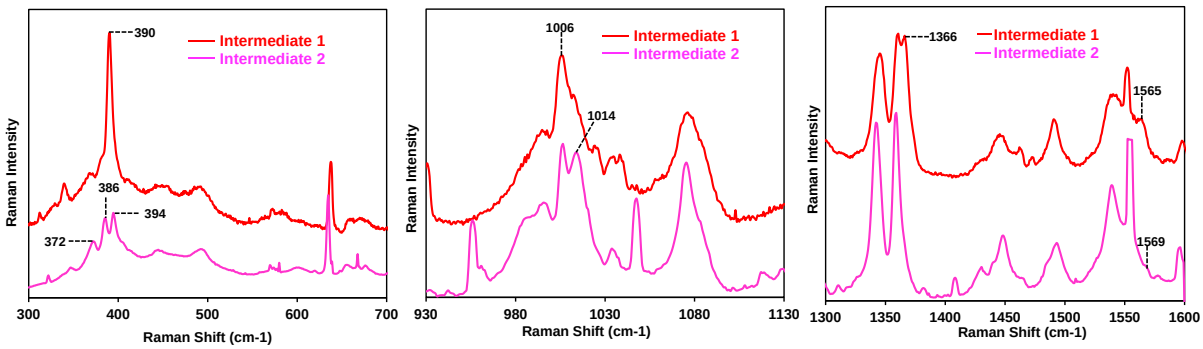

Figure 4.7 resonance Raman data overlay of the reaction Intermediate 1 (red spectra) and Intermediate 2 (pink spectra). For Intermediate 1, the reaction was performed at 193K and for Intermediate 2, the reaction was performed at RT, and after allowing both the reaction to proceed for 10 minutes, they were frozen. (A) shows the lower energy region, (B) shows the moderate energy region and (C) shows the higher energy region. All the spectra were recorded at 77K

The Intermediate 1 and 2 are two distinct species with easily discernible resonance Raman features. From their overlay (Figure 4.8) it can be observed that Intermediate 1 shows n_8 feature at 390 cm^{-1} (Figure 4.8, A, red spectra) while Intermediate 2 shows feature at 372, 386 and 394 cm^{-1} (Figure 4.8, A, pink spectra). The Intermediate 2 shows characteristic band at 1014 cm^{-1} (Figure 4.8, B, pink spectra) which corresponds to the unique 'S=O' stretching vibration of the MeOH-Fe^{III}TPP-SO Intermediate 2.[13] For Intermediate 1, that moderate energy region doesn't show any distinct peak other than at 1006 cm^{-1} (Figure 4.8, B, red spectra). Though Intermediate 1 is a Low Spin species, its nature is different from Intermediate 2. The former being an S=1/2 t_{2g}^5 Low Spin species with the unpaired e^- centered on the Fe^{3+}, gives rhombic EPR signal (Figure 4.4, red spectra)[18] while the latter being an S=1/2 t_{2g}^5 Low Spin species anti-ferromagnetically coupled to triplet SO, gives an axial EPR signal (Figure 4.4, green spectra).[13] This difference between the two S=1/2 Low Spin intermediates is also visible from the marker band region of the resonance Raman data. The marker band region of both the Intermediates are markedly different. The Intermediate 1 has n_4 and n_2 marker bands at 1366 and 1565 cm^{-1} (Figure 4.8, C, red spectra), characteristic of Low Spin Fe^{III} species[20] while the Intermediate 2 has n_2 marker band at 1569 cm^{-1} characteristic of Fe^{III} Low Spin, but the n_4 marker band corresponding to Fe^{III} Low Spin species is absent here. That can be possibly due to the fundamental difference in nature of these two Fe^{III} Low Spin species.

4.3.4 Intermediate 1 characterization studies:

In due course of SO_2 reduction using Fe^{II}TPP we stumble upon 2 intermediates, viz. Intermediate 1 and Intermediate 2. The Intermediate 2 is a 6C Low Spin MeOH-Fe^{III}TPP-SO species, which gets generated from Intermediate 1. As the Intermediate 2 has been

adequately characterized previously, the burden of proof for characterizing Intermediate 1 falls on us. What we know about Intermediate 1 is that via a proton dependent step, it generates MeOH-Fe^{III}TPP-SO (Intermediate 2). The Intermediate 1 also happens to be a Low Spin species. One thing can be guessed from here is that it's a 6C Low Spin MeOH-Fe^{III}TPP-SO_2^- species, which via a proton dependent step generates MeOH-Fe^{III}TPP-SO. In order to cement our guess on solid experimental evidence we did Isotope dependent resonance Raman studies, where Fe^{II}TPP was injected with $^{32}SO_2$ and $^{34}SO_2$ and their corresponding resonance Raman was recorded and Isotope shifts were looked into.

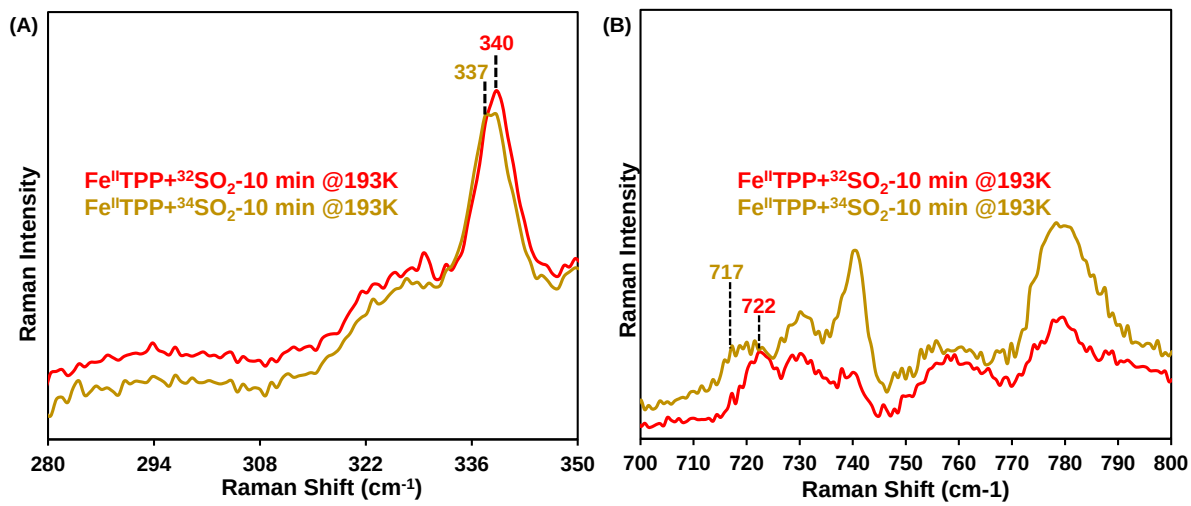

Figure 4.8 resonance Raman spectra of reaction between Fe^{II}TPP and $^{32}SO_2$-THF (red spectrum) and $^{34}SO_2$-THF (yellow spectrum) solution of low concentration, where reaction was allowed to proceed at 193K for 10 minutes and then frozen. Resonance Raman data were recorded on the frozen samples at 77K

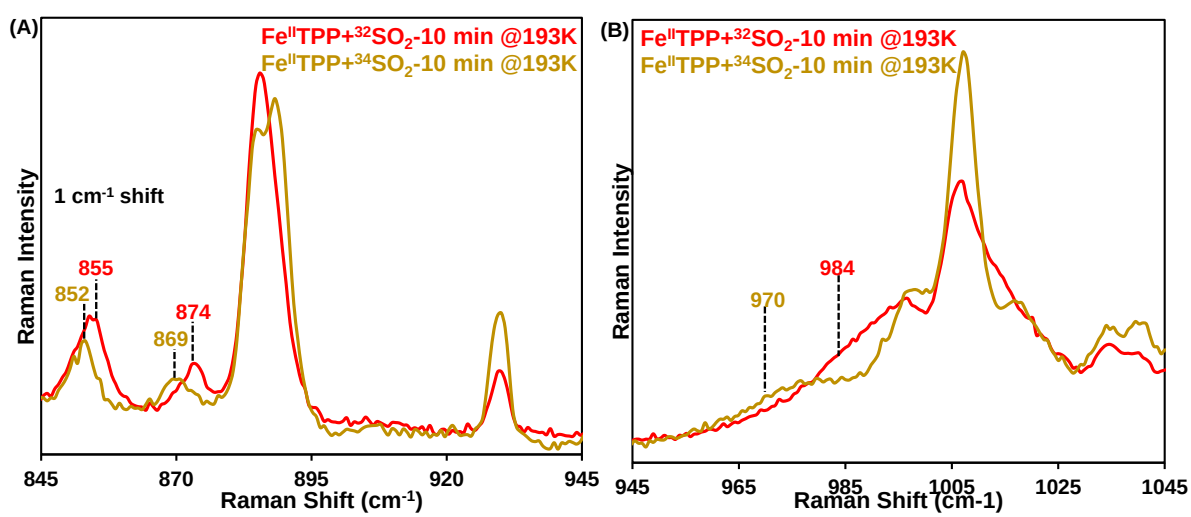

Figure 4.9 resonance Raman spectra of reaction between Fe^{II}TPP and $^{32}SO_2$-THF (red spectrum) and $^{34}SO_2$-THF (yellow spectrum) solution of low concentration, where reaction was allowed to proceed at 193K for 10 minutes and then frozen. Resonance Raman data were recorded on the frozen samples at 77K

On injecting $Fe^{II}TPP$ samples with $^{32}SO_2$-THF and $^{34}SO_2$-THF of low concentration and allowing the reaction to proceed at 193K for 10 minutes and freezing the reaction, Intermediate 1 was generated. Then their resonance Raman spectra were recorded. It was observed that the $^{34}SO_2$ injected samples were showing downshifts with respect to $^{32}SO_2$ injected $Fe^{II}TPP$ samples. A peak at 340 cm^{-1} shifted to 337 cm^{-1} (Figure 4.9, A). Another 5 cm^{-1} downshift was observed from 722 cm^{-1} to 717 cm^{-1} (Figure 4.9, B). Simultaneous downshifts were observed in other regions of the resonance Raman spectra. A 3 cm^{-1} downshift from 855 to 852 cm^{-1}, another 5 cm^{-1} downshift from 874 to 869 cm^{-1} (Figure 4.10, A) and an 14 cm^{-1} downshift from 984 to 970 cm^{-1} (Figure 4.10, B). These downshifts prove that these are S^{32}/S^{34} isotope sensitive vibrations. This proves that Intermediate 1 contains an Fe-S bond and collating the facts from the other spectroscopic experiments, we can say that the Intermediate 1 is a hexa Coordinated Low Spin Fe^{III} species bound to a S atom, and it also happens to be a proton dependent species. In this Intermediate 1 we have observed five S^{32}/S^{34} isotope sensitive bands; due to dearth in literature report about the isotope shifts of such systems, calls for computationally corroborating these bands. These experimental vibrations were compared against a Density Functional Theory (DFT) calculated vibrations of a 6C Low Spin MeOH-$Fe^{III}TPP$-SO_2^- species, where the S^{32} was systematically changed to S^{34} and protons to deuterium, as and where necessary.

4.3.5 DFT studies:

Experimental Data	DFT Data (BP86)	
Intermediate 1	**Low Spin MeOH-Fe^{III}-SO_2^- (^{34}S)**	**Assignment of vibration**
984 (970)	**973 (967)**	**S=O symmetric stretching**
340 (337)	**342 (341)**	**S=O bending**
722 (717)	**Unassigned**	
855 (852)		
874 (869)		

Table 4.2 The experimental spectral data has been compared to theoretical data, calculated using BP86 functional in DFT, a 6311g* basis set has been used for the calculations.

Geometrically optimized DFT calculations on 6C LS MeOH-Fe^{III}TPP-SO_2^- species were performed using BP86 functional. Theoretically calculated FTIR spectrum is used to measure the isotope shifts in various normal modes to compare them with experimental data. The experimentally observed isotope shift of 340 to 337 cm^{-1} (Figure 4.8, A) has also been observed in the calculated vibrational data, where 342 to 341 cm^{-1} shifts were observed (Table 2). These vibrations originate from S=O stretching vibrations.

Experimentally observed isotope shifts of 14 cm^{-1} where peak at 984 shifts to 970 cm^{-1} (Figure 4.9, B) was observed in theoretical calculations, where 973 shifts to 967 cm^{-1} (Table 2). The theoretical vibrations at 973 cm^{-1} were calculated to have symmetric S=O stretching vibrations, which shifts by 6 cm^{-1} on substituting ^{32}S with ^{34}S.

The other experimentally observed vibrations which shows shift with isotopic substitution, 722 to 717 cm^{-1}, 855 to 852 cm^{-1} and 874 to 869 cm^{-1} were not observed from the theoretical calculations. So they couldn't be assigned any particular vibrations and have been left unassigned.

All the above theoretical and experimental data points to the fact that the Intermediate 1 has Fe-S stretching, S=O bending and S=O stretching vibrations, which are isotope sensitive. These evidences, combined together with the evidences from UV-Vis and EPR spectroscopy, proves beyond reasonable doubt that the Intermediate 1 is indeed a MeOH-Fe^{III}TPP-SO_2^- species. The calculated Fe-S bond distance is 2.28 Å and S-O bond distance is 1.51 Ă, which is reasonably withing the range of acceptable Fe-S bond distance and charge delocalized bond distance of SO_2^- species.

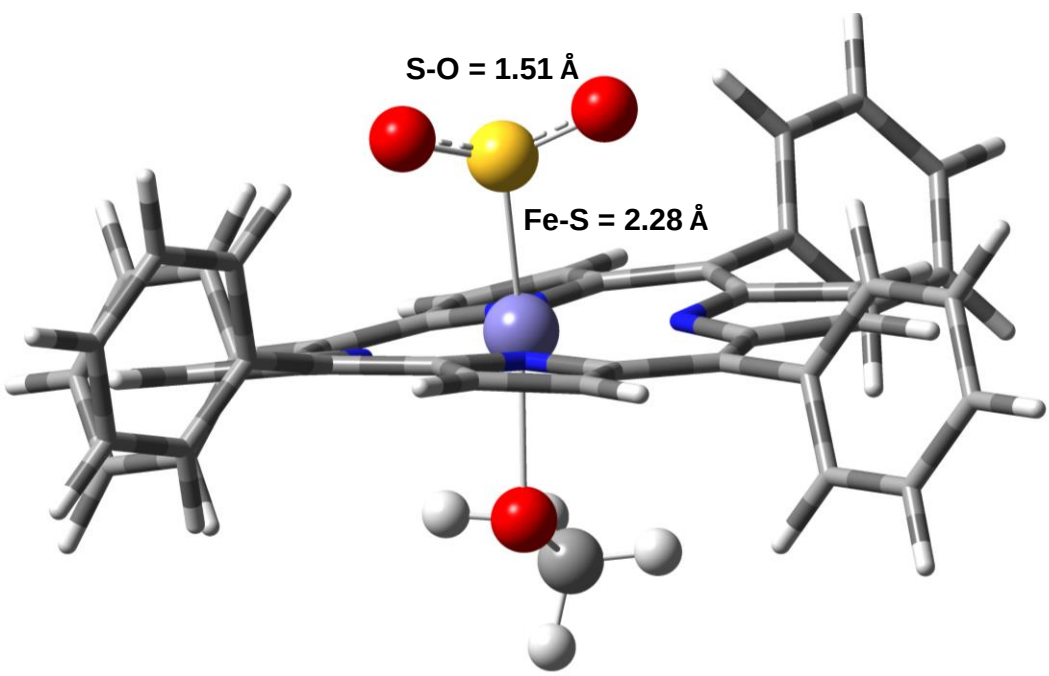

Figure 4.10. DFT optimized structure of Low Spin MeOH bound Fe^{III}TPP-SO_2^-. The Fe-S and S-O bond distances have been shown in the structure.

4.4 Conclusion:

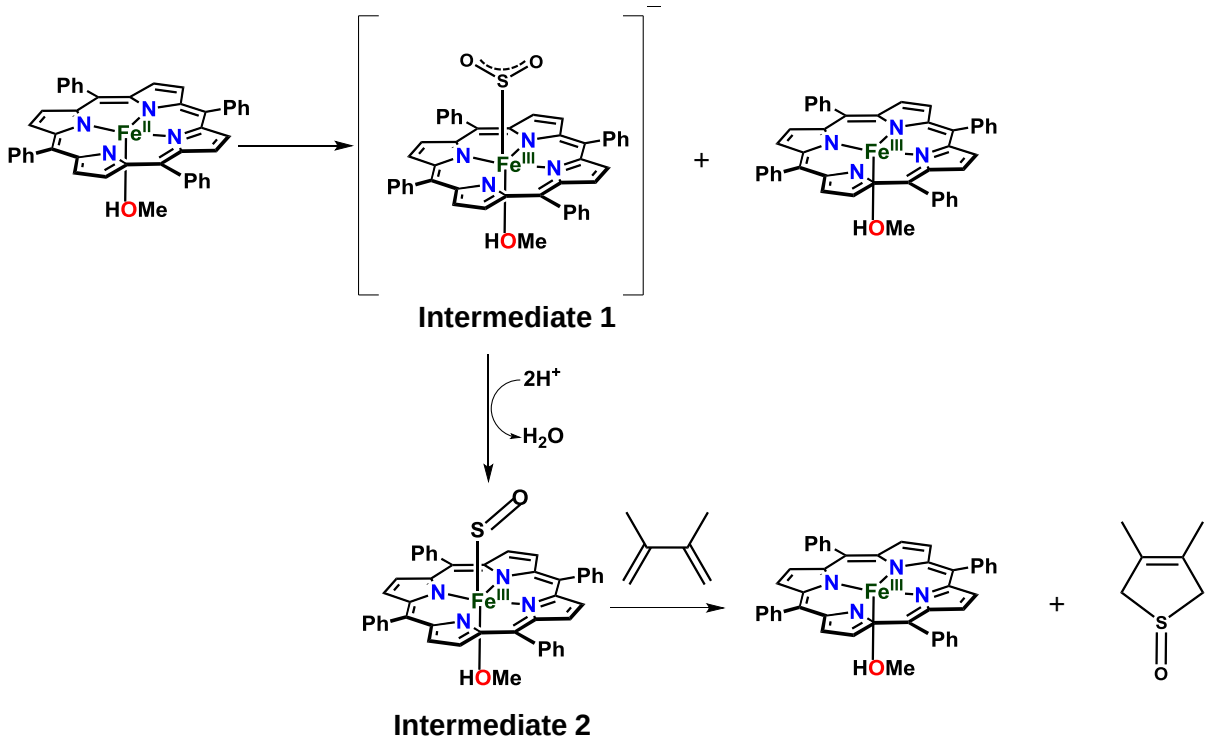

Scheme 4.1 The proposed mechanism of SO_2 reduction using $Fe^{II}TPP$, where the intermediates have been shown along with the side products

The reduction of SO_2 by $Fe^{II}TPP$ proceeds via a $2e^-/2H^+$ process, where the $2e^-$ are supplied by two molecules of $Fe^{II}TPP$, one from the $Fe^{II}TPP$ directly attached to the SO_2 and the other from a free $Fe^{II}TPP$. The SO_2 attached $Fe^{II}TPP$ generates two successive intermediates, Low Spin MeOH-$Fe^{III}TPP$-SO_2^- (Intermediate 1) and via a successive dehydration step another Low Spin MeOH-$Fe^{III}TPP$-SO (Intermediate 2). Both the intermediates have been adequately characterized. The Intermediate 1 characterization was done by Low Spin rhombic EPR signals and rR vibration bands, along with their isotope dependent shifts. They vibrations characteristic of the Fe-S and S-O bonds have also been corroborated with DFT where the Experimental and theoretical values go hand in hand. The generation of Intermediate 2 from Intermediate 1, via a proton dependent dehydration step has also been confirmed by proton dependent UV and EPR experiments. This is the first evidence of SO_2 reduction and intermediate characterization, outside a proton matrix, and this will help us in better understanding of the mechanism by which Sulfite Reductase enzyme reduces Sulfite into its other reduction products.

4.5 References:

1. Simon, J.; Kroneck, P. M. H., Chapter Two - Microbial Sulfite Respiration. In *Advances in Microbial Physiology*, Poole, R. K., Ed. Academic Press: 2013; Vol. 62, pp 45-117.
2. Murphy, M. J.; Siegel, L. M.; Kamin, H.; DerVartanian, D. V.; Lee, J. P.; LeGall, J.; Peck, H. D., Jr., An iron tetrahydroporphyrin prosthetic group common to both assimilatory and dissimilatory sulfite reductases. *Biochemical and biophysical research communications* **1973,** *54* (1), 82-8.
3. Crane, B. R.; Siegel, L. M.; Getzoff, E. D., Probing the Catalytic Mechanism of Sulfite Reductase by X-ray Crystallography: Structures of the Escherichia coli Hemoprotein in Complex with Substrates, Inhibitors, Intermediates, and Products. *Biochemistry* **1997,** *36* (40), 12120-12137.
4. Parey, K.; Warkentin, E.; Kroneck, P. M. H.; Ermler, U., Reaction Cycle of the Dissimilatory Sulfite Reductase from Archaeoglobus fulgidus. *Biochemistry* **2010,** *49* (41), 8912-8921.
5. Smith, K. W.; Stroupe, M. E., Mutational Analysis of Sulfite Reductase Hemoprotein Reveals the Mechanism for Coordinated Electron and Proton Transfer. *Biochemistry* **2012,** *51* (49), 9857-9868.
6. Finnegan, M. G.; Lappin, A.; Scheidt, W. R., Instability of the nitrite/iron (III) porphyrinate system. *Inorganic Chemistry* **1990,** *29* (2), 181-185.
7. Kuroi, T.; Nakamoto, K., Matrix-isolation infrared spectra of oxy(tetraphenylporphyrinato)iron(II) containing CS2 and SO2 as axial ligands. *Journal of Molecular Structure* **1986,** *146*, 111-121.
8. Reynolds, M. S.; Holm, R. H., Binding of oxysulfur anions to macrocyclic iron(II,III): [(Fe(TPP))2SO4] and Fe(Me6[14]-4,11-dieneN4)(S2O5)]. *Inorganica Chimica Acta* **1989,** *155* (1), 113-123.
9. Cocolios, P.; Lagrange, G.; Guilard, R.; Oumous, H.; Lecomte, C., Alkane (or arene)-sulphinato and -sulphonato-iron(III) porphyrins: synthesis and physicochemical properties; crystal structure of benzenesulphinato(5,10,15,20-tetraphenylporphyrinato)iron(III). *Journal of the Chemical Society, Dalton Transactions* **1984,** (4), 567-574.
10. Scheidt, W. R.; Lee, Y. J.; Finnegan, M. G., Reactions of sulfur dioxide with iron porphyrinates and the crystal structure of (hydrogen

sulfato)(tetraphenylporphinato)iron(III) hemibenzene solvate. *Inorganic Chemistry* **1988,** *27* (26), 4725-4730.

11. Crane, B. R.; Siegel, L. M.; Getzoff, E. D., Sulfite Reductase Structure at 1.6 Å: Evolution and Catalysis for Reduction of Inorganic Anions. *Science* **1995,** *270* (5233), 59-67.

12. Enemark, J. H.; Feltham, R. D., Principles of structure, bonding, and reactivity for metal nitrosyl complexes. *Coordination Chemistry Reviews* **1974,** *13* (4), 339-406.

13. Bhattacharya, A.; Kumar Nath, A.; Ghatak, A.; Nayek, A.; Dinda, S.; Saha, R.; Ghosh Dey, S.; Dey, A., Reduction of Sulfur Dioxide to Sulfur Monoxide by Ferrous Porphyrin**. *Angewandte Chemie International Edition* **2023,** *62* (10), e202215235.

14. Adler, A. D.; Longo, F. R.; Finarelli, J. D.; Goldmacher, J.; Assour, J.; Korsakoff, L., A simplified synthesis for meso-tetraphenylporphine. *The Journal of Organic Chemistry* **1967,** *32* (2), 476-476.

15. Mittra, K.; Singha, A.; Dey, A., Mechanism of Reduction of Ferric Porphyrins by Sulfide: Identification of a Low Spin FeIII–SH Intermediate. *Inorganic Chemistry* **2017,** *56* (7), 3916-3925.

16. Perdew, J. P., Density-functional approximation for the correlation energy of the inhomogeneous electron gas. *Physical Review B* **1986,** *33* (12), 8822-8824.

17. Pecul, M.; Marchesan, D.; Ruud, K.; Coriani, S., Polarizable continuum model study of solvent effects on electronic circular dichroism parameters. *The Journal of Chemical Physics* **2004,** *122* (2), 024106.

18. Walker, F. A., Magnetic spectroscopic (EPR, ESEEM, Mössbauer, MCD and NMR) studies of low-spin ferriheme centers and their corresponding heme proteins. *Coordination Chemistry Reviews* **1999,** *185-186*, 471-534.

19. Grainger, R. S.; Patel, B.; Kariuki, B. M.; Male, L.; Spencer, N., Sulfur Monoxide Transfer from peri-Substituted Trisulfide-2-oxides to Dienes: Substituent Effects, Mechanistic Studies and Application in Thiophene Synthesis. *Journal of the American Chemical Society* **2011,** *133* (15), 5843-5852.

20. Burke, J. M.; Kincaid, J. R.; Peters, S.; Gagne, R. R.; Collman, J. P.; Spiro, T. G., Structure-sensitive resonance Raman bands of tetraphenyl and "picket fence" porphyrin-iron complexes, including an oxyhemoglobin analog. *Journal of the American Chemical Society* **1978,** *100* (19), 6083-6088.

Chapter 5

SO_2 reduction using second sphere modified Ferrous Porphyrin

5.1 Introduction:

The reduction of SO_3^{2-} by ASiR and DSiR proceeds via a $6e^-/6H^+$ process. This $6e^-/6H^+$ reduction rection of Sulphite to Sulphide is facilitated by an enzyme present in these bacteria, known as Sulphite Reductase, which is also found in some archaea, plants and fungi.[1] This enzyme is a member of Oxidoreductase family of enzymes, falling under classification EC 1.8.1.2.[2] There are two different types of Sulfite Reductase enzymes: Assimilatory and Dissimilatory Sulfite Reductases. Assimilatory Sulfite Reductases (ASiR) have been extracted from *Escheria coli* bacteria while the Dissimilatory Sulfite Reductases (DSiR) have been extracted from Sulfate reducing bacteria. The DSiRs can again be classified into two classes: Desulfoviridin, extracted from *Desulfovibrio gigas* and Desulforubridin, extracted from *Desulfovibrio desulfuricans*. The ASiR catalyses Assimilatory Sulfite reduction, a minor pathway facilitating biosynthesis of cysteinyl amino acids, while the DSir catalyses Dissimilatory Sulfite reduction, which is a large-scale process linked to cellular respiration. The Dissimilatory pathway is observed in anaerobes, which evolved this pathway for cellular respiration in early anoxic conditions of earth.[3] The basic difference between Assimilatory and Dissimilatory pathway is the end product; in the former S^{2-} produced from SO_3^{2-} or SO_4^{2-} is assimilated in the cell to generate S containing biomolecules like Cysteine, which is further metabolised into Methionine, Glutathione and many other compounds.[4] While in the dissimilatory pathway, S^{2-} is generated from SO_4^{2-}, which acts as a terminal e^- acceptor. The generated S^{2-} in the dissimilatory pathway is released as Trithionates ($S_3O_3^{2-}$) or Thiosulphate ($S_2O_3^{2-}$).[5] This reduction of SO_3^{2-} (generated from SO_4^{2-} via some other enzymatic pathways) to S^{2-} proceeds via a $6e^-/6H^+$ pathway, the mechanism of which is still not clearly understood.[6] There is another uncommon DSiR, isolated from *Wolinella succinogenes* known as SirA having Octahaem cytochrome c MccA, which is a haem c-copper sulphite reductase, that also catalyses the $6e^-/6H^+$ reduction of SO_2 to S^{2-}.[7] Despite their difference in final products, both the ASiR and DSiR share common structures. Both the ASiR (extracted from *Escheria coli*) and DSiR (extracted from *Desulfovibrio desulfuricans*) contain pentacoordinate high spin siroheme moiety, however there is another type of ASiR (extracted from *Desulfovibrio vulgaris*) that has hexacoordinate low spin siroheme centre.[8] The Siroheme moiety of the heme chromophore belonging to ASiR is iron tetrahydroporphyrin of the isobacteriochlorin family, with octacarboxylic acid substitution around the porphyrin (Figure 3). There are some differences in the absorption spectra and EPR spectra of the ASiR and DSiR extracted from *E. coli* and *D. desulfuricans* but this difference is due to variation in their local environment, while residing inside their respective proteins.[9] The SiRs feature a siroheme cofactor (Figure 3) in its active site which is a member of the isobacteriochlorin family of heme cofactors.[10] The most extensively studied active site among the different Sulfite Reductaes are ASiR from *E.*

coli. The active site of the ASiR extracted from *E. coli* apart from having the siroheme moiety of the isobacteriochlorin family, via its proximal binding site, is covalently bridged to a Cysteine thiolate ligand, which again bridges it to a Fe_4S_4 cluster (Figure 2, bottom).[11] The Fe_4S_4 cluster acts as an e^- pump and transfers e^- via the Cysteine thiolate linkage to the Siroheme moiety, as a result of which the ASiR active site reduces the SO_3^{2-} ion to S^{2-} ions.[12] The Siroheme moiety remains in High Spin S = 5/2 state and the Fe_4S_4 cluster Fe centres are in the +2 diamagnetic oxidation state. The High Spin Fe centre of Siroheme is exchange coupled with the cluster. All the oxidation state and exchange coupling have been evidenced from EPR and Mössbauer spectroscopy on the isolated enzymes.[13] These observations have been further backed up by other spectroscopic evidences in the form of ^{57}Fe ENDOR (electron-nuclear double resonance), rR spectroscopy by Soret band excitation[14] paramagnetic NMR[15] and some crystallographic studies.[16] The siroheme active site sits on the surface of the protein and in a positively charged cavity containing several lysine and arginine residues. These residues stabilize the binding of the substrate and intermediates via H-bonding and provide protons needed for the reduction of SO_3^{2-} to H_2S. The distal site of SiRHP (Sulfite Reductase Hemoprotein) is designed to accommodate substrates like SO_3^{2-} and perform acid catalysis on them. The Lysine and Arginine residues present in the distal site helps in substrate binding and they act as conduits of proton transfer, either directly or via intervening H_2O molecules. This protonation plays a major role in $6e^-/6H^+$ reduction of SO_3^{2-} to S^{2-}.[11]

As the reason behind the substrate binding and protonation is the Lysine and Arginine Amino acid residues in the distal substrate binding site, study of the SO_2 reduction in presence of varying distal substrate binding site is worth pursuing, to better understand the mechanism of SO_2 reduction. In this regard the use of porphyrin based structural and functional model complexes of SiRHP can be explored. In our previous works, we have studied the SO_2 reduction using Fe^{II} Tetraphenylporphyrin and have achieved $2e^-/2H^+$ reduction of SO_2 and proposed a detailed mechanistic pathway of the reaction, where we stumbled upon two novel intermediates. In this work we would like to explore the SO_2 reduction reaction by using second sphere modified Iron metalated porphyrins, in the hope of exploring the role of second sphere modification on SO_2 reduction. To achieve that goal, we have used a second sphere modified porphyrin with distal basic residues which gets protonated *in situ* and supplies proton to the substrate SO_2, binding at the distal site with Fe. The porphyrin used in this case is a mononuclear Iron porphyrin having pendant Pyridyl group as a second sphere modified basic residue (FeL_2 or Fe Pydn), which is known to supply protons and perform facile and selective $4e^-/4H^+$ O_2 reduction.[17]

In this work we have done a comparative study, using Fe^{II}TPP and Fe^{II}Pydn, two porphyrins with and without second sphere modifications, of the SO_2 reduction reaction. In both cases we

are stumbling across the same set of intermediates, which might indicate that the reactions proceed via similar mechanisms, as elucidated in our previous works.[18] But the major difference happens in the reaction kinetics. There is clearly a difference in rate of SO_2 reduction when a basic second sphere modification is introduced in our system.

5.2 Experimental Section:

5.2.1 Materials:

All the reagents used were of the best commercially available quality. H_2SO_4 (98%, Merck), Na_2SO_3 (anhydrous, Merck), Silica (Merck), Na_2SO4 (Merck), all were bought from respective vendors and used without further purification. Benzaldehyde (Spectrochem), Pyrrole (Spectrochem), Glacial Acetic acid (Spectrochem), Na_2S (Spectrochem) were bought from respective vendors. 2,4,6-Trimethylpyridine (Sigma-Aldrich), Ferrous Bromide (anhydrous, Sigma-Aldrich), HCl (37%, Merck), were used for $Fe^{III}TPP$ synthesis. Tetrahydrofuran, Methanol, Hexane were sourced from Finar Chemicals and used only after subjecting them to adequate drying and distilling procedures. Dry and pure SO_2 gas was passed through a solution of conc. H_2SO_4 to remove any moisture and tested using GC-MS prior to use (Figure S1). The solubility of SO_2 in THF (after 20 mins purging) is assumed to be 0.3-0.5 M as is the case for commercial sources of the same (https://www.sigmaaldrich.com/catalog/product/aldrich/901592). All solvents used were dried and degassed before use. Absorption spectra were obtained by a UV-Vis diode array spectrophotometer (Agilent 8453). EPR experiments were performed at 77 K in a liquid nitrogen finger Dewar. EPR spectra were obtained by a JEOL FA200 spectrophotometer with the following parameters- modulation width: 10 gauss; amplitude: 20; time constant: 300 ms; power: 2 mW; frequency: 9.25 GHz. The EPR data was simulated using JEOL Anisotropic Simulation software. Resonance Raman (rR) data were collected using 413.1 nm excitation from a Kr^+ ion source (Sabre Coherent Inc.) and a Trivista 555 triple spectrophotometer (gratings used in the three stages were 900, 900, and 2400 grooves/mm) fit with an electronically cooled Pixis CCD camera (Princeton Instruments). The irradiation power kept at the sample is 8-10 mW, so that photodegradation does not take place. All the data were collected at 77 K in a liquid N_2 cooled finger Dewar after preparing the reaction mixtures at their respective reaction temperature and freezing them after a stipulated time.

5.2.2 Methods:

5.2.2 a) Synthesis:

Synthesis of Tetraphenylporphyrin (TPP):

Freshly distilled pyrrole (56 ml, 0.8 mol) and 80 ml (0.8 mol) of reagent grade benzaldehyde are added to 3 lit. of refluxing reagent grade propionic acid. (Note: crystalline material is not direct,ly obtained if acetic acid is used.) After refluxing for 30 min, the solution is cooled to room temperature and filtered, and the filter cake is washed thoroughly with methanol. After a hot water wash, the resulting purple crystals are air dried, and finally dried in vacuo to remove adsorbed acid to yield 25 g (20%, yield) of TPP. Spectrophotometric analysis shows that only 1% of the TPP yield remains in the filtrate and also that the filtered material is about 3% tetraphenylchlorin (TPC) by weight. This method was developed by Adler *et al.*[19]

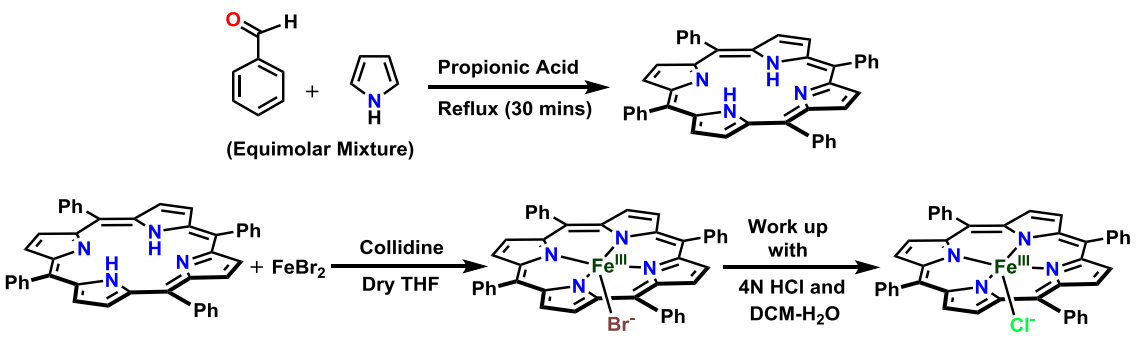

Scheme 5.1 Synthesis of TPP and Fe^{III}TPP by the reported procedure of Adler *et al*[19]

Synthesis of Fe^{III}TPP:

The synthesized 100mg, 0.162 mmol TPP was dissolved in dry degassed THF solvent inside a glove box and then stirred with 98.6 mg, 0.810 mmol 2,4,6-trimethyl pyridine (Collidine) for 30 minutes for the purpose of deprotonation of the pyrrolic protons. Then 350 mg, 1.62 mmol $FeBr_2$ metallic salt was added into the solution and left under stirring condition and the reaction was followed by TLC until disappearance of the TPP spot and appearance of a new spot. The reaction mixture was taken out of the glove box, the THF was removed from the reaction mixture *in vacuo* and the reaction was worked up with DCM and water after treating with 4N HCl to remove excess $FeBr_2$.The organic layer was dried with Na_2SO_4 and evaporated through a rotary evaporator. The solid compund was purified by column chromatography using 5:95 MeOH-DCM solution to afford the Fe^{III}TPP-Cl (HCl being the source of Cl^- in the resulting compound) (Scheme 1).

Synthesis of Monoaminephenylporphyrin:

The synthesis of o-aminophenyltris(phenyl)-porphyrin was done following well established reported procedures of Collman et al.[20]

Synthesis of FePydn:

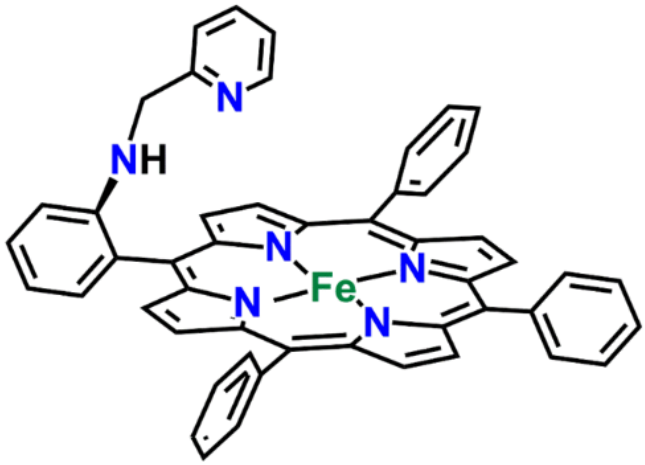

Figure 5.1 Synthesized Fe^{II} Pydn

The synthesis of FePydn was done following reported procedures of Bhunia et al.[17]

5.2.2 b) Sample preparation for UV-Vis Spectroscopy:

Synthesized Fe^{III}TPP and Fe^{III}Pydn was dissolved in THF to prepare 1 mM solution. It was subjected to reduction using a 0.5 eq. (20 mM stock solution) of Na_2S dissolved in dry degassed methanol or dry degassed CD_3OD.[21] The reduction was monitored using UV-Vis spectroscopy. Pure and dry SO_2 gas was bubbled in dry degassed THF to prepare a saturated solution of SO_2 in THF. 10-80 µL of SO_2 saturated THF (0.3-0.5 M) was added to the ferrous porphyrin and the absorption was recorded. For the kinetic runs, data at 0.5 s intervals were recorded.

5.2.2 c) Sample Preparation for EPR and Raman Spectroscopy:

Fe^{III}TPP and Fe^{III}Pydn were reduced to their Fe^{II} state inside the glovebox using 0.5eq. Na_2S dissolved in dry degassed MeOH and/or CD_3OD. In EPR Tubes, 20 µL, 5 mM solution of Fe^{II}TPP were taken and maintained at different temperatures like 193K, RT. Then they were injected with an 80 µL saturated solution of dry and pure SO_2 gas in THF (or $^{34}SO_2$ bubbled THF) to afford a 100 µL solution of 1 mM concentration reaction mixture. The reaction mixtures were allowed to progress for required time before freezing them in liq. N_2 for EPR analysis and resonance Raman analysis.

5.3 Results and Discussion:

5.3.1 UV-Visible studies:

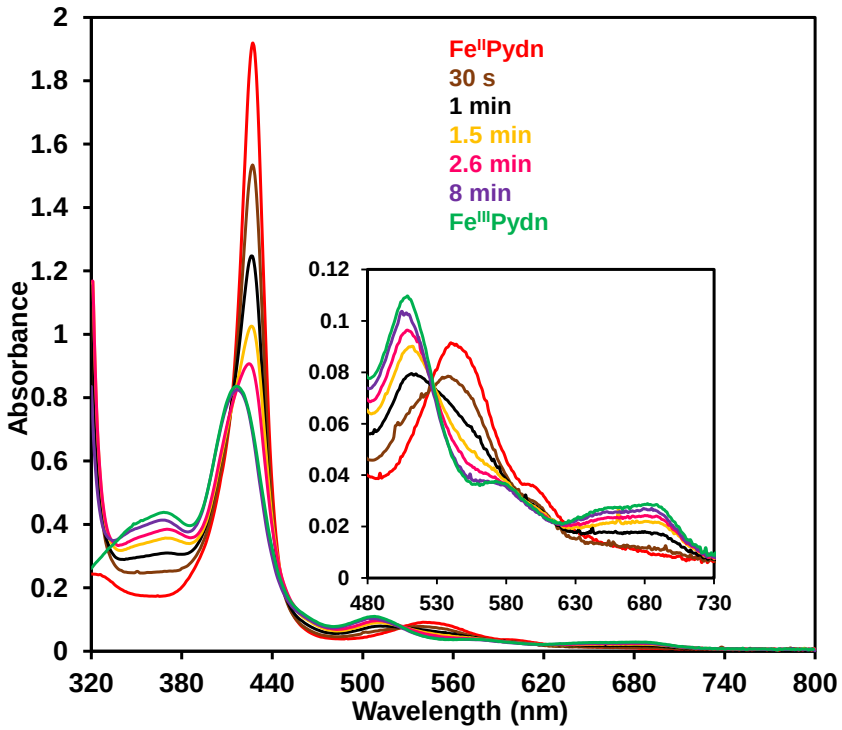

Figure 5.2 Absorbance data of the Fe^{II}Pydn (red), the resulting absorbance data at different time for the RT reaction between Fe^{II}Pydn+SO_2-THF, showing the Soret bands. Inset: Q-band region of the given spectra

A solution of Fe^{II}Pydn showing characteristic Soret and Q-bands at 426 and 540 nm[17] was injected with a saturated solution of SO_2-THF. The change in absorbance was studied for the reaction by recording absorbance data at different time, in due course of the reaction. On SO_2 injection the Fe^{II}Pydn got oxidized to Fe^{III}Pydn, showing its characteristic UV absorbance features[17]. The Uv features show a clear isosbestic point, which indicates the gradual oxidation of Fe^{II}Pydn to Fe^{III}Pydn in presence of SO_2.

To ascertain the effect of second sphere modification, a comparative study was done where both Fe^{II}TPP and Fe^{II}Pydn were subjected to SO_2 and their UV absorbance were recorded. But the reaction was done at a lower temperature. Due to lack of Low Temperature UV instrument set-up, two separate quartz cuvettes containing the Fe^{II}TPP and Fe^{II}Pydn solution had been kept in low temperature bath prepared at 193K and then they were injected with SO_2 and after certain time intervals their UV absorbance were recorded by bringing them out temporarily in Room Temperature conditions and recording the spectra as quick as possible, the cuvettes were returned back to the low temperature baths.

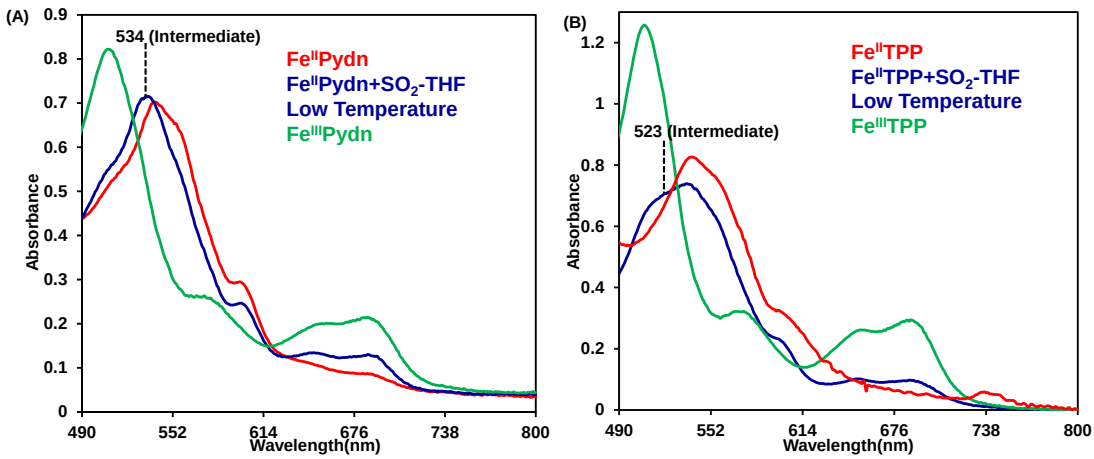

Figure 5.3 Absorbance data of (A) Fe^{II}Pydn (red), Fe^{II}Pydn reaction with SO_2-THF at low temperature (blue) and Fe^{III}Pydn (green) and (B) Fe^{II}TPP (red), Fe^{II}TPP reaction with SO_2-THF at low temperature (blue) and Fe^{III}TPP (green). Only the Q-region of the spectra has been studied under higher concentrations.

From the comparative study it has been observed that both the reaction passes through intermediates. The Fe^{II}Pydn on reacting with SO_2 makes way for Fe^{III}Pydn via a 534 nm intermediate (Figure 5.2. A, blue spectra) while the Fe^{II}TPP on reacting with SO_2 makes way for Fe^{III}TPP via an intermediate at 523nm. These kinds of intermediates are unprecedented and in the previous RT UV experiments on either of Fe^{II}TPP or Fe^{II}Pydn, no such intermediates were observed.

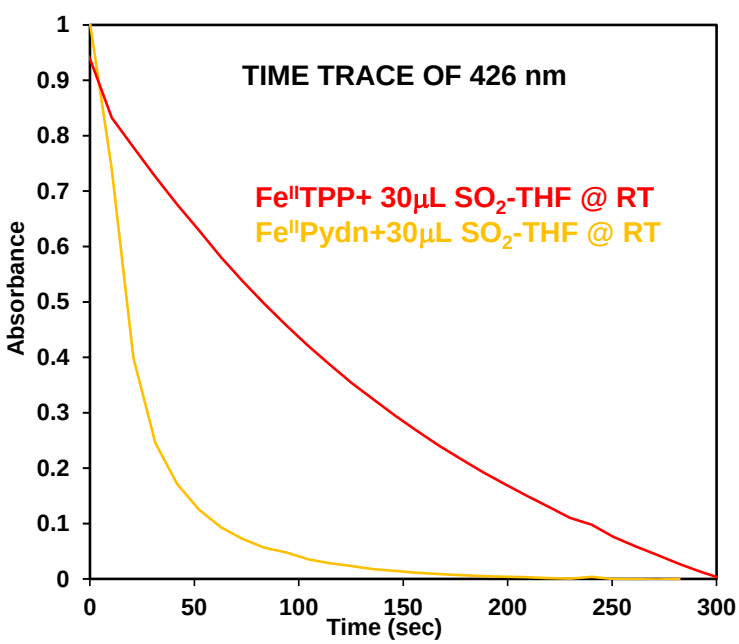

Figure 5.4 Absorbance vs Time Kinetic trace of 426 nm band of Fe^{II}TPP (red spectra) and Fe^{II}Pydn (yellow spectra) with 30 mL SO_2-THF. The reactions were performed at RT.

The time dependent decay of 426 nm band characteristic of both Fe^{II}TPP and Fe^{II}Pydn were studied in due course of RT reaction with SO_2. It was observed that reaction of Fe^{II}Pydn is faster than the reaction with Fe^{II}TPP.

So from the UV experiments it has become clear that Fe^{II}Pydn reacts with SO_2 to produce Fe^{III}Pydn, just like Fe^{II}TPP does. And the reaction rate of Fe^{II}Pydn is faster than Fe^{II}TPP, indicating a probable second sphere interaction in the reaction.

5.3.2 EPR spectroscopic studies:

Now, the Fe^{II}TPP reaction with SO_2 passes through a Low Spin Fe^{III}TPP-SO_2^- intermediate and another Low Spin Fe^{III}TPP-SO intermediate[18]. Whether the Fe^{II}Pydn reaction of SO_2 also passes via similar intermediates, it was necessary to study the reaction using EPR spectroscopy at lower temperature.

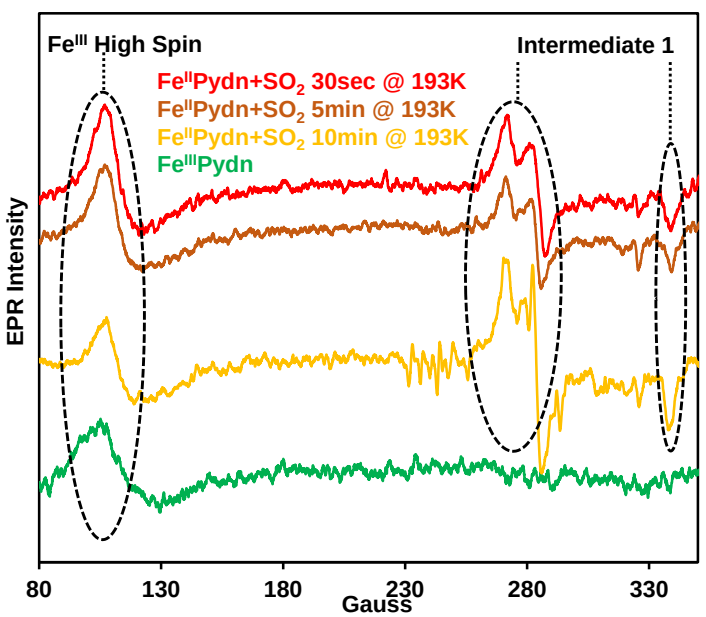

Figure 5.5 EPR spectra of reaction between Fe^{II}Pydn and saturated SO_2-THF solution where the reaction was performed at 193K and allowed to proceed for 30 s (red spectra), 5 min (brown spectra), 10min (yellow spectra) and Fe^{III}Pydn (green spectra). After allowing the reaction to proceed for different time intervals, the samples were frozen. X-band EPR data were recorded on the frozen samples at 77K

The reaction of Fe^{II}Pydn with SO_2 gave an indication of an intermediate. So, at low temperature of 193K the reaction was probed using EPR spectroscopy. Fe^{II}Pydn was allowed to react with SO_2 at 193K for different time periods. The reaction mixture of 30 s, 5min and 10 min (Figure 5.3 red, brown and yellow spectra) all g values at 2.37, 2.31 and 1.91, characteristic of Fe^{III} Low Spin rhombic signal[22], giving indication of a probable intermediate,

just like Fe^{II}TPP reaction with SO_2. Apart from this signal, there was also associated generation of Fe^{III} High Spin signal. Appearance of these two signals indicate that the reaction between Fe^{II}Pydn and SO_2 generates a High Spin Fe^{III} signal as indicated by the UV studies and also proceeds via an Fe^{III} Low Spin intermediate species, having similarity to the reaction between Fe^{II}TPP and SO_2.

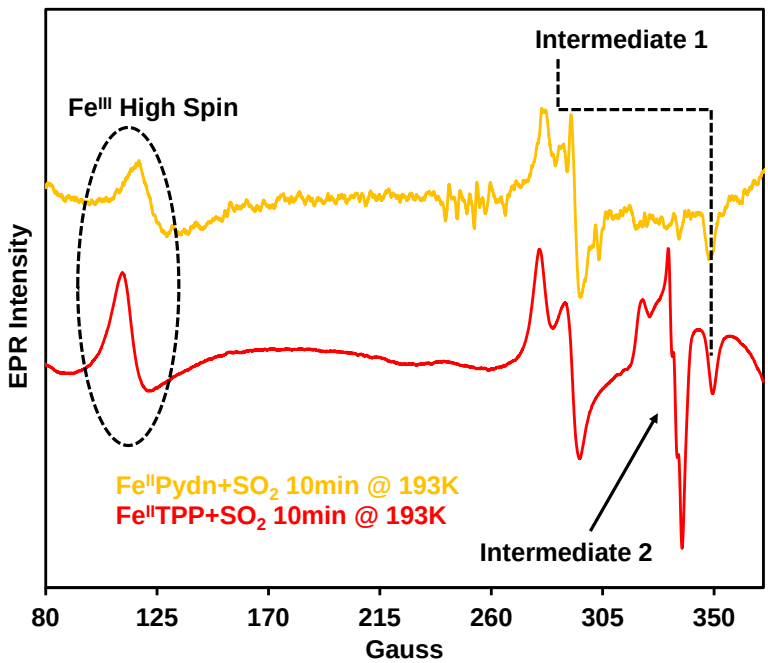

Figure 5.6 EPR spectra of reaction between Fe^{II}Pydn (yellow) and Fe^{II}TPP (red) and saturated SO_2-THF solution, where reaction was allowed to proceed at 193K for 10 minutes and then frozen. X-band EPR data were recorded on the frozen samples at 77K

To get a better understanding about the nature of second sphere interaction in the course of SO_2 reduction using Fe^{II}Pydn, a comparison was done where both Fe^{II}Pydn and Fe^{II}TPP were reacted with saturated SO_2-THF at 193K and the reaction was allowed to proceed for 10 minutes. The Fe^{II}TPP generated the expected intermediates, Intermediate 1 and Intermediate 2 along with Fe^{III} High Spin signal. What is interesting is that Fe^{II}Pydn also generated signales similar like Intermediate 1 but the Intermediate 2 signal was very weak. This implies that either the reaction has been frozen at Intermediate 1 stage or the reaction proceeds via some other pathway, where Intermediate 2 is not generated at all. From our UV-Vis Kinetics study of this comparative RT reaction, it was clear that Fe^{II}Pydn generates Fe^{III}Pydn after reacting with SO_2 at a much faster rate than Fe^{II}TPP (Figure 5.2), but the EPR data points at a slower reaction. If the first implication of the EPR data is correct that the Fe^{II}Pydn reaction has not proceeded beyond Intermediate 1 stage while Intermediate 2 signal clearly develops in Fe^{II}TPP reaction, then the EPR contradicts the UV-Vis data. But it is also possible that the Fe^{II}Pydn might

entirely bypass the Intermediate 2 stage and generates Fe^{III}Pydn via some other pathway. In that case we won't be able to observe Intermediate 2 properly. This apparent contradiction has to be ruled out by further reaction studies.

5.3.3 resonance Raman studies:

To further ascertain the intermediates observed from the EPR spectroscopic studies of the SO_2 reduction using Fe^{II}Pydn, probing of the same employing resonance Raman (rR) spectroscopy was necessary. So, we subjected the reaction mixtures prepared for EPR studies to rR spectroscopy.

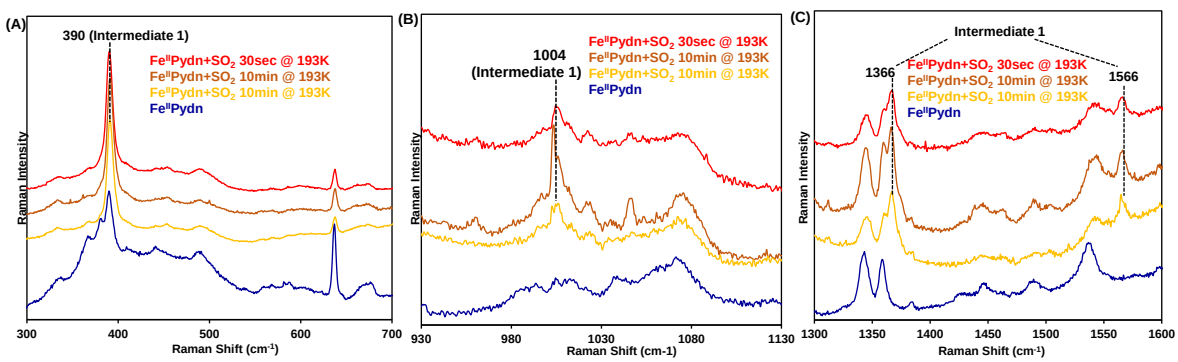

Figure 5.7 resonance Raman data of the reaction Fe^{II}Pydn with saturated SO_2-THF. The reaction was performed at 193K and frozen after allowing to proceed for 30 s (red), 5 min (brown), 10 min (yellow). Resonance Raman data of Fe^{II}Pydn (blue spectra) of similar concentrations have also been overlayed. (A) shows the lower energy region, (B) shows the moderate energy region and (C) shows the higher energy region. All the spectra were recorded at 77K

The samples prepared for EPR spectroscopy were also subjected to resonance Raman spectroscopy. The reaction mixture at 193K where Fe^{II}Pydn was injected with saturated SO_2-THF, which showed rhombic Fe^{III} Low Spin signals corresponding to Intermediate 1 in EPR, yielded some characteristic features in resonance Raman. The band at 390 cm^{-1} (Figure 5.5, A), the band at 1006 cm^{-1} (Figure 4.5, B) and 1366 cm^{-1} & 1565 cm^{-1} (Figure 4.5, C) all are characteristic resonance Raman features of Intermediate 1, also identified from EPR spectroscopy. The 1366 cm^{-1} and 1565 cm^{-1} bands observed for Intermediate 1 are typical of 6 Coordinated Fe^{III} Low Spin n_4 and n_2 oxidation and spin state marker bands respectively.[23] Generation of Intermediate 1 necessitates the simultaneous generation of a High Spin Fe^{III} signal. In the resonance Raman spectra of the higher energy region along with the Low Spin Fe^{III} species, n_4 and n_2 marker bands at 1360 and 1552 cm^{-1}, characteristic of Fe^{III} High Spin species (Figure 4.5, C, red spectra), were also obtained.[23] The observation of Fe^{III} Low Spin species along with Fe^{III} High Spin species in resonance Raman spectra, proves the

observation from EPR spectroscopy that Intermediate 1 is generated vis-à-vis Fe^{III} High Spin species.

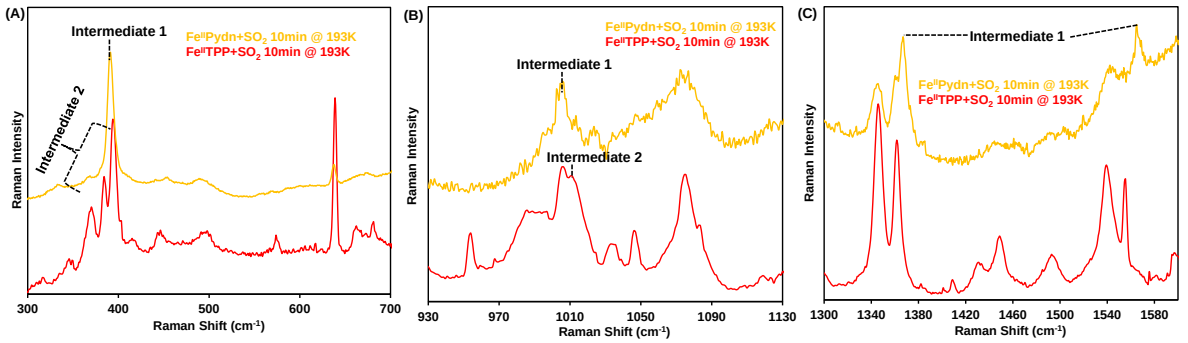

Figure 5.8 resonance Raman data overlay of the reaction between SO_2-THF and Fe^{II}Pydn (yellow) and Fe^{II}TPP (red). Both the reactions were performed at 193K, and after allowing both the reactions to proceed for 10 minutes, they were frozen. (A) shows the lower energy region, (B) shows the moderate energy region and (C) shows the higher energy region. All the spectra were recorded at 77K

Comparing the Fe^{II}Pydn and Fe^{II}TPP reaction with saturated SO_2-THF, performed at 193K for 10 mins, it was observed that Fe^{II}Pydn reaction generates rR peaks corresponding to Intermediate 1 while the Fe^{II}TPP reaction generates rR peaks corresponding to Intermediate 2. This observation goes hand in hand with our EPR spectroscopic results. This goes on to prove, when Fe^{II}Pydn and Fe^{II}TPP reacts with SO_2 under similar time scale, the former generates only Intermediate 1 while the latter generates a mixture of Intermediate 1 and Intermediate 2. Apparently, the Fe^{II}Pydn reaction is slower than the Fe^{II}TPP reaction and the contradiction with UV-Vis data still stands.

The rR peaks obtained from the Fe^{II}Pydn reaction with SO_2 reaction, which indicates formation of Low Spin Fe^{III} intermediate, cannot be confirmed as Fe^{III}Pydn-SO_2^- species. Since, their DFT corroboration and isotopically labelled rR shifts studies are yet to be done. Without doing those experiments and the theoretical calculations, one can only speculate that the reaction proceeds, via an Intermediate 1, since all the UV-Vis, EPR and rR data bears some similarities with the well characterized reaction intermediates of Fe^{II}TPP reaction with SO_2-THF. It is expected that Fe^{II}Pydn being different from Fe^{II}TPP only in respect of the second sphere pendant groups, won't alter the course of the reaction much, but only tamper with the reaction kinetics up to some extent.

5.4 Conclusion:

Here it is observed that using second sphere modified prophyrins having pendant Pyridyl group, the SO_2 reduction proceeds by a Low Spin Fe^{III} intermediate, which is likely to be $Fe^{III}TPP\text{-}SO_2^-$, but we cannot be sure about the nature of the intermediate with the data we have. Based on some follow-up work which involves DFT corroboration, isotope dependent studies and a lot of kinetic experiments supplemented by more elaborate spectroscopic results we will be able to elucidate the effect of second sphere modification. But what we can say conclusively from here that the rate of SO_2 reduction is different in presence and in absence of second sphere modified porphyrins, Fe^{II} Pydn and $Fe^{II}TPP$. So, it's worth mentioning that such kind of studies on SO_2 reduction reaction has not been done outside protein matrices. This opens up a lot of possibilities of further exploration of this field of work, which will help us in better understanding of the SO_2 reduction reaction and the mechanism of action of Sulfite Reductase enzyme and the role which the amino acid residues like Arginine and Lysine performs in the distal site of SiRHP.

5.5 References:

1. Brychkova, G.; Yarmolinsky, D.; Ventura, Y.; Sagi, M., A Novel In-Gel Assay and an Improved Kinetic Assay for Determining In Vitro Sulfite Reductase Activity in Plants. *Plant and Cell Physiology* **2012,** *53* (8), 1507-1516.

2. Siegel, L.; Murphy, M.; Kamin, H., Reduced Nicotinamide Adenine Dinucleotide Phosphate-Sulfite Reductase of Enterobacteria. *Journal of Biological Chemistry* **1973,** *248*, 251-264.

3. Grein, F.; Ramos, A. R.; Venceslau, S. S.; Pereira, I. A. C., Unifying concepts in anaerobic respiration: Insights from dissimilatory sulfur metabolism. *Biochimica et Biophysica Acta (BBA) - Bioenergetics* **2013,** *1827* (2), 145-160.

4. Leustek, T.; Martin, M. N.; Bick, J. A.; Davies, J. P., PATHWAYS AND REGULATION OF SULFUR METABOLISM REVEALED THROUGH MOLECULAR AND GENETIC STUDIES. *Annual review of plant physiology and plant molecular biology* **2000,** *51*, 141-165.

5. Kobayashi, K.; Takahashi, E.; Ishimoto, M., Biochemical Studies on Sulfate-reducing Bacteria

XI. Purification and Some Properties of Sulfite Reductase, Desulfoviridin. *The Journal of Biochemistry* **1972,** *72* (4), 879-887.

6. Barton, L. L.; Fauque, G. D., Chapter 2 Biochemistry, Physiology and Biotechnology of Sulfate-Reducing Bacteria. In *Advances in Applied Microbiology*, Academic Press: 2009; Vol. 68, pp 41-98.

7. Hermann, B.; Kern, M.; La Pietra, L.; Simon, J.; Einsle, O., The octahaem MccA is a haem c–copper sulfite reductase. *Nature* **2015,** *520* (7549), 706-709.

8. Wolfe, B. M.; Lui, S. M.; Cowan, J. A., Desulfoviridin, a multimeric-dissimilatory sulfite reductase from Desulfovibrio vulgaris (Hildenborough) Purification, characterization, kinetics and EPR studies. *European Journal of Biochemistry* **1994,** *223* (1), 79-89.

9. Murphy, M. J.; Siegel, L. M.; Kamin, H.; DerVartanian, D. V.; Lee, J. P.; LeGall, J.; Peck, H. D., Jr., An iron tetrahydroporphyrin prosthetic group common to both assimilatory and dissimilatory sulfite reductases. *Biochemical and biophysical research communications* **1973,** *54* (1), 82-8.

10. Murphy, M. J.; Siegel, L. M.; Tove, S. R.; Kamin, H., Siroheme: a new prosthetic group participating in six-electron reduction reactions catalyzed by both sulfite and nitrite reductases. *Proc Natl Acad Sci U S A* **1974,** *71* (3), 612-616.

11. Crane, B. R.; Siegel, L. M.; Getzoff, E. D., Sulfite Reductase Structure at 1.6 Å: Evolution and Catalysis for Reduction of Inorganic Anions. *Science* **1995,** *270* (5233), 59-67.

12. Brânzanic, A. M. V.; Ryde, U.; Silaghi-Dumitrescu, R., Why does sulfite reductase employ siroheme? *Chemical Communications* **2019,** *55* (93), 14047-14049.

13. Moura, I.; LeGall, J.; Lino, A. R.; Peck, H. D.; Fauque, G.; Xavier, A. V.; DerVartanian, D. V.; Moura, J. J. G.; Huynh, B. H., Characterization of two dissimilatory sulfite reductases (desulforubidin and desulfoviridin) from the sulfate-reducing bacteria. Moessbauer and EPR studies. *Journal of the American Chemical Society* **1988,** *110* (4), 1075-1082.

14. Han, S. H.; Madden, J. F.; Siegel, L. M.; Spiro, T. G., Resonance Raman studies of Escherichia coli sulfite reductase hemoprotein. 3. Bound ligand vibrational modes. *Biochemistry* **1989,** *28* (13), 5477-85.

15. Kaufman, J.; Spicer, L. D.; Siegel, L. M., Proton NMR of Escherichia coli sulfite reductase: the unligated hemeprotein subunit. *Biochemistry* **1993,** *32* (11), 2853-2867.

16. McRee, D.; Richardson, D.; Richardson, J.; Siegel, L., The heme and Fe4S4 cluster in the crystallographic structure of Escherichia coli sulfite reductase. *Journal of Biological Chemistry* **1986,** *261* (22), 10277-10281.

17. Bhunia, S.; Rana, A.; Roy, P.; Martin, D. J.; Pegis, M. L.; Roy, B.; Dey, A., Rational Design of Mononuclear Iron Porphyrins for Facile and Selective 4e–/4H+ O2 Reduction: Activation of O–O Bond by 2nd Sphere Hydrogen Bonding. *Journal of the American Chemical Society* **2018,** *140* (30), 9444-9457.

18. Bhattacharya, A.; Kumar Nath, A.; Ghatak, A.; Nayek, A.; Dinda, S.; Saha, R.; Ghosh Dey, S.; Dey, A., Reduction of Sulfur Dioxide to Sulfur Monoxide by Ferrous Porphyrin**. *Angewandte Chemie International Edition* **2023,** *62* (10), e202215235.

19. Adler, A. D.; Longo, F. R.; Finarelli, J. D.; Goldmacher, J.; Assour, J.; Korsakoff, L., A simplified synthesis for meso-tetraphenylporphine. *The Journal of Organic Chemistry* **1967,** *32* (2), 476-476.

20. Collman, J. P.; Brauman, J. I.; Doxsee, K. M.; Halbert, T. R.; Bunnenberg, E.; Linder, R. E.; LaMar, G. N.; Del Gaudio, J.; Lang, G.; Spartalian, K., Synthesis and characterization of "tailed picket fence" porphyrins. *Journal of the American Chemical Society* **1980,** *102* (12), 4182-4192.

21. Mittra, K.; Singha, A.; Dey, A., Mechanism of Reduction of Ferric Porphyrins by Sulfide: Identification of a Low Spin FeIII–SH Intermediate. *Inorganic Chemistry* **2017,** *56* (7), 3916-3925.

22. Walker, F. A., Magnetic spectroscopic (EPR, ESEEM, Mössbauer, MCD and NMR) studies of low-spin ferriheme centers and their corresponding heme proteins. *Coordination Chemistry Reviews* **1999,** *185-186*, 471-534.

23. Burke, J. M.; Kincaid, J. R.; Peters, S.; Gagne, R. R.; Collman, J. P.; Spiro, T. G., Structure-sensitive resonance Raman bands of tetraphenyl and "picket fence" porphyrin-iron complexes, including an oxyhemoglobin analog. *Journal of the American Chemical Society* **1978,** *100* (19), 6083-6088.

List of Publications:

1. Reduction of Sulfur Dioxide to Sulfur Monoxide by Ferrous Porphyrin

Aishik Bhattacharya[1], Arnab Kumar Nath[1], Arnab Ghatak[1], Abhijit Nayek, Souvik Dinda, Rajat Saha, Somdatta Ghosh Dey*, Abhishek Dey*
https://doi.org/10.1002/anie.202215235

2. Silver nanostructure-modified graphite electrode for in-operando SERRS investigation of iron porphyrins during high-potential electrocatalysis

Samir Chattopadhyay[1], Soumya Samanta[1], Ankita Sarkar, **Aishik Bhattacharya**, Suman Patra, Abhishek Dey*

https://doi.org/10.1063/5.0136333

Manuscript under preparation:

1. Intermediates involved in the Reduction of SO_2: Insight into the mechanism of Sulfite Reductases

Aishik Bhattacharya[1], Soumya Samanta, Arnab Kumar Nath, Arnab Ghatak, Somdatta Ghosh Dey*, Abhishek Dey*